INSTITUT FÜR GEOTECHNIK
STUTTGART

1999
Mitteilung 46
Herausgeber P.A. Vermeer

Akinsola Emmanuel Akinrogunde

Propagation of Cement Grout in Rock Discontinuities Under Injection Conditions

INSTITUT FÜR GEOTECHNIK
STUTTGART

1999
Mitteilung 46
Herausgeber P.A. Vermeer

Akinsola Emmanuel Akinrogunde

Propagation of Cement Grout in Rock Discontinuities Under Injection Conditions

Herausgeber:
Prof. Dr.-Ing. P.A. Vermeer
Institut für Geotechnik
Universität Stuttgart
Pfaffenwaldring 35
70569 Stuttgart
Telefon 0711/685-2436
Telefax 0711/685-2439
e-mail: vermeer@igs.uni-stuttgart.de

ISBN 3-921837-46-4

Herausgegeben 1999 im Eigenverlag des Instituts für Geotechnik.

Propagation of Cement Grout in Rock Discontinuities Under Injection Conditions

Von der Fakultät Bauingenieur- und Vermessungswesen
der Universität Stuttgart zur Erlangung der Würde
eines Doktors der Ingenieurwissenschaften (Dr.-Ing.)
genehmigte Abhandlung

vorgelegt von

AKINSOLA EMMANUEL AKINROGUNDE

geboren in Iju-Odo, Nigeria.

Hauptberichter: em. Prof. Dr.-Ing. U. SMOLTCZYK

Mitberichter: Prof. Dr. h. c. H. KOBUS, PhD.

Tag der mündlichen Prüfung: 27. Juli 1998

Vorwort der Herausgeber

Die vorliegende Arbeit entstand ursprünglich aufgrund einer Anregung der Zementindustrie, ein Verfahren zu entwickeln, mit dem man die Eignung von Suspensionen aus Ultrafeinzement zur Verpressung von Rissen in Felsgestein mit Spaltweiten unter 0,5 mm testen könnte.

Es stellte sich sehr bald heraus, daß Versuchsanordnungen mit künstlich eingestellten und damit definierten Spaltweiten nicht zum Ziel führten, sondern ein Verfahren mit Probekörpern aus dem zu untersuchenden Gestein zu entwickeln war. Außerdem stellte sich dann die Frage, wie die Wandrauhigkeit und die variable Rißweite berücksichtigt werden könnten.

Damit geriet die Aufgabenstellung zur Grundlagenforschung - insbesondere nachdem der Bearbeiter, Herr Akinrogunde aus Iju-Odo, Nigeria durch umfangreiche Schrifttumsrecherchen erkennen mußte, daß es für die Berücksichtigung der Raughigkeit natürlicher Klüfte international keine verwertbaren Quellen gab, obwohl gerade dieser Parameter den Erfolg eines Verpreßvorgangs nachhaltig steuert und den viskosen Fließvorgang bis zum Stillstand abbremst.

Dank der Förderung der Deutschen Forschungsgemeinschaft war es möglich, diese Fragen sowohl experimentell als auch theoretisch so weit zu bearbeiten, daß der Baupraxis ein Weg zur Prognose der Eignung von Verpreßmitteln gewiesen wird. Dabei ist bemerkenswert, daß dies nur durch eine fachübergreifende wissenschaftliche Arbeitsweise möglich war.

em. Prof. Dr.-Ing. Dr.-Ing.E.h. U. Smoltczyk o.Prof. Dr.-Ing. P.A. Vermeer

Ausbreitung von Zement-Suspensionen in Felsklüften unter Injektionsbedingungen

(Deutsche Kurzfassung)

Arbeitziele und Untersuchungsumfang

Die bisher veröffentlichten Studien zur mathematischen Analyse des Fließvorgangs von Injektionsmitteln in Felsklüften (*Gustafson/Stille*, 1996;*Hässler*, 1991; *Lombardi*, 1985; *Wallner*, 1976; *Wittke*, 1968) gehen von der Idealvorstellung aus, die Diskontinuität durch glatte, parallele Platten zu simulieren. Eine solche Modellbildung kann aber nicht die Blockade des Fließvorgangs erklären, wie er sowohl im Labor als auch in situ zu beobachten ist. Die Ziele die Untersuchung sind:

1. Die Entwicklung eines Verfahrens zur Berücksichtigung geometrischer Unregelmäßigkeiten längs des Fließweges in einer Kluft, und zwar auf der Grundlage vergleichender Wasserdruck-Versuche;

2. die Erarbeitung einer theoretischen Methode zur Abschätzung der Ausbreitung eines Injektionsmittels in Felsklüften unter Berücksichtigung der Felsdeformation, der Varianz der Fließweg-Geometrie und der Blockade der Klüfte im Zuge der Injektion;

3. die Entwicklung eines Verfahrens zur Qualitätskontrolle.

Die Untersuchung gliedert sich in drei untereinander verknüpfte Komponenten, nämlich Theorie, Experiment und Software-Entwicklung. Im theoretischen Teil werden die Gleichungen für den instationären Fließvorgang des Fluids in den Felsklüften aufgestellt und ihre progressive Versiegelung erklärt. Im versuchstechnischen Teil werden

- die Laborverfahren zur Bestimmung der im theoretischen Teil erforderlichen Eingangsparameter ausgewählt,
- Verfahren zur Erfassung der Oberflächenrauhigkeit der Kluftwandungen erprobt,
- Wasserdruckversuche ausgeführt,
- eine physikalische Simulation des Injektionsvorgangs im Labormaßstab entwickelt und
- Laborverfahren zur Eignungsprüfung dargestellt.

Bei der Software-Entwicklung ging es um die numerische Lösung der aufgestellten Gleichungen und die Inversionstechnik zur Erfassung der geometrischen Unregelmäßigkeit des Fließweges.

Die Anwendung der entwickelten Verfahren ist m.E. geeignet, die Planung, Ausführung und Überwachung von Verpreßmaßnahmen transparenter zu machen. Insbesondere kann das Verfahren zur Qualitätskontrolle bei Ausschreibungen und Angeboten von Injektionsmaßnahmen angewendet werden.

Stand der Technik der Felsverpressung

Der gegenwärtige Trend der Forschung auf diesem Gebiet widmet sich bevorzugt der Suche nach geeigneten, umweltverträglichen Verpreßmitteln, um die Ausbreitung toxi-

scher oder radioaktiver Eluate zu verhindern. Die traditionelle bautechnische Anwendung von Injektionen im Untertagebau und beim Dammbau wird heute zunehmend erweitert bei Maßnahmen zur Einschließung toxischer und radioaktiver Abfälle, s. dazu etwa die Diskussion von *Franklin/Dusseault* (1989). Die hier hauptsächlich verwendeten Substanzen sind Zement, Ton, Gesteinsmehl und ihre Mischungen. Der Trend bei der Injektionstechnik geht in Richtung auf Automatisierung und Qualitätskontrolle, siehe hierzu die State-of-the-Art-Berichte von *Kutzner* (1991), *Müller (1993)*, *Houlsby* (1994), *US Dept. of Energy* (1995). *Wittke* (1968) diskutierte das Problem, die Ausbreitung stabiler Zement-Suspensionen in Klüften zu untersuchen. Er wies darauf hin, daß eine exakte Behandlung der instationären Ausbreitung einer Zement-Suspension als Bingham-Flüssigkeit bei einem irregulär gestalteten Fließweg, wie es eine Kluft ist, mit den seinerzeit verfügbaren mathematischen Verfahren nicht zu leisten sei. Er verwendete Gleichgewichts-Betrachtungen, um die Reichweite des Injektionsmittels in einer durch glatte und parallele Wandflächen idealisierten Kluft abzuschätzen. *Wallner* (1976) modellierte das Fließverhalten von Zementsuspensionen mit der Bingham-Gleichung. Mittels FEM löste er numerisch das instationäre Problem der Felsverpressung. Seine numerischen Ergebnisse stimmten gut mit Versuchsergebnissen überein, die er beim Durchströmen von aus Plexiglas modellierten Diskontinuitäten gewonnen hatte. *Hässler* (1991) analysierte den Binghamschen Fließvorgang in einem Netzwerk eindimensionaler Klüfte mit glatten und parallelen Wandflächen. Auch seine numerischen Ergebnisse paßten gut zu Versuchsdaten in Simulationsmodellen aus Plexiglas und den Wallnerschen Resultaten. Wie aus den Versuchen *(Kennedy, 1958)* hervorgeht, beeinflußt die Wandrauhigkeit der Klüfte jedoch das Fließverhalten entscheidend. So zeigte sich bei den ersten Versuchen von *Smoltczyk/Akinrogunde*, daß Plexiglas für eine Simulation des viskosen Fließens selbst dann ungeeignet war, wenn man die künstlich eingestellten Kluftflächen mit einem rauhen Belag versah: die natürliche Wandrauhigkeit in einer engen Felskluft von Zehntelmillimeter-Weite war so nicht zu simulieren. Somit basieren die bisher vorliegenden theoretischen Arbeiten auf der Annahme glatter und paralleler Kluftwände. Dagegen sind die natürlichen Kluftwände ganz unregelmäßig beschaffen (*Sharp/Maini*, 1972; *Neuzil/Tracy, 1981*; *Ewert*, 1985; *Bourke*, 1987; *Tsang/Tsang*, 1987 und 1989; *Abelin et al.*, 1991; *National Research Council*, 1996). Ein besseres Verständnis des Fließverhaltens von Suspensionen in Klüften läßt sich aus Versuchsergebnissen an natürlichen Felsprobekörpern herleiten, wenn man sie mit den Ergebnissen numerischer Simulation unter Einbeziehung der Rauhigkeit vergleicht, wie das in der vorliegenden Untersuchung vorgenommen wurde.

Zum Stand der Qualitätssicherung

Die Auftraggeber verlangen in zunehmendem Maße eine Qualitätskontrolle bei Injektionsarbeiten. Die meist angewendete Methode, um den Versiegelungseffekt einer Injektionsmaßnahme in situ festzustellen, ist der Wasserdruckversuch (WD-Test). Andere Verfahren, die bisher aber nur in Forschungsprojekten benutzt wurden, sind die Crosshole-Seismik, Radarverfahren zur Durchdringung von Injektionsmassen, elektromagnetische Feldmessungen, Strahlungssonden (Neutronen) und Temperaturprofilmessungen (*Dwyer, 1994*). *Nonveiller* (1989) beschreibt einen Laborversuch zur Bestim-

mung des Erosionswiderstandes von einem Injektionsmittel in teilgefüllten Klüften. Dabei wurde ein 8 mm großes Loch in der Achse einer zylindrischen Probe aus Injektionsmittel gebohrt und dann Wasser unter einem bestimmten Druck für eine festgelegte Zeit eingepreßt. Der Gewichtsunterschied des Prüfkörpers vor und nach dem Versuch wurde als Maß für den Erosionswiderstand genommen. Dieses Verfahren eignet sich aus zwei Gründen nur sehr bedingt für eine Qualitätskontrolle: (1) simuliert es nicht die Verbundwirkung zwischen Gestein und Injektionsmittel; (2) bleibt die Durchlässigkeit des Injektionsmittels außer Betracht. *Hooton/Konecny* (1990) berichten über ihren Versuch, die Wirksamkeit der Injektion im Labor zu bestimmen, wobei sie künstlich gebrochene Felsproben verwendeten. Das von ihnen verwendete Gerät erlaubte jedoch keinen dreiaxialen Einschluß des Prüfkörpers, wie er für seine Injektion erforderlich gewesen wäre. In der Folge verwendeten sie dann Kluft-Modellkörper aus Plexiglas und Stahl, die aus den bereits erörterten Gründen keine zuverlässigen Bewertungen erlauben.

Aufstellung der Gleichungen für den Durchfluß in Felsklüften

Grundlagend für alle Strömungsvorgänge sind die Navier-Stokes-Gleichungen. Ihre Anwendung auf das instationäre Fließen bei irregulären Randbedingungen, die sich nur unklar definieren lassen, ist sehr schwierig. Aus diesen Gründen werden die Erhaltungssätze für Massen und Momente direkt auf den Fließvorgang in der Kluft angewendet, um zu vereinfachten Gleichungen für den Durchfluß zu kommen. Dabei werden folgende Annahmen getroffen

1. Die Wandflächen der Diskontinuitäten sind rauh;
2. die Dichte der Flüssigkeit ist konstant;
3. der Fließvorgang ist eindimensional;
4. die Veränderungen des mittleren Querschnitts, S_y, ist allein mit dem Druck korreliert;
5. die mittlere Fließgeschwindigkeit ist klein genug, um den konvektiven Term sowie quadratische und Glieder höherer Ordnung vernachlässigen zu können;
6. der mittlere Querschnitt für den Durchfluß ist klein;
7. die Injektion ist ein isothermer Prozeß, so daß die Energiegleichung nicht eingesetzt wird.

Geometrisches Modell des Fließweges

Der Wandabstand ergibt sich dabei zu

$$a_c(l, y) = \alpha_1(l, y) + \alpha_2(l, y) \tag{0.1}$$

wo $a_c(l,y)$ die zusammengesetzte Topographie und $\alpha_1(l,y)$ und $\alpha_2(l,y)$ die Rauhigkeitserhebungen über der mittleren Oberfläche sind.

Wenn der Querschnitt des Fließweges an einer bestimmten Stelle mit S_s bezeichnet wird, ist die mittlere Fließgeschwindigkeit $u_s = \frac{1}{S_s}\int u dS$. Der mittlere Wandabstand ist a_s. Es wird angenommen daß die mittlere Querschnittsbreite $b_s = S_s/a_s$ konstant ist.

Es seid dA ein Element des betrachteten Querschnitts, $d\mathcal{V}$ das Volumenelement,ρ die Flüssigkeitsdichte, $\mathbf{V}$ die Fließgeschwindigkeit und η die auf die Masse bezogene Eigenschaft N der Flüssigkeit (Massenmoment und Energie) innerhalb des betrachteten Volumens. Dann lautet die Reynoldssche Transportgleichung

$$\frac{dN}{dt} = \frac{\partial}{\partial t}\left(\int_{cv}\eta\rho d\mathcal{V}\right) + \left(\int_{cs}\eta\rho\mathbf{V}\cdot\mathbf{n}dA\right)_{out} - \left(\int_{cs}\eta\rho\mathbf{V}\cdot\mathbf{n}dA\right)_{in} \tag{0.2}$$

wo $\mathbf{n}$ der Normalvektor des Flächenelements dA ist.

Mit der Masse $N = m$ und dem Massenerhaltungssatz folgt aus Gl.(5):

$$\frac{\partial S_s}{\partial t}\delta l - u_s S_s + (u_s S_s + \frac{\partial}{\partial l}(u_s S_s)\delta l) + \chi p S_s \delta l = 0 \tag{0.3}$$

worin χ die Einspeisung, bezogen auf Einheitsvolumen und Einheitsdruck, in den Fels und p der Druck sind.

Mit den eingangs genannten Annahmen 4 und 5 vereinfacht sich diese Gleichung zu

$$\boxed{\beta\frac{\partial p}{\partial t} + \chi p + \frac{\partial u_s}{\partial l} = 0} \tag{0.4}$$

worin $\beta = 1/S_s\frac{dS_s}{dp}$ eine Funktion der Kompressibilität der Felsmasse und von a_s ist. Unter der Voraussetzung, daß das Felsmassiv elastisch und isotrop ist, erhält man mit dem Elastizitätsmodul E und der Poissonzahl ν mit der Annahme 4 die Gleichung

$$\boxed{\beta = \frac{1}{a_s}\frac{da_s}{dp} = 2\frac{\mathcal{C}_d\mathcal{L}(1-\nu^2)}{Ea_s}} \tag{0.5}$$

Hierin ist $\mathcal{L}$ die charakteristische Länge und $\mathcal{C}_d$ ein Koeffizient (*Wylie, 1992*), deren Werte hängen jeweils vom Grad der Diskretisierung ab.

Für die Bedingung von der Erhaltung des Moments werden in Gl.(5) $N = m\mathbf{V}$ und $\eta = \mathbf{V}$ gesetzt:

$$\frac{d}{dt}(m\mathbf{V}) = \sum\mathbf{F} = \frac{\partial}{\partial t}\int_{cv}\mathbf{V}\rho d\mathcal{V} + \int_{cs}\mathbf{V}\rho(\mathbf{V}\cdot\mathbf{n})dA \tag{0.6}$$

woraus bei Berücksichtigung der Annahme 5 die vereinfachte Gleichung

$$\boxed{\frac{\partial p}{\partial l} + \theta + \rho\frac{\partial u_s}{\partial t} = 0} \tag{0.7}$$

folgt.

Bei Wasser, einer Newton-Flüssigkeit, ist $\tau = \mu\dot{\gamma}$, was auf $\theta = \frac{12\mu}{a_s^2}u_s$ führt. Eingesetzt in Gl.0.7 ergibt sich

$$\frac{\partial p}{\partial l} + \zeta u_s + \rho\frac{\partial u_s}{\partial t} = 0 \tag{0.8}$$

mit der Abkürzung $\zeta = \frac{12\mu}{a_s^2}$

Wenn Gl.0.4 nach t und Gl.0.8 nach l differenziert werden, folgt nach weiteren Vereinfachungen die Gleichung

$$\boxed{(\beta\zeta + \chi\rho)\frac{\partial u_s}{\partial t} + \beta\rho\frac{\partial^2 u_s}{\partial t^2} + \chi\zeta u_s = \frac{\partial^2 u_s}{\partial l^2}} \tag{0.9}$$

Analog erhält man durch Differentiation der Gl. 0.4 nach l und Gl.0.8 nach t:

$$\boxed{(\beta\zeta + \chi\rho)\frac{\partial p}{\partial t} + \beta\rho\frac{\partial^2 p}{\partial t^2} + \chi\zeta p = \frac{\partial^2 p}{\partial l^2}} \tag{0.10}$$

Zur Lösung läßt sich die formale Analogie mit der sog. "Telegraphengleichung" heranziehen, mit der die Signal-Übermittlung in Kabeln berechnet wird. Die dort verwendeten Parameter sind, jeweils verteilt über die Länge und bezogen auf die Längeneinheit, die Induktivität L_f [Henry/m], der Widerstand R_f [Ohm/m], die Kapazität C_f [Farad/m] und die Leitfähigkeit G_f [Siemens/m]. Die elektrischen Gleichungen lauten damit:

$$\boxed{(C_l R_l + G_l L_l)\frac{\partial i}{\partial t} + C_l L_l\frac{\partial^2 i}{\partial t^2} + G_l R_l r i = \frac{\partial^2 i}{\partial l^2}} \tag{0.11}$$

$$\boxed{(C_l R_l + G_l L_l)\frac{\partial v}{\partial t} + C_l L_l\frac{\partial^2 v}{\partial t^2} + G_l R_l v = \frac{\partial^2 v}{\partial l^2}} \tag{0.12}$$

Ein Vergleich der Gleichungen (0.11) und (0.12) mit den Gleichungen (0.9) und (0.10) zeigt ihre mathematische Gleichartigkeit.

Die elektrische Analogie kann also angewendet werden, um den Wasserdruckversuch zu analysieren. Das Verfahren wird hier kurz angesprochen. Wenn der Wasserdruck auf die Felskluft einwirkt, stellt sich ein Fließvorgang ein, dessen Druckverlauf von der Geometrie der Kluft abhängt. Bei Anwendung eines konstanten Injektionsdruckes p nimmt die Fließgeschwindigkeit von 0 aus zu, bis ein stationärer Zustand erreicht ist. Dies kann symbolisch ausgedrückt werden in der Form

$$q(t) = f(a_s(l))$$

Wenn unterschiedliche Drücke p erzeugt werden, erhält man eine entsprechende Kurvenschar

$$q(p,t) = g(a_s(l)) \tag{0.13}$$

wo g die Beziehung zwischen der Verteilung des durchschnittlichen Abstandes $a_s(l)$ der Kluftwände und der gemessenen Wassermenge $q(p,t)$ angibt. Die Transformation dieser Gleichung wird gewöhnlich symbolisch in der Form

$$a_s(l) = g^{-1}(q(p,t)) \tag{0.14}$$

ausgedrückt. Dieses Transformationsverfahren wurde folgendermaßen in einem Rechenprogramm implementiert:

1. Festlegung einer annehmbaren Fehlertoleranz,
2. Schätzung der Verteilung von a_s.
3. Lösung der Gln. 0.9 und 0.10 mit den geschätzten Eingangsdaten mittels elektrischer Analogie (*Chistopoulos*, 1995),
4. Vergleich der analytischen Lösung mit den Versuchsergebnissen und Fehlerermittlung,
5. Bleibt der Fehler innerhalb der Toleranz, endet die Iteration. Falls nicht, wird anhand eines Fehlerausgleichs ein neuer Datensatz bestimmt und das Verfahren mit den Schritten 3 bis 5 wiederholt, bis die Toleranz eingehalten ist.

Für den Fehlerausgleich im Sinne einer Optimierung gibt es viele Verfahren. Hier wurde die Hybridmethode nach Powell gewählt (*Powell, 1964*), weil ihr Algorithmus sehr schnell ist, da sie keine Differentiation anwendet, die das gemeinsame Merkmal von Optimierungsver-fahren ist.

Es sei erwähnt, daß es auch andere Verfahren zur Lösung der Telegraphengleichungen gibt. Ein häufig angewendetes Verfahren ist die *Finite Difference Time Domain-Methode* (FDTD). Das gewählte Verfahren (TLM) hat den Vorteil, einfach und robust zu sein (*Pomeroy*, 1991). Außerdem kann ein TLM-Modell im kleinen Maßstab entwickelt und getestet werden und läßt sich auf großmaßstäbliche Probleme anwenden, ohne instabil oder ungültig zu werden. Aus dem Gesagten wird deutlich, daß die Lösung eines inversen Problems nicht eindeutig ist, sondern prinzipiell von der gewählten Fehlertoleranz, der Optimierungsmethode und dem Algorithmus abhängt.

Fließ- und Blockade-Mechanismen bei Zementinjektionen in Felsklüften

Die beiden Hauptfaktoren für das Strömungsverhalten in Leitern von der Art der Felsklüfte sind die Geometrie des Leiters und die rheologischen Eigenschaften der Flüssigkeit. Letztere lassen sich nach *Ashikmen and Pronina (1986)* bei einer Zementverpressung mit Hilfe der Bingham-Gleichung modellieren:

$$\begin{aligned} \tau &= 0, \quad && \tau < \tau_y \\ \tau &= \tau_y + \mu_p \dot{\gamma}, \quad && \tau \geq \tau_y \end{aligned} \tag{0.15}$$

wobei die Scherspannung τ und $\dot{\gamma}$ die Scherrate sind. μ_y und τ_y sind die *plastische Viskosität* und die *Fließgrenze*. Dies wurde von vielen Forschern bestätigt, siehe dazu etwa *Banfill* (1981) und *Murata/Kikukawa* (1992). Das Bingham-Modell besagt mathematisch, daß die so beschriebene Flüssigkeit nur bei Überschreiten der Fließgrenze fließt. Wenn angenommen wird, daß der Fließweg in der Kluft durch parallele Platten begrenzt und der Injektionsdruck ausreicht, die Suspension durch den Prüfkörper zu pressen, dann ist $\tau > \tau_y$, und es ergibt sich nach Gl.(0.15) ein kontinuierliches Fließen durch die Kluft. Der wirkliche Verlauf zeigt ein ganz anderes Bild, als es sich bei der Annahme paralleler, glatter Kluftwände ergeben sollte. Würde man den Versuch mit Plexiglas-Platten machen, ergäbe sich nach den Berichten von *Wallner* (1976) und *Hässler* (1991) ein Verhalten, das der theoretischen Voraussage aufgrund der Annahme paralleler, glatter Wände ähneln würde. Es war also notwendig, die Arbeitshypothese durch Berücksichtigung der Blockadewirkung zu erweitern.

Beim Prozeß der progressiven Blockade des Fließvorgangs ist von folgenden Beobachtungen auszugehen:

1. die Wandabstände innerhalb der Kluft variieren beträchtlich;
2. die Blockade ist ein kontinuierlicher Vorgang und stellt sich an Engstellen des Fließweges ein;
3. Engstellen in der Nähe des Eintrittsquerschnitts beinflussen die Geschwindigkeit, mit der sich die Blockade entwickelt, stärker als entferntere Engstellen;
4. Blockaden können folgenden interaktiven Faktoren notwendig und hinreichend zugeordnet werden: Fließgrenze des Injektionsmittels, Zementkorngröße, Hindernisse oder Ende des Fließweges, Van-der-Waals-Kräfte;
5. Eine Erhöhung des Injektionsdruckes hebt eine Blockade nicht unbedingt auf.

Zur Veranschaulichung des Blockade-Mechanismus betrachte man Abbildung 5.4 (Seite 77) Wenn die Front des Injektionsmittels das Hindernis (Wandabschnitt 1) erreicht, wird ein Teil der Masse zurückgehalten, während der Rest durch den Querschnitt 2 weiterfließt. Es entsteht ein Staudruck, der rückwärts bis zum Einpreßquerschnitt reflektiert wird, so daß die Verpreßleistung geringer wird. Für das durch Querschnitt 2 gepreßte Injektionsmittel wiederholt sich dieser Vorgang am Wandabschnitt 3: die Injektionsleistung nimmt progressiv bis zur vollständigen Blockade ab, wobei die Größe der Rauhigkeitserhebungen das Tempo des Vorgangs bestimmt. So kann es auch vorkommen, daß sich ein auf dem Fließweg entfernteres größeres Hindernis bremsend auf davor liegende kleinere Hindernisse auswirkt. Bei all diesen Erscheinungen spielt es keine Rolle, ob der Injektionsdruck oszilliert oder nicht. Makroskopisch handelt es sich um den bekannten Energieverlust durch Reibung in Transportleitungen. Zu dem Energieverlust durch die Wandrauhigkeit (äußere Reibung) kommt der Verlust durch Viskosität (innere Reibung) hinzu. Unabhängig von diesen Reibungsverlusten besteht naturgemäß auch ein kritisches Verhältnis zwischen dem größten Durchmesser D_c des Zements und der lokalen Kluftweite . Nach *Lau/Crawford (1986)* soll das Verhältnis $D_c > 3$ sein, um ein stetiges Fließen zu gewährleisten. Im übrigen spielen auch die Van-der-Waals-Kräfte insofern eine die Blockade fördernde Rolle, als durch

sie die Grenzschicht zwischen bereits zur Ruhe gekommenen und noch im Fluß befindlichen Teilchen vergrößert wird. Der Vorgang läßt sich formal mit der zuvor genannten Methode der Signalfortleitung erfassen, wenn man vereinfachende Annahmen einführt. Es ist nicht möglich, sämtliche beteiligten Faktoren einzeln mathematisch zu berücksichtigen. So wird in dem folgenden Ansatz die Wirkung der Van-der-Waals-Kräfte vernachlässigt. Angenommen, die Geometrie des Fließweges ist definierbar, dann wird μ in dem Term $\zeta = \frac{12\mu}{a_z^2}$ der Gl. 08 durch

$$\mu_m = \mu_p + \frac{\tau_y(1 - e^{-m|\dot{\gamma}|})}{|\dot{\gamma}|} \tag{0.16}$$

ersetzt, wobei μ_p und τ_y die plastische Viskosität und die Fließgrenze der Suspension bedeuten und m eine konstantes Abklingungsmaß seien. Dieser von *Papanastasiou* (1987) eingeführte Ansatz ersetzt den Knick im Bingham-Diagramm durch einen stetigen Übergang. Er wurde von *Abdali et al.*(1992) und von *Donier/Tichy* (1992) für die Analyse der Bingham-Flüssigkeit verwendet. Dabei wird für m derjenige Wert gewählt, der die für eine bestimmte Viskosität gültige Bingham-Kurve am besten approximiert. Mit diesem Ansatz wurden auch von uns die Gln. 0.11 und 0.12 mit dem geschilderten Verfahren gelöst, wobei davon ausgegangen wurde, daß sich eine Blockade jederzeit einstellt, wenn der lokale Druckabfall einen kritischen Wert unterschreitet.

Labormessungen

Die Labormessungen umfaßten die Charakterisierung des Fließweges durch Messung der Kluftflächen-Geometrie bzw. durch den Wasserdruckversuch, die verfeinerte Bestimmung der Viskosität der Zementsuspension, die physikalische Simulation des Injektionsvorganges und die Entwicklung eines Eignungstestes.

Laser-scannen von Bruchflächen

Zylindrische Felsproben wurden axial abgedrückt, um natürliche Bruchflächen auf ihre Rauhigkeit hin zu untersuchen. Dabei wurde ein laser-Verfahren des Institut für Navigation der Universität Stuttgart verwendet um eine digitale Auswertung der Datenfelder der Topographie zu ermöglichen.

Integrative Erfassung der Kluftflächen-Geometrie durch Wasserdruckversuche

Die Versuchsanordnung für den Wasserdruckversuch zeigt Abbildung 7.7 (Seite 107). Der Durchflußmesser F und der Hahn V3 werden rechnergesteuert. Der Druck im Tank T1 wird konstant gehalten, nachdem das Injektionsrohr mit Wasser gefüllt ist. Der Einpreßvorgang beginnt mit dem Öffnen von V3. Die Durchflußrate wird automatisch registriert. Bei Erreichen des stationären Zustandes wird V3 abgeschaltet.

Abbildung 8.6 (Seite 118) zeigt ein typisches Flußdiagramm für variable Drücke zwischen 50 und 250 kPa. Das Resultat dient dann bei der Lösung der Gln. 0.11 und

0.12 dazu, die Varianz des Kluftquerschnitts innerhalb eines Fließweges als Integralmittelwert zu berücksichtigen. Bei allen diesen Versuchen stellte sich der stationäre Zustand innerhalb von 6 sec ein.

In gleicher Weise wurde auch der Injektionsversuch gefahren mit dem Unterschied, daß V3 durch einen mechanischen Sperrschieber ersetzt wurdet. Die Durchflußmenge der Zementsuspension wurde bei diesen Versuchen durch die Aufzeichnung der Gewichtsänderung des Tanks T1 gemessen.

Bestimmung der Eigenschaften der Zementsuspension

Für diese Bestimmung sind grundsätzlich zwei Versuche erforderlich - die Messung der Viskosität und der Dichte. Die Dichtewerte liegen zwischen 1,30 und 1,37 g/ml. Die Viskosität wurde mit einem hoch empfindlichen Rotationsviskosimeter (Rheometer MC1) bestimmt, um 1. bei gegebenem W/Z-Faktor die optimale Zugabemenge an Verflüssiger, und 2. die Materialkennwerte τ_y und μ_p für die Analyse zu ermitteln. Das Meßsystem besteht im wesentlichen aus einem zylindrischen Behälter mit der Suspension, in die ein rotierender innerer Zylinder eintaucht. Die Behälterwand ist rauh, um einen Schlupf der Suspension zu verhindern. Die Theorie für die Auswertung wurde entwickelt. Als Zement wurde Microcem A, ein Produkt der Heidelberger Baustofftechnik, verwendet. Die optimale Dosis des Verflüssigers lag zwischen 1,5 und 3

Eignungsversuch

Die Einrichtung für den Eignungsversuch zeigt Abbildung 7.11 (Seite 111). Der an eine Handpumpe angeschlossene Tank T3 beaufschlagt den Tank T2 über eine Drossel V6 mit dem Druck, der den Druck des Grundwassers simulieren soll.

Der Tank T1 dient sowohl für die Injektion mit Wasser als auch Zementsuspension. Er ist über den Hahn V1 an eine Druckluftversorgung angeschlossen, die im Tank einen konstanten Luftdruck aufrechterhält. Der Tank T2 enthält den Probenhalter SH, der im wesentlichen aus einer Kopf- und einer Fußplatte besteht, die durch Spindeln zusammengespannt werden. Die Platten haben Bohrungen für die Injektion. Der Durchflußmesser F wird auch hier wieder nur bei Versuchen mit Wasser eingesetzt.

Es wurden zwei Gesteinsarten gewählt - Granit und Sandstein. Die aus ungeklüftetem Gestein herausgedrehten Prüfkörper hatten 64 mm Durchmesser und waren 125 mm lang. Die Trennfläche im Prüfkörper wurde in der Weise des "Brazilian Tests"hergestellt. Dabei ergaben sich auch die Daten für den Elastizitätsmodul und die Poissonzahl. Die Bruchhälften wurden wieder zusammengefügt, mit einem dicht anschließenden Gummimantel überzogen und in stählerne Halbschalen gestellt, die mit Metall-Sprengbändern verbunden wurden. Die Endflächen des Prüfkörpers wurden mit Silikonschichten versehen, so daß sie gegen die Platten des Probenhalters druckdicht verspannt waren. Der Versuch läuft folgendermaßen ab:

1. Wasserdruckversuch mit konstanten Drücken von 50 - 100 - 150 - 200 - 250 kPa, um die Wasserdurchlässigkeit des Prüfkörpers zu ermitteln: als Maß wird das Integral T_0 der Durchflußmenge in Abhängigkeit vom Injektionsüberdruck [Pa] in dem untersuchten Druckbereich festgelegt.

2. Injektion.
3. Wiederholung des Wasserdruckversuchs 24 h nach der Injektion und Ermittlung des Wertes T_1.
4. Berechnung der Effektivität der Injektion durch das Verhältnis

$$\frac{T_0 - T_1}{T_1} \tag{0.17}$$

Abbildung 8.8 (Seite 120) zeigt ein Beispiel für die auf diese Weise gemessenen Kurven und die daraus errechnete Effektivität.

In allen untersuchten Fällen widerstand das Injektionsmittel dem maximal verfügbaren Druck von 250 kPa, ohne ausgewaschen zu werden. Ferner war festzustellen, daß sich bei konstantem Injektionsdruck der Durchfluß zunächst bis zu einem Maximum steigerte, um dann progressiv abzufallen. Beim nachträglichen Aufsägen der Prüfkörper zeigte sich, daß das Injektionsmittel die Bruchfläche vollständig benetzt hatte, obwohl durch das Zusammendrücken der Hälften praktisch keine definierbare Kluftweite vorhanden gewesen war. Dennoch ergab sich, wie der Wasserdruckversuch zeigte, keine vollständige Versiegelung, d.h. der gewählte Eignungsversuch liefert ein sehr empfindliches Maß für die Effektivität.

Bestimmung der Wandrauhigkeit

Abbildung 8.4 (Seite 117) vergleicht ein typisches Ergebnis der Computerrechnung mit dem entsprechenden Laborergebnis aus direkten Messungen. Als allgemeine Tendenz ist zu erkennen, daß die berechneten Werte von in der Nähe des Injektionsquerschnitts den direkt gemessenen ähneln, während sich bei größeren Abständen erhebliche Unterschiede ergeben. Da die aus der Rechnung hergeleitete Geometrie des Fließweges von der direkt gemessenen abwich, wurde letztere eingesetzt, um die Zeit zu ermitteln, die für eine Blockade erforderlich war. Die so berechnete Zeit ergab sich um etwa 20% größer als die im Versuch gemessene.

Schlußfolgerungen und Empfehlungen

Im Verlauf dieser Untersuchung wurde ein Eignungsversuch für die Versiegelung von Trennflächen im Fels durch Injektionen entwickelt, wobei sowohl die Eignung des Injektionsmittels als auch der Versiegelungseffekt getestet werden. Ebenso sind damit Untersuchungen des Widerstandes von Injektionsmitteln gegen chemisch verunreinigte Wässer möglich. Die ausgeführten Versuche mit einem Ultrafeinzement haben gezeigt, daß mit diesem Injektionsmittel auch sehr enge Trennflächen gefüllt werden können. Der Versiegelungseffekt liegt sehr hoch, selbst wenn sich eine 100 %ige Versiegelung nicht erreichen läßt. Der Versuch kann somit für die Ausschreibung von Injektionsarbeiten als Qualitätskontrolle eingesetzt werden.

Die in dieser Untersuchung vorgenommene Nachrechnung des Wasserdruckversuchs ermöglicht nur die Voraussage der Wandrauhigkeit im Nahbereich des Injektionspunktes. Die Anwendung der Transmissionstheorie zur Modellierung des Verpreßvorgangs lieferte Ergebnisse mit Abweichungen in der Größenordnung von 20%

im Vergleich zu Werten aus Laborversuchen. Dies läßt sich wahrscheinlich durch weitere Forschungen verbessern, wenn insbesondere durch eine räumliche Anordnung von Sensoren die Datenbasis für die Transmissionstheorie und ihren Inversions-Algorithmus erweitert werden könnte. Damit sollte es möglich sein, mit den Vorhersagen über den Nahbereich hinauszukommen. Jedenfalls dürfte der Wasserdruckversuch angesichts seiner weit verbreiteten Anwendung in der Praxis die geeignete Möglichkeit zur Entwicklung verfeinerter Verfahren sein.

Die Simulation des Verpreßvorgangs mit der Transmissionstheorie erscheint jedenfalls vielversprechend. Feldversuche wären hier angezeigt, konnten aber im Rahmen der in diesem Vorhaben vorhandenen Mittel und angesichts der unerwartet umfangreichen Vorarbeiten bisher nicht durchgeführt werden. Ein wesentlicher Vorteil des theoretischen Modells ist seine von äußeren Bedingungen unabhängige Stabilität.

Ein wissenschaftliches Ergebnis dieser Arbeit ist das für die Felsverpressung entwickelte theoretische Modell, in dem die zur Zeit vorhandenen Theorien dadurch erweitert werden, daß die Rauhigkeit der Diskontinuitätsflächen systematisch einbezogen und damit der Blockade-Effekt als progressives Phänomen des Injektionsvorganges erklärt werden kann.

Propagation of Cement Grout in Rock Discontinuities Under Injection Conditions

Akinsola Emmanuel Akinrogunde

Preface

This work was presented to the Faculty of Civil Engineering and Surveying, University of Stuttgart in fulfillment of the award of the Dr.-Ing. degree.

My deep heart felt gratitude goes to my *Doktorvater*, Professor Dr. -Ing. Dr. -Ing. E.h U. Smoltczyk who not only gave me the opportunity to run the doctoral programme under his supervision but also went to very great extent in ensuring my wellbeing and that of my family.

My thanks goes to Professor Kobus for accepting to be my co-supervisor.

Professor P. Vermeer and Professor Reinhardt, put the facilities of their institutes at my disposal during this work. For this, I am very grateful.

The research was financed through the fund granted to Professor Smoltczyk by the German Research Society. The Rotary Club, Stuttgart and the Heidelberger Baustofftechnik GMBH, Leimen provided support at different stages of the work. To these organizations, I am most grateful.

All the computer work on the research was done using Linux, the free Unix operating system and many free softwares downloaded from the Internet. To the authors of these softwares, I express my appreciation.

My thanks also go to many people, who, through different Internet resources provided information at different times during this work.

Finally I would like to thank my wife, Patience and my children, Morayo and Olaseji. They gave me every reason to continue when the obstacles seemed insurmountable.

Akinsola E. AKINROGUNDE

Contents

List of Figures

List of Tables

Chapter 1

Introduction

1.1 Background Information

Engineering structures such as dams, tunnels, storage facilities for crude oil and food, power plants, repositories for toxic and radioactive waste are usually sited in or on rock masses. Underground spaces in rocks are increasingly being used for recreational, art and cultural purposes. Rock masses contain discontinuities. On one hand, the presence of discontinuities in the rock masses enhances the flow of economically important fluid such as water and crude oil. On the other, discontinuities not only weaken the rock masses, they also serve as conduits for toxic fluids which pollute the environment and groundwater.

For the engineering structures sited in or on rocks masses to fulfill their intended purpose(s), sealing of the discontinuities is usually necessary during construction and maintenance work. In some structures such as dams and tunnels, partial sealing of the discontinuities may be supplemented with additional measures such as drainage facilities. However, in structures such as repositories for radioactive waste, complete sealing of the discontinuities is desirable. In petroleum extraction, sealing of some discontinuities is also implemented to control the flow of crude oil towards wells. Groundwater can also be protected from toxic waste through sealing of rock discontinuities.

Grouting is one of the major methods of sealing rock discontinuities. It involves the injection of substances (grouts) into the discontinuities in order to improve strength and/or impermeability of the rock mass. Rock grouting is basically different from soil grouting. This work deals only with rock grouting. Therefore, rock grouting is implied in all subsequent references to grouting. Rock grouting can, in general, be classified into two major types — permeation grouting and hydrofracture grouting. In permeation grouting the injection pressure is lower than that which can fracture the rock mass. The injection pressure in hydrofracture is deliberately made high enough to fracture the rock mass in order to enhance pen-

etration of the grout. In this work only permeation grouting is considered because it is the type usually employed in most grouting projects.

Commercially available grouts can be broadly grouped into particulate grouts and chemical grouts. Cement and clay suspensions — with or without additives are examples of particulate grouts while resin and bitumen are examples of chemical grouts. According to Koerner (1984), in his overview of commonly used chemical grouts, chemical grouts are toxic and corrosive to some extent. Cement grout on the other hand is non-toxic. When in contact with water, its active component turns into Calcium Hydroxide $Ca(OH)_2$, which is harmless (Mouxaus, 1978). Consequently, in terms of environmental compatibility, cement based grouts are better than chemical grouts. Common cements cannot be used to grout fine discontinuities because of their relatively large grain size. This draw-back has largely been removed with the introduction of ultra-fine cement which has been successfully used to seal fine discontinuities (Moller et.al., 1983; Smoltczyk and Akinrogunde, 1995). In addition, cements suspensions are cheaper than chemical grouts.

As environmental laws around the world become more stringent, cement suspensions will continue to be the grout of choice until a more environmentally friendly grout is developed. The importance of environmental protection in grouting projects was highlighted recently when a manufacturer of chemical grout in France was forced to stop production because his product was implicated in the groundwater pollution cases in Norway and Sweden (Soudain, 1997). On the basis of its relative advantages over chemical grouts, cement grout has been selected for use in this work. Therefore, cement suspension and grout are used synonymously in this report.

An ideal rock grouting project would involve complete mapping of the rock discontinuities, drilling of boreholes to intersect the discontinuities and the injection of just enough quantity of grout to improve strength and impermeability, at the least cost. The ideal grouting, however, does not exist because of the following reasons:

1. Discontinuities cannot be completely mapped with the present level of technological advancement because of their 3-dimensional nature and their limited exposure in outcrops, boring or tunnels (Dershowitz and Einstein, (1988)).

2. The geometry of the flow paths in the discontinuities are irregular and difficult to describe quantitatively.

3. The flow property of the cement grout is not completely understood.

4. The grouting process is complex and difficult to model mathematically.

These difficulties have hindered efforts at understanding the physics of rock grouting. A situation in which rock grouting is considered more of an art than science has resulted (Bradbury, 1987). Some practitioners (e.g Lombardi and Deere, 1993) have even gone to the extent of advocating for the simplification of rock grouting process to suit mathematical analysis. There are no generally accepted methods to assess the need for grouting or a method to assess its effectiveness. Basic questions such as the quantity of grout required to achieve a given level of impermeability or strength cannot be answered reasonably. In spite of the considerable improvement made in the development of machinery and instruments (e.g. Müller, 1984 and ÖDK (1991)) used for the execution and monitoring of grouting, planning and execution of grouting are more of gambling than scientific processes. With all the tools at the disposal of the modern engineer, it is possible to improve on the present situation. This work is directed towards understanding the mechanics of the flow of cement grout in rock discontinuities and the development of a laboratory test for investigating the effectiveness of the injected grout.

1.2 Objective and Scope

The basic pre-requisite for the analysis of fluid flow is the description of the geometry of the flow path. The idealization of the rock discontinuities as parallel plates on the macroscopic scale was employed in all published studies (Gustafson and Stille (1996), Hässler (1991), Lombardi (1985), Wallner (1976), Wittke (1968)) on the flow of grout in rock discontinuities known to the author. This idealization however, oversimplifies the description of the geometry of the flow path of the grout within rock discontinuities. Furthermore, the idealization cannot be used to explain the blockage process of the rock discontinuities as observed both in the laboratory and on the field. An objective of this research work is therefore:

- The development of a method of geometric characterization of rock discontinuities suitable for investigating the flow of cement grout in rock discontinuities.

Existing models of the flow of grout in rock discontinuities (e.g. Gustafson and Stille (1996), Hässler (1991), Lombardi (1985), Wallner (1976), Wittke (1968)) did not consider blockage of the discontinuities as grouting progresses. Another objective of this research is:

- The development of a theoretical method for estimating the spread of grout in rock discontinuities, under injection conditions, taking into consideration the blockage of the discontinuities as injection progresses.

The last objective of this work is:

- The development of a method for assessing the effectiveness of injected grouts.

The research is divided into three interrelated components:

1. Theoretical,
2. Experimental, and
3. Computational.

In the theoretical parts, new equations are developed for the transient analysis of the flow of injected fluids in rock discontinuities. The developed equations are used within numerical inversion process to obtain information on the variation of the geometry of the flow path within the rock discontinuities. In addition, the mechanics of the flow of cement grout in rock discontinuities are explained, taking into considerations

- the effects of irregular geometry of the walls of the discontinuities and
- blockage of the discontinuities as injection progresses.

The experimental part involves:

1. Determination of the rheological properties of the rock grout.
2. Measurement of the geometry of the flow path within the rock discontinuity using
   - transient water pressure test and
   - surface morphology of the walls of the discontinuity
3. Physical simulation of grouting on the laboratory scale.
4. Laboratory method for assessing the effectiveness of injected grout.

The computational component deals with the numerical simulation of the flow of water and grout under transient conditions using the transmission line modeling and the numerical inversion process for estimating the geometry of the flow path within the rock discontinuity.

The mechanics of rock grouting as explained in this research extend the current level of understanding the physics of rock grouting. Within the framework of the research a new method of analyzing the results of water pressure test was developed to obtain information on the variation of the geometry of the flow path within the rock discontinuities.

The application of the new procedure to grouting projects will make planning , execution and monitoring of injection more transparent. In particular, the method of assessing the effectiveness of injected grout can be used to write precise specifications and tenders for grouting projects.

1.3 Outline of the Report

The report is divided as follows: The state of the art in rock grouting is presented in Chapter 2. In Chapter 3, the review of the mechanics of fluid flow in rock discontinuities and the description of flow path geometry is presented.

In Chapter 4, fundamental conservation laws are combined with constitutive equation of water to develop a new equation which is used for the transient analysis of the result of water pressure test. The developed equation is similar to the transmission line equation. The numerical inversion process for estimating the geometry of the flow path is also discussed.

The mechanics of the flow of cement grout in rock discontinuities is discussed in Chapter 5 with the concept of *progressive blockage* of the rock discontinuities. In addition, equations are developed for estimating the extent of propagation cement grout in the rock discontinuities using the description of the geometry of the flow path obtained from the method developed in Chapter 4.

The transmission line modeling (TLM) is the subject of Chapter 6. The theory of transmission line modeling is discussed. The numerical implementation of the TLM is also presented.

In chapter 7, laboratory procedure for the measurement of the rheology of cement grout is presented. The procedure for measuring surface geometry of the walls of the discontinuity using laser beam is also presented. Furthermore, the the method of obtaining the void geometry within the rock discontinuity from the measured surface geometry is discussed. Transient water pressure test for the numerical inversion process is highlighted. Finally, physical simulation of grouting and the method of assessing the effectiveness of injected grout is the laboratory is discussed.

Both Laboratory and numerical results are discussed in Chapter 8 while conclusions are presented in Chapter 9.

Chapter 2

State of the Art

2.1 Rock Grouting

As stated in chapter 1, rock grouting involves the injection of substances (grout) into the rock discontinuities with the aim of decreasing permeability and/or increasing strength. In recent time, especially within research work on sealing radioactive waste repository, other types of grouts are being investigated for sealing rock discontinuities. Börgesson and Pusch(1993) investigated the rheological and sealing capability of of less commonly used grouts. The materials they investigated are — smectite-rich clay with quartz and salt as additives; and cement with silica fume and superplasticizer as additive. They concluded that both grout mixtures are suitable grouting materials. These materials are yet to find their way into main stream rock grouting. The US Department of Energy is currently testing two new grouts—*montan wax* and *glyoxal-modified sodium silicate*. The first, a mineral wax and bentonite emulsion was developed by MIBRAG and DBI in Germany and the second was developed in France. Tentative field and laboratory testing of the materials showed that they have good penetrating and sealing properties, but they may have problems satisfying environmental protection regulations (US Department of Energy).

A successful grouting project requires a comprehensive knowledge of the structural geology and strength characteristics of the rock mass, flow behavior of the grout and grouting equipment. The applications of grouting, current practices in grouting, present knowledge on the physics of grouting and methods of assessing injected grout are discussed in this chapter.

2.2 Applications of Rock Grouting

The commonest use of rock grouting is in the construction and rehabilitation of dams. In form of blanket curtain and/or cut-off wall, it is used for one or more of

the followings:

1. Strengthening of foundation and abutment,
2. Reduction of seepage through the foundation, abutment and body of the dam,
3. Checking the build-up of pore pressure (in conjunction with drainage facilities) in the foundation, and abutment.

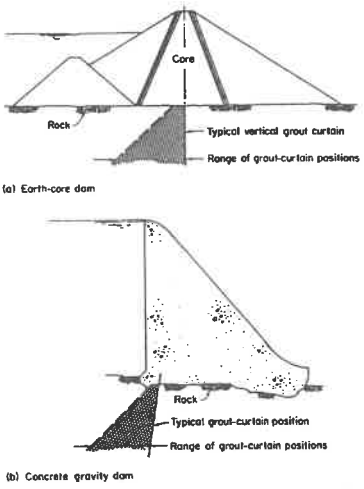

Figure 2.1: Application of grouting in dam rehabilitation and construction (a) Grout curtain under earth dam (b) Grout curtain under concrete dam (after Kosmatka,1990)

In mines, grouting is used to check the flow of water, and strengthening of support. It is also carried out during construction and rehabilitation (e.g. underpinning) of foundations for structures such as multi-storey buildings, launching pads for spacecrafts, airport runways, nuclear reactors, conventional power plants, silos etc.

A promising application of grouting is the containment of hazardous waste from seeping into groundwater. A recent application of grouting in this area was

nominated for the American Society of Civil Engineers' 1996 Outstanding Civil Engineering Achievement. In the $6.8 million project, grouting was used to prevent impounded waste water from seeping into the underlying aquifer. It was also used to fill a sinkhole underneath a disposal area used for storing phosphogypsum (a by-product of the concentration of phosphate manufacturing process that contains acidic water) (Robinson, 1996). Franklin and Dusseault (1989) discusses the areas of investigations in grouting applications in the treatment of repositories for radioactive and toxic waste. These investigations include vault grouting, borehole sealing, buffer packing and backfilling (see Figure 2.2). Under these applications,

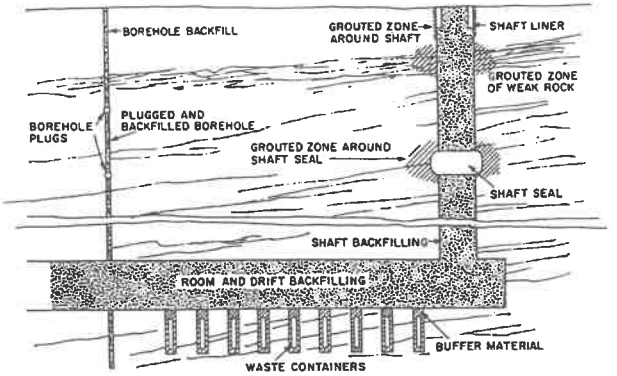

Figure 2.2: Application of grouting in radioactive waste disposal (after Lopez et al., 1984)

grouting is used to seal discontinuities in the rock to ensure complete containment of the waste and protection of the groundwater. The basic requirements for grout for these applications are low hydraulic conductivity, ease of injection and long term erosion and chemical resistance. Leading grouts for this special applications are cement, clay, rock dust and their combinations. Kleinschnittger and Holtgrene (1989) and Pierau (1996) reported the result of experimental grouting at Konrad Mine (a proposed site for radioactive waste repository in Germany). Their result showed that ultrafine cement*(Microdor S)* grout with mix ratio water/cement of 1.5 was able to provide the necessary level of impermeability (below $10^{-14}m^2$) required for the safe operation of the repository.

Another major application of grouting is in tunneling where it is used for one of the followings:

1. Prestress the linings using anchors to reduce the amount of artificial lining.
2. Sealing-off water and strengthening of weak rock ahead of tunnels (Figure 2.3.
3. Repair of blasting damages in rocks surrounding tunnels to enhance stress transmission.

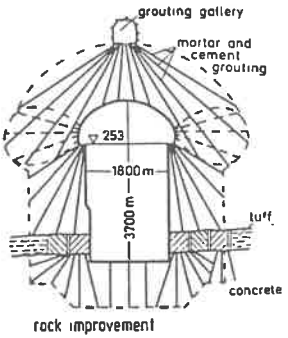

Figure 2.3: Applications of grouting in tunnel construction (after Kutzner and Schetelig, 1985)

In rocky countries such as Finland, underground space are put to permanent use for such facilities as gymnasium, concert hall, power generation plants and cavern for storing crude oil (Saari, 1988). All these facilities require permanent sealing of the discontinuities in the rock by grouting.

In the exploration for water and petroleum, grouting is usually carried out to prevent groundwater contamination and loss of drilling mud. Furthermore in artesian aquifer grouting can be implemented to prevent the loss of artesian pressure.

For completeness, grouting can also be used for rock excavation where disturbance to the rock mass should be minimized. In this application, boreholes are drilled on a pattern (see Figure 2.4) into the rock mass which are grouted with highly expansive cement. On hydration the special cement expands and breaks up the rock mass.

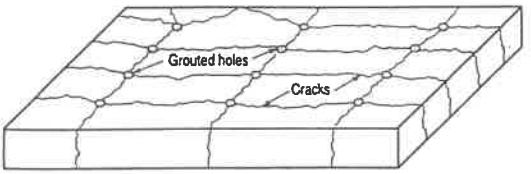

Figure 2.4: Application of grouting in rock excavation (After Kosmatka, 1990)

2.3 Grouting Process

The grouting process begins with its planning. Information required for the planning of a grouting project include:

1. Hydro-geological information.
2. Characteristics (flow, strength and toxicity) of the grout.
3. Available machinery.

The hydro-geological information required are:

1. Location (strike, dip, persistence, position and spacing) of the discontinuities.
2. Size (aperture) of the discontinuities.
3. Strength of the rock mass.
4. Groundwater level.
5. Dissolved chemical in the groundwater.

From the available information on discontinuities, flow property of the grout and equipment, the engineer designs the grouting project by supplying the grouter (the operator of the field equipment) with the following information.

1. The maximum grouting pressure.
2. Mix ratio of the grout.
3. Spacing and orientation of of the grout holes.

2.3.1 Geological Information

The geological information is usually acquired through core drills from boreholes, surface observation of the rock mass and results from water pressure tests. Other methods which have been used for investigating in-situ characteristics of the discontinuity are: borehole television cameras (Figure 2.5) and televiewers, Lau et al., 1987), borehole impression packers (Figure 2.6 (Brown and Boodt, 1987). National Research Council (1996) cataloged methods of acquiring information

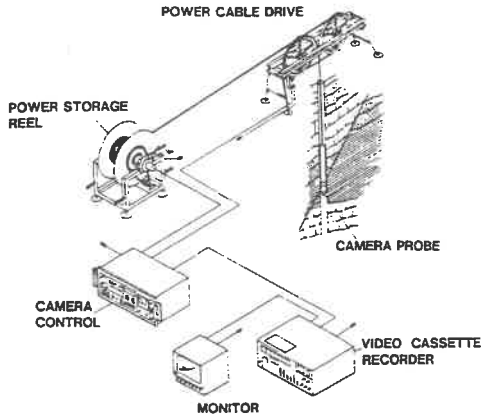

Figure 2.5: Schematic layout of the borehole television survey system (after Lau et al., 1987)

on discontinuities. These methods are grouped under the following categories: differential, elastic, electrical, electromagnetic, radar,conventional well logs, geological observation, tiltmeter and flowmeters. The strength characteristics of the rock mass can be measured in the laboratory using the usual direct and indirect compressive methods — triaxial, biaxial and uniaxial Brazilian methods. On the field, plate bearing test, flat jack test, water loading test are some of the methods commonly used.

2.3.2 Flow Characteristics of Grout

The flow characteristics of grout can be completely specified with its density and the constitutive equation. The constitutive equation (sometimes referred to as flow model) expresses the relationship between the shear stress (τ) and the shear

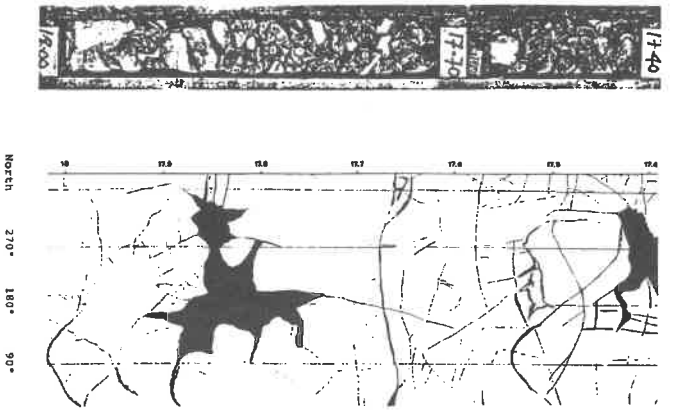

Figure 2.6: Comparison between rock core the tracing of the oriented impression packer obtained from the same length of borehole (after Harper and Hinds, 1977)

strain ($\dot{\gamma}$). In grouting, the shear stress is related to the grouting pressure and the geometry of the flow path while shear strain is a function of the geometry of the flow path, flow rate and molecular structure of the grout.

In the laboratory, the density is measured using measuring cylinder—the mass of a sample is divided by its volume. On the grouting site the *mud balance* is commonly used to measure the specific gravity which can be converted to grout density by multiplying with the density of water.

The use of sediment stable grout in rock grouting project is becoming the standard practice. The constitutive equation of sediment stable grout can be approximated using the Bingham equation (see section 5.1). The Bingham flow model uses two flow parameters— plastic viscosity (μ_p) and yield stress (τ_y) for its characterization. Presently, measurement of flow characteristics of grout on most grouting sites is mainly for assessing the performance of the mixer and for quality control of the grout (Houlsby, 1990). Measurement of flow properties of the grout with the aim of estimating the extent of its propagation is currently being practiced by few grouting consultants and firms.

The most commonly used instrument on grouting site for measuring the flow behavior of grout is the *flow cone*. As pointed out by Houlsby (1990) and Lombardi (1985), there are many varieties of flow cones in use. This has made almost impossible, the comparison of measurements of the flow properties of grout using flow cones. The results of the flow cone test are expressed in the time required for

a given quantity of grout to flow out of the cone. This time is not directly related to physics of flow, it is therefore not possible to obtain the parameters (μ_p and τ_y) of Bingham flow model using flow cone.

Lombardi (1985) is his widely referenced paper presented a chart which correlates the results of a particular flow cone and *plate cohesion meter* (used for measuring dynamic yield stress) with flow parameters of a grout obtained from a laboratory concentric cylinder viscometer. The chart was implicitly based on the assumption that the flow parameters of a Bingham fluid are unique material properties. However, these parameters depend on the rate of shearing. They are therefore not unique material properties. The chart presented by Lombardi is applicable only to his experimental conditions and cannot be generalized. Knoblauch (1987) compared the repeatability and accuracy of instruments— falling-body viscometer, flow cone, flow-channel, concentric-cylinder viscometer— for measuring the flow properties of grouts. He concluded that concentric-cylinder viscometer is best in terms of both accuracy and repeatability. Marsland and Loudon (1963) described a capillary viscometer shown in Figure 2.7 and procedure for obtaining the flow parameter of cement grout from the experimental result. The viscometer

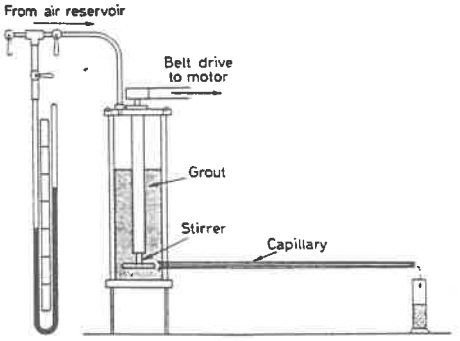

Figure 2.7: Capillary Viscometer for measuring flow parameters of cement suspension (after Marsland and Loudon, 1963)

was specifically constructed for measuring the flow parameter of cement grout.

The concentric and capillary viscometers which can be used to obtain both flow parameters of a Bingham fluid such as cement suspension are very expensive and not suitable for field environment. Other measuring equipment suitable for

site environment have been introduced. The plate cohesion meter (mentioned earlier) was described by Lombardi (1985). It is used for measuring the dynamic yield stress of the grout. The plate cohesion meter is a flat thin steel plate with rough surfaces. The plate is completely submerged in a container of grout and lifted out. According to Lombardi (1985), the thickness of the grout sticking to the plate equals the dynamic yield stress per unit weight.

Håkansson et al. (1992) presented Equation 2.1 for estimating the dynamic yield stress of cement grout from the height to which the grout rises in a cylinder with rough internal walls inserted into a container of grout (Figure 2.8(a)).

$$\tau_y = \frac{\gamma R}{2} \frac{\Delta h}{(h_1 - \Delta h)} \tag{2.1}$$

where h_1 is length of the cylinder submerged, h_2 is the height to which the grout rises in the cylinder, R radius of the cylinder, γ specific weight of the grout and Δh equals $h_1 - h_2$.

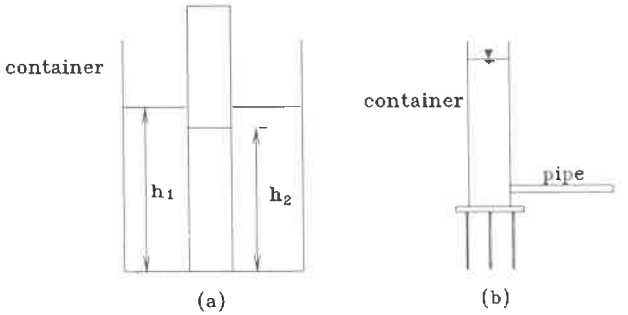

Figure 2.8: (a)Estimating dynamic yield stress (adapted from Håkansson et al., 1992) (b) *The Kasumeter* (after Schulze et al. (1991)

The *Kasumeter* (Figure 2.8(b)) was designed for measuring the dynamic yield stress of cement grout. It was presented by Schulze et al (1991). For a given grout, the height of the suspension in the reservoir cylinder of the kasumeter is correlated to the dynamic yield stress of the suspension.

In recent time, due to the effect of slip at the fluid/solid boundary of conventional viscometers, the shear vane used in testing shear strength of soil has been used to measure yield stress of cement suspension. Haimoni and Hannant,

(1996) compared rheological measurements of cement suspension using a conventional concentric-cylinder viscometer and confirmed the superiority of shear vane in measuring yield stress .

2.3.3 Grouting Equipment

Houlsby (1990), Kutzner (1991) and Müller (1993) provided state of art information on grouting equipment. Typical configuration of grouting equipment is shown in Figure 2.9 and Figure 2.10.

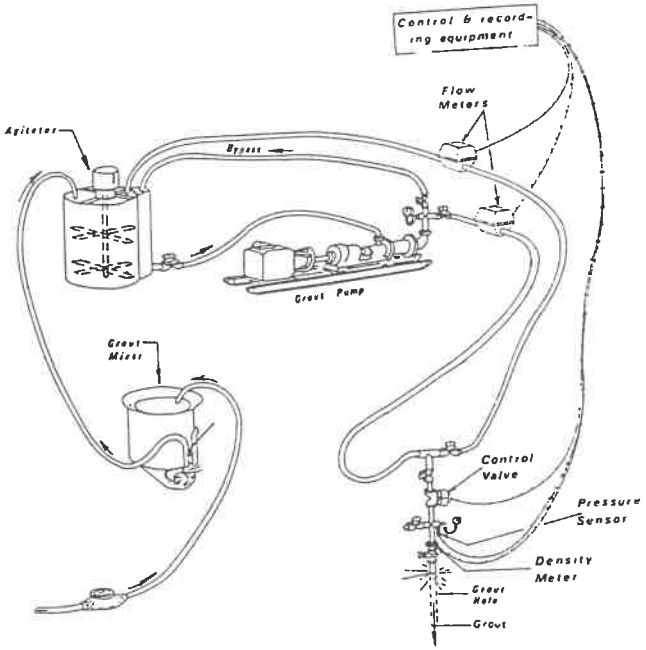

Figure 2.9: Typical configuration of grouting equipment for cement suspension (after Houlsby, 1992)

The batcher (not shown in Figure 2.9) weighs the right proportion of cement and water (and admixture, if used) and pours them into the mixer where they are mixed together. From the mixer, the grout flows to the agitator for storage. The agitator serves as the reservoir from which the the pump pumps the grout into the

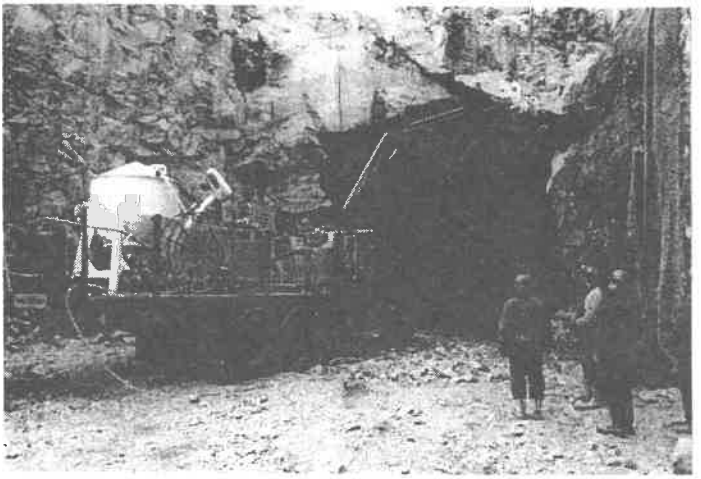

Figure 2.10: A Mobile grouting equipment (courtesy of Häny and CIE Ag.)

grouting circuit. The valves at the standpipe controls the quantity of grout that flows into the grout hole and excess grout flows back into the agitator.

The most important of all the equipment is the mixer. It controls the quality of the grout. The mixer must have the capability to stir the grout vigorously so that maximum hydration and homogeneous mixture are achieved. Example of such mixers are: paddle, continuous, and high-shear mixers (Müller, 1993). The characteristics of the pump influence the grouting pressure and the volume that can be injected within a given time. The pump must be capable of optimum operation irrespective of the consistency of the grout. Examples of pumps employed in grouting are: helical rotor (progressive cavity), centrifugal, piston, ram, and diaphragm pumps (Houlsby, 1990). In this work, because the pressure produced by the pumps will be used in the theoretical analyses, it is important to highlight that oscillatory pressure are produce by piston, ram,diaphragm pumps while helical rotor pumps produce steady pressure. However, Houlsby (1990) discussed methods of obtaining steady or almost steady pressure from pumps producing oscillatory pressures. According to him, installation of air dome on the grout line and the use of several cylinders reduces flow pulsation. The commonest type of valves used in grouting are diaphragm, ball (certain types) and plug cocks valves.

In order to ensure the production of high quality and uniform grout mixes, the trend in grouting plant manufacturing is the automation of the batching—weighing of the cement and water (and admixture when used). An example of such batch plant is discussed by Müller (1993).

Currently, the acquisition of grouting data such as grouting pressure, flow rate of the grout, displacement within the rock masses is automated using sophisticated sensors and computer (ÖDK, 1991; Müller, 1984; ANON, 1983, and ANON, 1984). The acquired data are usually displayed in graphical form so that injection process can be followed. Figure 2.11 shows an example of instrument for real-time acquisition of data during grouting and a typical printout from such equipment.

The state of the art of instrumentation in grouting as described by Kutzner (1991), may have made him, in his review of the history of grouting to predict that, there may not be dramatic development in grouting as it is currently being practiced. Unfortunately, the advancement in instrumentation has not been matched with theoretical development.

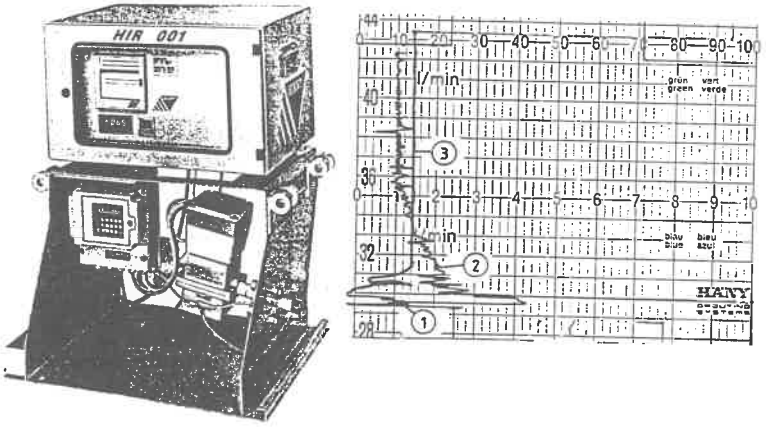

Figure 2.11: (a) Instrument for automatic measurement of flow rate and pressure during grouting (courtesy of Häny and CIE Ag. (b) Typical Print-Out from A Data Acquisition Equipment (after Kutzner, 1991).

2.4 Grouting Methods

The basic method of grouting is called the *split-spaced* grouting. In this method, the first set of holes (primary holes) are drilled , usually between 3 to 12 m

apart, and grouted. Secondary holes are drilled midway between the primary and grouted. Tertiary holes may be drilled and grouted if necessary. The decision on when to stop drilling and grouting is usually made by the engineers as the grouting progresses. This makes it difficult to estimate the quantity of grout required for a particular project. As mentioned in Chapter 1 there is presently no generally agreed method of determining when grouting should stop.

For a particular borehole, grouting methods are classified into the following (USBR, 1987):

1. Stage Grouting. This method is also called successive stage grouting, descending stage grouting (Kosmatka, 1990). It involves: Drilling of the grout hole to a predetermined depth, washing of the grout hole, execution of water pressure test, grouting of the hole and washing out -injected grout from the bore hole. The above procedure is repeated for successive stage until the final depth of the borehole is reached.

2. Stop Grouting, also called packer grouting, upstage grouting(Kosmatka, 1990). In this method, the grout hole is drilled to its full depth. Different sections of the hole, starting from the bottom to the top, are sealed off with packers and grouted after washing and execution of water pressure test.

3. Series Grouting. Series grouting has almost the same procedure as the stage grouting. The only difference is that, instead of washing out of the grout after injection, the grout is allowed to set. Subsequent stages are then drilled through the set grout.

4. Circuit Grouting. This method of grouting employs an out-line in addition to the usual in-line. Grout is pumped into the section being grouted and allowed to circulate out of section if it does not penetrate the discontinuity. This method is usually combined with other methods.

5. Gravity Grouting. This method is usually used to fill cavity in the rock. It involves pumping the grout into the grout hole and allow it to penetrate the discontinuity under the influence of gravity. The grout hole is refilled as necessary.

It is a common practice to begin grouting with a thin mix. The thickness of the grout is then progressively increased at interval until *grout refusal* state is reached. The grout refusal state is defined within the specification for the project and it is reached when a given volume of grout cannot be injected within a given time. For example, the U.S. Corp of Engineers defines grout refusal state as either no grout take at three-fourths of the maximum grout pressure or 28 liters or less of grout take in 10 minutes (USBR, 1987).

A recent alternative grouting process in which stable grout (water/cement < 2.0, by weight) of the same thickness is used for the entire project is presented by Lombardi and Deere (1993). The procedure is based on the *Grout Intensity Number* (GIN) principle. The GIN is the product of total volume of grout injected and grouting pressure. For a particular project, the designer of the project, on the basis of his experience selects a GIN for the project. The criteria for ending injection is when the GIN for the project has been reached. As with other aspects of grouting, there is no theoretical base for the selection of the GIN for a particular project. The GIN principle has been criticized by Ewert (1996) for its emphasis on the properties of the grout at the expense of the geology of the rock mass.

The general trend in rock grouting is the use of stable mixes. The pressure at which grout is injected still remains a subject of controversy. For example, in the US, the rule of the thumb maximum pressure is 22.6 kPa/m thickness of overburden, while it is 100 kPa/m in Europe (Kosmatka, 1990). Furthermore, some practitioners believe grouting should be executed at a pressure lower than the overburden pressure to prevent hydrofracture, others (e.g. Ewert, 1996) have argued that the pressure a rock mass can withstand without failure depends more on its strength than on the overburden pressure. From the GIN principle grouting pressure is expected to increase with depth because the size of the discontinuities decreases with depth. And higher pressure is required to grout fine discontinuities.

2.5 The Physics of Rock Grouting

For a long time, there has been interest in the mathematical analysis of the injection of grout into the ground. The earliest work in this area was done by Kollbrunner (1948). In the work, a set of formulae based on the Newtonian fluid model (Equation 5.2) were given for estimating the extent of propagation of injection material in homogeneous ground. Raffle and Greenwood (1961) extended the work of Kollbrunner to cover flow of Bingham fluids (Equation 5.3) in the soil. Kaiser (1969) subsequently based his work on the flow of cement suspension in the soil on the formulations of Raffle and Greenwood (1961). All these reports were aimed at injection work in the soil and based on the assumption that injection is a steady state process.

The earliest work on the theoretical studies of rock grouting known to the author was done by Jähde (1953). In the work, Jähde divided the injection process of grout into three phases shown in Figure 2.12. The explanation given for the phases are as follows—during the *filling phase*, the rock discontinuities are being filled with grout at almost constant pressure. However, if the borehole is not properly washed before injection or the discontinuities are blocked, a temporary increase in pressure which subsequently disappears may occur. The rate of grout

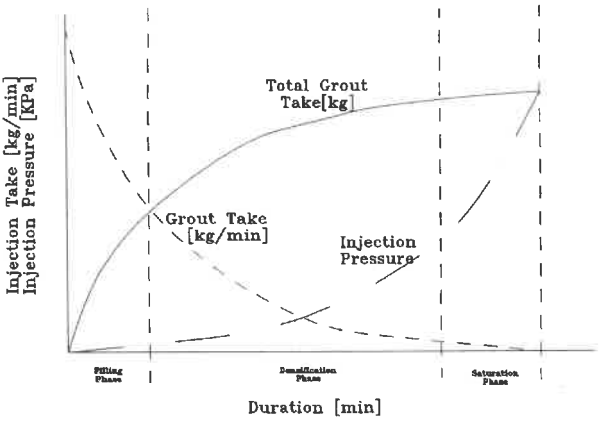

Figure 2.12: Theoretical phases of injection process (after Jähde, 1953)

take is highest at this phase. The *densification phase* is characterized with decreasing rate of grout take, At this phase the injection pump runs at a slower rate. If a injection pressure is high enough to widen the discontinuities or previously blocked discontinuities are opened up, the phase reverts to filling phase. The *saturation phase* involves the consolidation of injected grout. The duration of this phase is short and injection take very low. Kutzner, 1964 confirmed the theoretical phases developed by Jähde in an experiment using a grout with water/cement ratio 6.0. Houlsby (1990), highlighted different deviations from the ideal situation described by Jähde and recommended methods of handling them.

Kennedy, (1958) discussed results of experimental grouting aimed at highlighting factors affecting the propagations of cement grout in rock discontinuities. In the investigation, standard grouting equipment was used to inject horizontal discontinuities with sizes 0.254 mm, 0.508 mm and 0.762 mm. The discontinuities were modeled using shim stock inserted between two reinforced concrete slabs (177.8 mm x 1320.8 mm). In 11 of the total 97 injections the surfaces of the simulated discontinuities were rough while the remaining were smooth surfaces. The grout mixtures used are: (1) neat cement with and without additives, (2) cement and fly ash with and without additives. The mix ratio of water to cementing medium (cement and/or fly-ash) ranged from 0.33 to 4.30 (by weight). The simulated discontinuities were injected at pressures of 172.5 kPa, 345 kPa and 690

kPa. The major conclusions drawn from these extensive tests are as follows:

1. The surface roughness of the discontinuities has tremendous effect on the thickness of the grout that can be injected into the discontinuities, the rougher the surface the higher the water/cement ratio required.

2. The grouting pressure required to inject a given grout is almost independent of the thickness of the grout if the discontinuity is greater than 0.508 mm. For discontinuities with size 0.254 mm, the pressure required for injection depends on the thickness of the mix.

3. The pressure gradient along discontinuities is a straight line only if the discontinuity has sufficient size. In the test, discontinuities with aperture size 0.254 mm were too small and the pressure gradient was non-linear. Furthermore, for discontinuities with 0.245 mm , the pressure loss close to the injection point was very high.

Unfortunately, the surface roughness of the discontinuities in Kennedy's work was not quantified.

Wittke (1968) discusses the problem of investigating the propagation of stable cement grout in rock discontinuities. He pointed out that exact mathematical solution of the propagation (unsteady state problem) of cement suspension(a Bingham fluid) in an irregular conduit such as rock discontinuity cannot be obtained using currently available mathematical tools. He used equilibrium method to estimate the extent of propagation of grout in an idealized discontinuity with smooth and parallel walls. The geometrical layout of the problem and the equation derived by Wittke are shown in Figure 2.13 and Equation 2.2 respectively.

$$R_o(\phi) = \frac{\frac{a}{2\tau_y}(p_{io} - p_{wo}) + r_o}{1 + \frac{a}{2\tau_y}(\gamma_i - \gamma_w) sin\alpha \, cos\phi} \tag{2.2}$$

where

$R_o(\phi)$ = extent of propagation within the discontinuity.
ϕ = angle which the plane of the discontinuity makes with the horizontal.
a = size of the discontinuity
p_{io} = pressure at the center of the grout hole.
p_{wo} = water pressure at the centre of the bore hole.
τ_y = yield stress of the grout.
r_o = radius of the borehole.
α = angle which the discontinuity makes with the horizontal.
ϕ = directional angle on the plane of the discontinuity.
γ_w = unit weight of water.
γ_i = unit weight of grout.

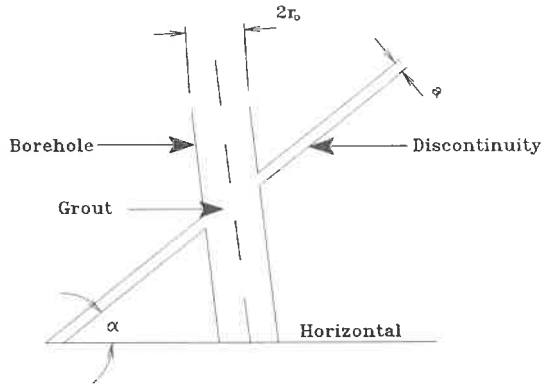

Figure 2.13: Geometry of borehole and discontinuity (adapted from Wittke, 1968)

If the discontinuity is horizontal Equation 2.2 becomes:

$$R_o = \frac{a}{2\tau_y}(p_{io} - p_{wo}) + r_o \tag{2.3}$$

Wittke (1968) injected a grout mix with water/solid content = 0.37 into a simulated discontinuity with aperture size of 2 mm. The solid content of the mix consisted 3% bentonite and 97% cement. The yield stress of grout was measured with concentric cylinder viscometer. It amounted to about 23 Pa. This, however, differs from the yield stress obtained from the graph of pressure difference (Δp) versus extend of propagation(R) as predicted by Equation 2.3. To reconcile the difference, he suggested multiplying the yield stress obtained from the viscometer with a correction factor. Although he did not provide enough details on his experimental measurement of yield stress using concentric viscometer, a reason which could have led to his obtaining a lower yield stress value with the concentric viscometer is — the Haake's SV II measuring system used by him has a smooth surface. It is therefore not suitable for rheological measurement of cement suspension which is known to exhibit slip characteristics. Slip has the effect of reducing rheological parameters, especially yield stress. As discussed in section Chapter 7, yield stress is not a unique material property, measurement of rheological parameters should therefore be subjected to the conditions similar to that being modeled. There is no evidence that this was the case in Wittke's report. A flow measurement using a measuring system with rough surface and which sim-

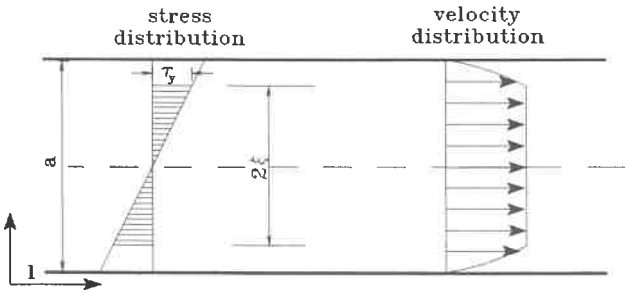

Figure 2.14: Flow of Bingham fluid within parallel wall discontinuity (adapted from Wallner, 1976)

ulates conditions similar to those within the discontinuity would have led to flow parameters similar to those obtained from the simulated discontinuity. There is therefore no need for the correction suggested by Wittke, (1968).

Wallner (1976), modeled the flow behaviour of cement grout using the Bingham equation (see chapter 3). He solved numerically, using finite element method, the non-steady state problem of rock grouting. He made the assumption that the walls of the rock discontinuities are smooth and parallel to each other. In the solution, the non-steady state was approximated using independent time sequence of steady states. The steady state equation of flow for Bingham fluid used by Wallner is shown in Equation 2.4.

$$\overline{v} = \frac{g(a)^2\rho}{12\mu}\frac{dp}{dl}\left(1 - 3\frac{\xi}{a} + 4\left(\frac{\xi}{a}\right)^3\right) \tag{2.4}$$

where ξ is as shown in Figure 2.14. $\overline{v}$ is the average flow velocity, a the size of the discontinuity, p is the pressure and g acceleration due to gravity. Wallner's numerical results were in good agreement with his experimental results obtained from flow in discontinuities simulated using Plexiglas.

Hässler, (1991) using Equation 2.4 analyzed the flow of a Bingham's fluid in a network of one dimensional discontinuities with smooth and parallel walls. He used the network channel method for his analysis. His computational results were in good agreement with experimental results obtained from flow simulations using Plexiglas and the results obtained by Wallner (1976). As evident from the work of Kennedy, (1958) the effect of surface roughness is of utmost importance in the

flow of grout in discontinuities. In addition, on the basis of laboratory studies of discontinuities simulated with Plexiglas Smoltczyk and Akinrogunde (1995) concluded that Plexiglas is not suitable for simulating flow in rock discontinuities because of the difference in the surface morphology of Plexiglas and rock.

There is a recent surge of interest in the theoretical investigation of rock grouting. This is in part due to the prospect of using grouting in the potentially big market of sealing repositories for toxic and radioactive waste and containment of impounded waste water from seeping into the groundwater. Theoretical studies of rock grouting is on the agenda of the Rock Grouting Commission of the International Society of Rock Mechanics (ISRM) (Kuhling and Widmann, 1996 and Widmann, 1994). The US Bureau for Reclamation has also published a review of reported work on theoretical investigations of rock grouting (USBR,1987).

Lombardi (1985) used the equilibrium method to statically analyze the extent of propagation of cement suspension in an idealized horizontal discontinuity with smooth and parallel walls. He arrived at a set of equations (equations 2.5, 2.6), the first of which corresponds to the equation earlier derived by Wittke (1968), which can be used to monitor the trend of grouting.

$$R_o = p_{max}\frac{a}{2\tau_y} \tag{2.5}$$

$$\mathcal{V}_{max} = \pi p_{max}^2 \frac{a^3}{4\tau_y^2} \tag{2.6}$$

$$F_{max} = \pi p_{max}^3 \frac{a^2}{12\tau_y^2} \tag{2.7}$$

where:

R_o	= maximum radius of grout penetration
p_{max}	= maximum applied grouting pressure
a	= size of the discontinuity
τ_y	= yield stress of the grout
$\mathcal{V}_{max}$	= maximum volume of grout injected
F_{max}	= maximum total uplift force

Monitoring of grouting is only possible, using Lombardi's set of equations, if real-time data acquired with the computer are available. Lombardi did not quantify surface roughness in his report. He suggested that the effects of surface roughness can be taken into consideration by reducing the flow parameter (plastic

viscosity (μ_p) and yields stress(τ_y)) in boundary layer of thickness δ by a factor α. Obviously, α will depend on the surface roughness and the flow characteristics of the grout. There was no given guideline for estimating the relationship between surface roughness and the parameter α in his report. In his subsequent published work (Lombardi and Deere (1993)) where his equations were employed, surface roughness of the discontinuity was not mentioned.

Börgesson (1993) and Börgesson and Jönsson (1990), on the basis of the assumption that vibration reduces the viscosity of cement grout and enhances penetration of the grout into the rock discontinuities, analyzed the flow of grout subjected to oscillatory pressure in a single discontinuity with smooth and parallel walls using Equation 2.9 (one dimensional pressure transient flow)

$$\frac{\partial h}{\partial t} + \frac{u_{wav}^2}{gS}\frac{\partial q}{\partial x} = 0 \tag{2.8}$$

$$\frac{1}{gS}\frac{\partial q}{\partial t} + \frac{\partial h}{\partial x} + \frac{\tau_y}{\gamma R_h} = 0 \tag{2.9}$$

where h is the pressure head, q flow rate, S cross sectional area, a_{wav} propagation velocity, g acceleration due to gravity, R_h hydraulic radius and τ_y the yield stress.

Their analytical results were different from the results obtained in the laboratory flow experiment conducted in a discontinuity, simulated using parallel steel plates. They attributed the difference in the results to their inability to model adequately the complex rheological properties of the grout under oscillatory conditions. It is interesting to note that Houlsby (1990) (page 34) claimed that oscillatory pressure hinders penetration of grout into the discontinuities rather enhances it. This type of contradictory claims is very common in grouting.

Recently, Gustafson and Stille (1996) published a report on their work on rock grouting. They incorporated variations in the distance between the walls of the discontinuity using channel network method earlier used by Hässler, 1991. However, within a section of the discontinuity with constant aperture they used the equilibrium approach earlier used by Wittke (1968) and Lombardi (1985). The report essentially highlights the current state of the art in the physics of rock grouting.

All the theoretical work done so far on flow of cement suspension in rock discontinuities has been based on the assumption that the surfaces rock fissures are smooth and parallel. Real rock surfaces are known to be rough and the flow path is known to be tortuous. A better understanding of the flow of cement grout can be gained by comparing results obtained using real rock samples with numerical simulation which take into consideration surface roughness. This approach is used in this current work. Apart from the works cited above no other report on the theoretical treatment of grouting is known to the author.

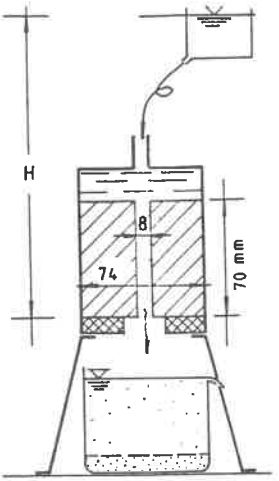

Figure 2.15: Experimental setup for testing erodibility of grouts (after Nonveiller, 1989)

2.6 Effectiveness of Injected Grout

The most widely used method for assessing the sealing effectiveness of injected grout on the site is the water pressure test. It is normally executed usually after 24 hours of grouting. Other methods being tested under research programs include cross hole seismic tomography, grout penetrating radar, electromagenetic induction, neutron probe and downhole temperature logs (Dwyer, 1994). These methods are currently research tools. Nonveiller (1989) described a laboratory test for assessing the resistance of injected grout in partially filled discontinuities against erosion. The experimental setup for the test is shown in Figure 2.15. A hole 8 mm in diameter is drilled at the center of a cylindrical sample prepared from grout material. Water under the desired pressure is passed through the hole for a specified period of time. The difference in the weight of sample before and after the test is taken as measure of the resistance of the grout to erosion. The lower the loss in weight the higher the resistance to erosion. Obviously, this test has limited use in assessing the effectiveness of injected grout because of (1) it does not simulate the bond between the rock surface and the injected grout, (2) the permeability of the injected grout was not considered.

Hooton and Konecny (1990) reported their attempt to investigate the effec-

tiveness of injected grout in the laboratory. They used artificially fractured rock samples. The apparatus they used was unable to provide the triaxial confinement required for the injection of the sample. They subsequently used a discontinuity simulated using Plexiglas and steel. As mentioned earlier Plexiglas and steel are not good materials for simulating rock discontinuities under this type of investigation because of the difference in the surface characteristics of rock and Plexiglas or steel.

The impetus for the development of means of assessing the effectiveness of placed grout is coming from the need to completely contain hazardous waste from polluting the environment. Governments around the world are not satisfied that a barrier (for example grout curtain) against hazardous waste is in place, they want proof that injected grout is performing its intended purpose. They are therefore putting regulations into place to make mandatory, the continuous monitoring of the effectiveness of barrier for containment of hazardous waste.

The US Department for Energy has developed an electronically based system for continuous monitoring of the effectiveness of injected grout. The system which is called *Time Domain Reflectometry with Waveguides* (Figure 2.6) consists of sensors which are located within or adjacent to grout barrier and the

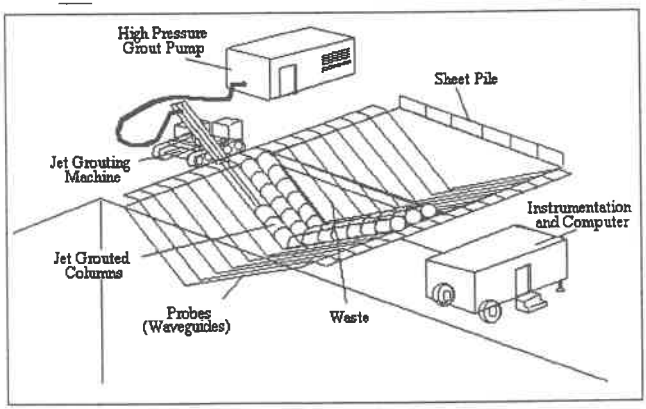

Figure 2.16: Time domain reflectometry with waveguides (after US Department of Energy)

electronic component which analyses the signal from the sensor. The sensor essentially monitors the change in moisture content and the electronic part sends appropriate signal if the change in moisture content is not within the limit allowed (US Department of Energy, 1995). This type of device can also be used in writing project specifications and it is also a means of assuring the client that the placed grout is performing as planned.

Chapter 3

Fluid Flow in Rock Discontinuities and Flow Path Geometry

In most grouting projects, especially in dams and waste disposals, the aim is to create an impermeable barrier to the flow of fluid within the rock discontinuities. To achieve this aim, analysis of the flow of the fluid within rock discontinuity is usually done, both before and after grouting to assess the effectiveness of the injected grout. Flow analysis is possible only with a complete description of the flow path of the fluid within the rock discontinuities. The classical methods of fluid mechanics are widely used for the analysis of fluid flow within rock discontinuities. In this chapter, a general look is taken at the classical mechanics of fluid flow. Problems involved in its direct application to the flow of fluid in rock discontinuities are highlighted. Modifications of the relevant equations of classical fluid mechanics to suit the peculiar case of fluid flow in rock discontinuities and their limitations are discussed. Methods of obtaining information on the geometry of the flow path are also discussed.

3.1 Fluid Flow in Closed Conduit

If electro magnetic, chemical, surface tension and nuclear effects are neglected, kinetic energy, potential energy and pressure energy can account for almost all the energies of a flowing fluid (e.g. water) in a closed conduit (e.g. flow between parallel plates or pipe). The energy per unit mass of a flowing fluid has the unit of length and it is defined as

$$H = \frac{p}{\gamma} + \frac{1}{2}\overline{v}^2 + h \tag{3.1}$$

in which p is the pressure, γ the unit weight of water, $\overline{v}$ the average velocity and h the height about an arbitrary datum.

Figure 3.1 shows the velocity distribution for both *laminar* and *turbulent* flows within a parallel plate, at a section far away from entrance of the conduit. For the

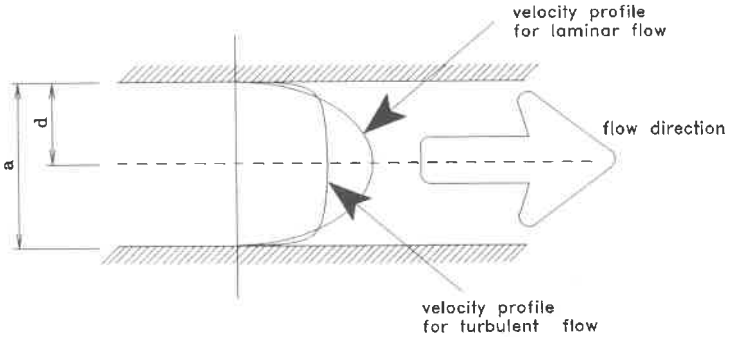

Figure 3.1: Velocity distribution for laminar and turbulent flows

one dimensional flow analysis, the usual practice is to assume that the pressure at a cross-section is uniform. The pressure, however varies along the direction of flow. If different layers of fluid slide over each other without particles moving across layers, the flow is said to be laminar and the parabolic velocity distribution curve shown in Figure 3.1 results. If fluid particles move across layer boundaries *turbulent* flow occurs. The velocity distribution at a cross-section for a turbulent flow is more uniform than that of laminar flow,but the energy loss in turbulent flow is more.

The generalized *Reynolds number*, Re_h, is defined as

$$Re_h = \frac{\rho D_h \overline{v}}{\mu} \tag{3.2}$$

in which D_h, ρ, and μ are *hydraulic diameter* of the conduit, density of the fluid and viscosity of the fluid respectively. $\overline{v}$ is the average flow velocity. The Reynolds number is the ratio of *inertial forces* to *viscous forces* acting on the fluid and it is used to describe the flow condition. For a given flow situation, there is a critical Reynolds number when the flow starts changing from laminar to turbulent. The transition from laminar to turbulent is gradual. Therefore, there exist flow conditions which are neither completely laminar or turbulent.

The concept of hydraulic diameter was developed so that established method of flow analysis in circular pipes can be extended to flow in conduits with any cross-sectional shape. The hydraulic diameter is defined as

$$D_h = \frac{4 \text{ x cross} - \text{sectional area}}{\text{wetted perimeter}} = 4 \text{ x hydraulic radius} \tag{3.3}$$

The *hydraulic radius* for flow between parallel plates equals half the distance between the plates, $a/2$.

The flow rate through a parallel plate for the laminar flow case can be calculated using the well known *cubic flow law*

$$q = \frac{ba^3}{12\mu L}\Delta p \tag{3.4}$$

where

q = flow rate
L= length of the flow channel
b = width of the flow channel
a = distance between plates
Δp = pressure gradient
μ= dynamic viscosity of water.

Huit (1956) and Sharp (1972) referenced Lamb (1957) who stated that Equation 3.4 is approximately valid for

1. Gradual variations in the depth of flow channel, a.
2. Curved channel, provided a is small with respect to the radii of curvature of the channel walls.

The $\overline{v}$ in Equation 3.1 equals

$$\overline{v} = \frac{a^2}{12\mu L}\Delta p \tag{3.5}$$

3.1.1 Major Head Losses

As the fluid flows along the conduit, it looses energy mainly due to :

1. Friction at the walls of the conduit.
2. Internal resistance of the fluid to flow due to its viscosity.

Consequently, the total energy of the fluid at point 1(Figure 3.2) is lower than that at point 2, hence

$$\frac{p_1}{\gamma} + \frac{1}{2g}\bar{v}_1{}^2 + h_1 = \frac{p_2}{\gamma} + \frac{1}{2g}\bar{v}_2{}^2 + h_2 + h_f \tag{3.6}$$

The difference between the energy level as the points 1 and 2 , h_f is called

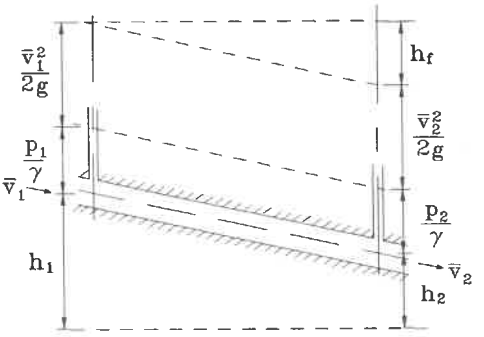

Figure 3.2: Head loss in conduit flow

head loss or *major loss*. Over the years the following facts about major head loss in a close conduit with regular cross section have been established (Hwang and Houghtalen, 1996).

1. It is linearly proportional to the length of the flow conduit.
2. It is independent of pressure driving the flow.
3. It is proportional to some power of the average velocity.
4. The roughness of walls of the conduit has influence only if the flow is turbulent.
5. It is inversely proportional to height of the conduit.

3.1.2 Darcy Friction Factor

A widely used relationship between the head loss, h_f and other flow parameters is the Darcy-Weisbach Equation

$$h_f = f\left(\frac{L}{D_h}\right)\frac{\overline{v}^2}{2g} \tag{3.7}$$

in which f is the *Darcy friction factor*, L the length of the section of the flow channel under consideration and D_h the hydraulic diameter. Equation 3.7 is valid for flow in all types of cross-sections. It is important to point out that some authors (e.g Huit, (1956), Longwell, (1966)) prefer to use the *Fanning friction factor*. The Fanning friction factor is $f_F = f/4$. The friction factor is obtained by balancing forces acting on the fluid within a section of the conduit. The relationship between the friction factor and the other flow parameters for steady laminar flow between parallel plates is

$$f = \frac{24\mu}{\rho V D_h} = \frac{24}{Re_h} \tag{3.8}$$

Equation 3.8 is valid for Newtonian fluid such as water and it shows that the friction factor for laminar flow is independent of the surface roughness of the walls of the conduit. If the Reynolds number, Re_h increases due to flow condition, a critical Reynolds number (for flow between parallel plate, about $Re_h = 2800$ (Longwell, 1966)) is reached at which the flow starts changing from laminar to turbulent. At Reynolds much higher than 2800 the friction factor becomes dependent on the *relative roughness*, e/D_h of the flow channel— e is the arithmetic mean elevation of surface roughness of the wall of the flow channel. In practice, e is not measured directly. It is determined by comparing friction factors at high Reynolds number, when turbulent is guaranteed, with those determined by Nikuradse (1933) (Figure 3.3) for an artificially roughened flow channel for which the roughness has been obtained with sand of known size.

At the wall of the flow conduit, there exists a thin layer of fluid called the *laminar sublayer*. This layer exists even when the flow is turbulent. The thickness of the laminar sublayer, δ, decreases with increasing Reynolds number. If the average roughness of the wall of the flow channel e, is less than the thickness of the laminar sublayer, the roughness of the pipe wall has no effect on the friction factor, f. Under this condition the pipe is said to be *hydraulically smooth*. This does not mean that the walls of the conduit are geometrically smooth. For steady turbulent flow, if $\delta > 1.7e$ the roughness of the walls of the conduit is submerged in the laminar sublayer and the conduit is hydraulically smooth. The relationship between friction factor, f, and Reynolds number, Re_h, for this flow situation is

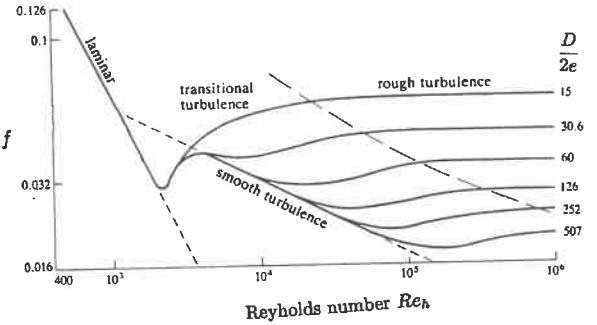

Figure 3.3: Nikuradse's experimental result

given in Equation 3.9. The relationship is based on experimental results and it is attributed to von Karman:

$$\frac{1}{\sqrt{f}} = 2\log\left(\frac{Re_h\sqrt{f}}{2.51}\right) \tag{3.9}$$

If $\delta < 0.08e$ the friction factor, f, becomes independent of the Reynolds number, Re_h, and becomes dependent on the relative roughness of the pipe. The relationship between relative roughness and the friction factor, also based on von Karman's work is

$$\frac{1}{\sqrt{f}} = 2\log\left(\frac{3.7D}{e}\right) \tag{3.10}$$

For the flow situation $0.08e < \delta < 1.7e$, the conduit's behaviour is neither completely smooth nor rough. An approximate relationship for the intermediate range which is called the Colebrook formula is

$$\frac{1}{\sqrt{f}} = -2\log\left(\frac{\frac{e}{D}}{3.7} + \frac{2.51}{R\sqrt{f}}\right) \tag{3.11}$$

The *Moody diagram of friction factors* (Figure 3.4) which is a plot of the above equations has been provided to simplify their application in practice.

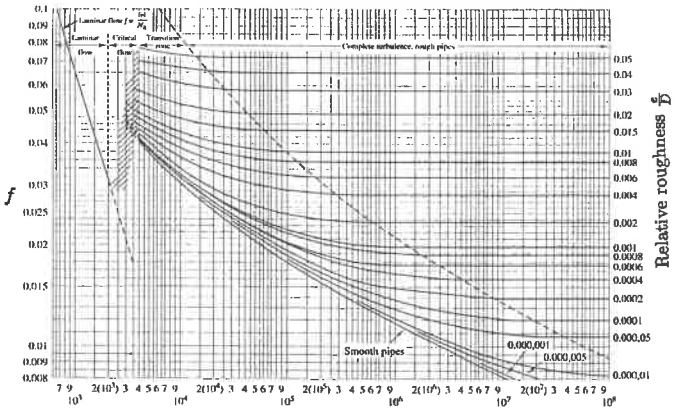

Figure 3.4: Moody plot of friction factor

Churchill (1977), has also published an equation which can be used in place of the Moody diagram. The equation is shown in Equation 3.12

$$f = 8\left[\left(\frac{8}{R}\right) + \frac{1}{(A+B)^{3/2}}\right]^{1/12} \tag{3.12}$$

where

$$A = \left[2.457 \ln \frac{1}{\left(\frac{7}{R}\right)^{0.9} + \frac{0.27e}{D}}\right]^{16}$$

$$B = \left(\frac{37530}{R}\right)^{16}$$

The equation is valid for all flow situations. Here it is noted that there are other empirical formulae for flow analysis in closed conduit. These other methods are not discussed here because their use follow the same general procedure discussed above.

$$h_e = K_e \left(\frac{\bar{v}^2}{2g} \right)$$

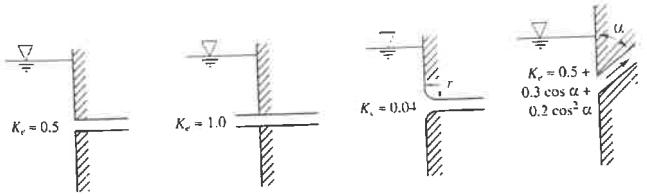

Figure 3.5: Minor losses and their formulas

3.1.3 Minor Head Losses

Losses other than frictional loss also occur as the fluid flows through the conduit. These losses are usually referred to as minor losses. They include

1. Head loss due to contraction.
2. Head loss due to enlargement.
3. Head loss due to bends.
4. Head loss due to fixtures (e.g valves).

The last item is added for completeness. It is not related to subsequent discussion. The formulas for calculating these losses are given in terms of velocity head as shown in figure 3.5.

3.2 Flow of Water in Rock Discontinuities

The basic laws governing the flow of fluids is the same both in man-made conduits or in natural conduits such as rock discontinuities. It is therefore logical that researchers working on flow analysis in rock discontinuities apply directly classical methods of flow analysis discussed above to flow in rock discontinuities. Results from these studies were presented in form of Reynolds number-Friction factor relationships. For example, according to Lious (1967), for the flow of water within rock discontinuities, the relationship between friction factor and Reynolds

number for laminar flow is

$$f = \frac{96}{Re_h}\left[1 + 8.8\left(\frac{e}{D_h}\right)^{1.5}\right] \tag{3.13}$$

whilst

$$\frac{1}{\sqrt{f}} = -2log\frac{\frac{e}{D_h}}{1.9} \tag{3.14}$$

is valid for turbulent flow when $e/D_h > 0.032$. A common feature of earlier studies of the flow of water in rock discontinuities is the idealization that the walls of the discontinuities are parallel. In studies involving laboratory work, non-rock materials were used for the physical simulation of rock discontinuities. For example Baker, (1955) used a discontinuity simulated with cement concrete, Huit (1956) used sand glued to steel plates, Lious (1969) used cement concrete and Rißler, (1977) used Plexiglas with roughened surfaces.

The question that was never addressed until recently is whether the physical models used in these studies actually simulate discontinuities in real rock masses. Reports (Tsang and Tsang, 1989) on recent studies of flow of fluid in rock discontinuities have shown that the physical models used in all the above experiments are over simplifications of the flow of fluid in rock discontinuities. The distance between the walls of a discontinuity is not constant because the walls are not parallel. Furthermore, completely opened discontinuities which these models simulated rarely occur in nature. Sharp and Maini (1972) noted in their work that there is a wide variation in the geometry of natural discontinuities and classified them into three idealized geometries shown in Figure 3.6. They posited that natural discontinuities are probably a combination of the idealized forms. They also asserted that the Reynolds number-Friction factor approach of classical fluid mechanics is not applicable to a flow within rock discontinuities. Their reason was that Reynolds number-friction factor method is valid only for parallel and irrotational flow cases—the ratio e/D_h is very small; and that the flow in rock discontinuities does not exhibit these characteristics.

The following facts about the flow of water in rock discontinuities are widely accepted (Tsang and Tsang, 1987 and National Research Council, 1996):

1. Surface geometry of the rock discontinuity has tremendous influence on flow through rock discontinuities.

2. Flow does not take place in all available voids within the discontinuities—there is flow channelization (see Figure 3.7).

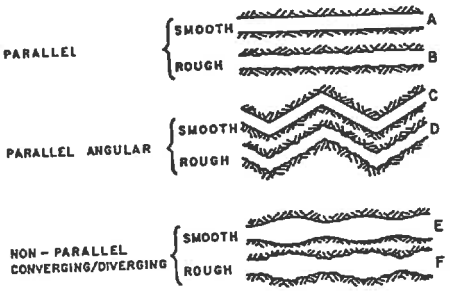

Figure 3.6: Idealized geometry of flow path in rock discontinuities (after Sharp and Maini, 1972)

3. The conventional method of characterizing surface roughness of flow channel in classical fluid mechanics—e/D_h is not adequate for characterizing surface geometry of rock discontinuity which varies widely.

4. The distribution of void within the rock discontinuity alone is not sufficient to describe the flow path. Additional information on interconnection of conduction void is required.

From the above, concentration of flow in preferred channels within a discontinuity in rock masses as observed and reported by Ewert (1985),Abelin et al. (1991) and Bourke (1987) can be attributed to the variation in the distance between the walls of the discontinuities and interconnection of conducting voids(see Figure 3.7).

Figure 3.2 shows a possible geometry of rock discontinuity in nature. In addition to the frictional loss which will occur as fluid flows through the discontinuity, losses due to bend, enlargement and contraction will also occur at points 1,2, 3 respectively. The analysis of flow in this discontinuity, using classical fluid mechanics approach, requires that the locations of points at which losses occur be known in addition to shape of the channel in the plane of the discontinuity . As mentioned

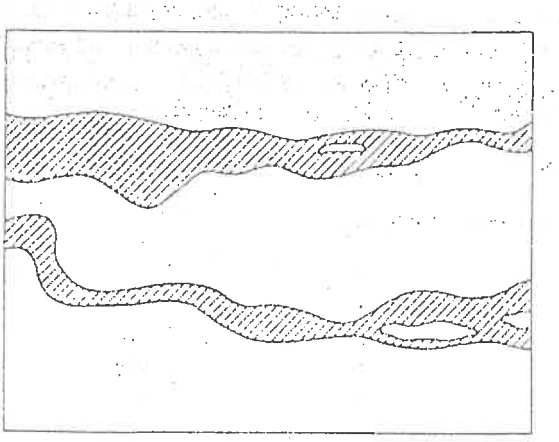

Figure 3.7: Dyestreak showing flow channelization(taken from Neuzil and Tracy, 1981 — attributed to Maini, 1971)

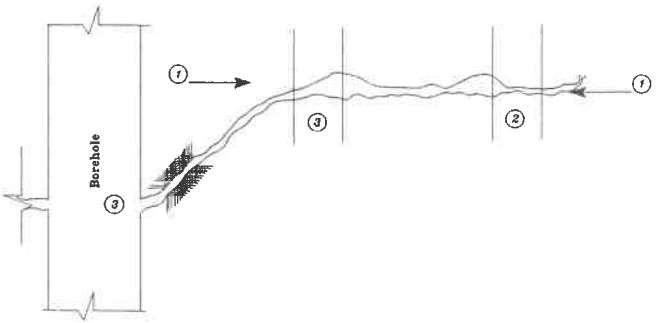

Figure 3.8: Possible geometry of rock in nature

in Chapter 1, it is not presently possible to acquire all geometric information of rock discontinuities using available technology. In addition, the geometry of the flow channel within the plane of the discontinuity is not known. Geometric parameters (e.g. hydraulic diameter) which are easily determined in flow in artificial conduits are not known in rock discontinuity. The variation in surface roughness which can be controlled during manufacturing process of artificial conduit is also not known in rock discontinuities. The lack of information on the geometry of the flow path within the rock discontinuities explains the continuous use of the parallel plate assumption in flow analysis within rock discontinuities; in spite of repeated demonstrations of its invalidity.

3.3 Geometry of Flow Path In Flow within Rock Discontinuities

In this section, methods of obtaining limited information on the geometry of rock discontinuities on the site are discussed. In addition laboratory methods which have been used to acquire geometry information on the sample rock discontinuity are also discussed.

3.3.1 Methods Limited to Exposures

There are different instruments for acquiring the geometry information on rock discontinuity at exposures. These include— automotive feeler gauge, borehole impression packers (Brown and Boodt, 1987) and borehole television cameras and televiewers (Lau et al. 1987) (see section 2.3). The use of these equipment is restricted to limited exposures such as outcrops, tunnels and boreholes. The distance between the walls of the discontinuities measured with the automotive feeler gauge can be used to estimate the mechanical aperture, a_m (Barton et al., 1985).

3.3.2 Water Pressure Test

A widely used method of measuring the distance between walls of a discontinuity both in the laboratory and in the field is the *water pressure test*. In practice, there are two types of water pressure test—the linear flow and the radial flow. The linear flow is restricted to laboratory use while the radial flow is used both in the laboratory and in the field. Figure 3.10 show the two types of water pressure tests. The water pressure test involves the injection of water into the discontinuity at a constant rate. Usually the test is run at different pressures in the sequence– p1, p2, p3, p2, p1. Typical flow rate-curves and their interpretations are given in

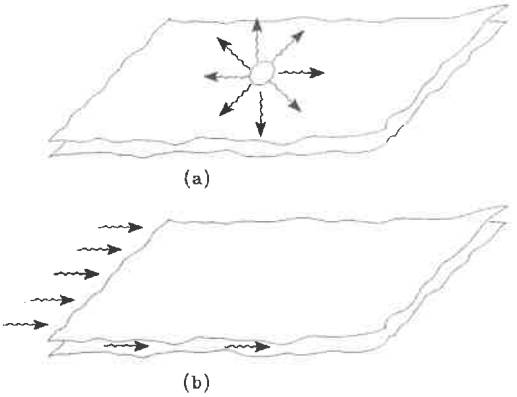

Figure 3.9: Linear and radial flow

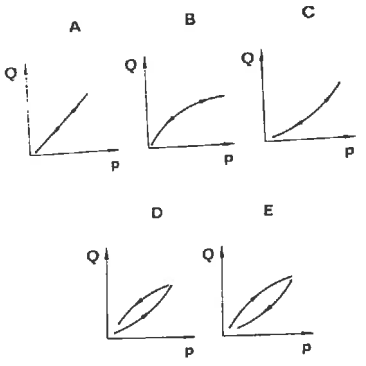

Figure 3.10: Possible results from water pressure test and their interpretations (Q - discharge, p -pressure, A -laminar, B - turbulent, C - elastic deformation, D - cracking or erosion, E - void filling)

Figure 3.10. These interpretations are not universally accepted. The analysis of the water pressure test is usually based on the following assumptions:

1. The distance between the walls of the discontinuity is constant throughout the discontinuity.
2. The flow is laminar
3. The applied pressure does not alter the distance between the walls of the discontinuity.

With the above assumptions, the single valued ***hydraulic aperture***, a is calculated from Equations 3.4 and 3.15[1] for linear and radial flow respectively.

$$a = \left[\frac{6q\mu}{\pi\Delta p}\log\left(\frac{R}{r}\right)\right]^{\frac{1}{3}} \tag{3.15}$$

where

Δp = pressure gradient between r and R
R = radius of influence
r = radius of the borehole

[1]Equation 3.15 is usually applied on the site where an arbitrary value is assigned to R

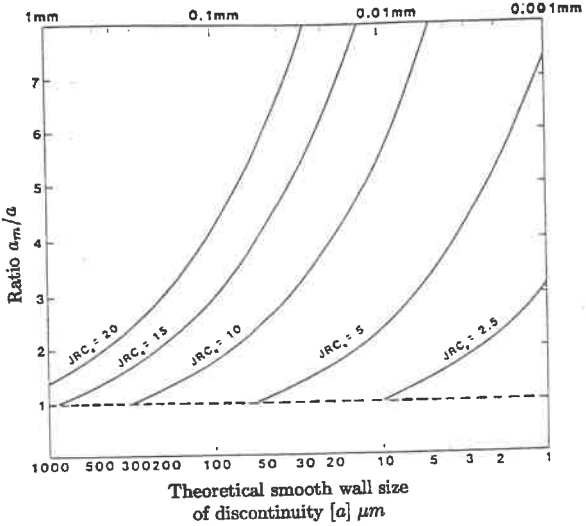

Figure 3.11: Relationship between hydraulic aperture (a) and real mechanical aperture (a_m), (after Barton et al., 1985)

The hydraulic aperture, a is different from mechanical aperture a_m which can be estimated using feeler gauges. Barton et al. (1985) presented a graphical relationship (shown in Figure 3.11) between a_m and a. The major deficiency of this relationship is that the Joint Roughness Coefficient (JRC) on which it is based, is highly subjective parameter (see Section 3.3.4).

There are different modifications to the basic cubic flow law to take account of variation in the distance between the walls of the discontinuity and change in the distance between the walls of the discontinuities due to applied water pressure. For example, Witherspoon et al. (1980) introduced the friction factor f into the cubic flow law to account for the geometric irregularities on the surface of the walls of the discontinuity. Equation 3.4 then becomes

$$q = \frac{1}{f}\frac{a^3}{12\mu L}\Delta p \tag{3.16}$$

Equation 3.16 is valid only for completely open discontinuity
(National Research Council, 1996). A major deficiency of this modification is the possibility of finding completely open discontinuity in nature to which the formula is applicable.

Walsh (1981) derived an analytical expression based on the analogy between the flow of water in rock discontinuities and the flow of heat in a conductor with

holes. On the assumption that the surface geometry of the walls of the discontinuities are randomly distributed, he expressed the dependency of conductivity on confining stress, σ_0 and pressure of water within the discontinuity, σ_w as:

$$\frac{< k >}{< k_0 >} = \left[1 - \sqrt{2}\left(e_{rms}/\frac{a_0}{2}\right) \ln \frac{\sigma_0}{\sigma_p}\right]^3 \left[\frac{(1 - \eta(\sigma_0 - \sigma_w)}{1 + \eta(\sigma_0 - \sigma_w)}\right] \tag{3.17}$$

where

$$< k >= \frac{1 - c}{1 + c} \frac{a^3}{12\mu}$$

and

$$\eta = \sqrt{\frac{\frac{3l_a}{e_{rms}}}{E(1 - \upsilon^2)}}$$

k_0 and a_0 are respectively hydraulic conductivity and local distance between the walls of the discontinuity at some reference stress σ_p. c is the ratio of contact area to total surface are of the continuity; e_{rms} is the root mean square values of the height distribution of the surface. l_a is the auto-correlation distance, E and υ are Young's modulus and Poisson's ratio respectively. Walsh's relationship was based on the assumption that the surface geometry of the discontinuity is normally distributed. This assumption is yet to be confirmed.

3.3.3 Void Geometry

In recent years, research efforts have been directed at obtaining information on *void geometry*— the variation in the distance between the walls of the discontinuities. The methods commonly used to obtain the void geometry within the discontinuity can be classified into the following:

1. Method based on measurement of surface geometry of the two walls of the discontinuity.
2. Methods based on casting replica of the void geometry.
3. Direct Measurement.

The different methods of describing the geometry of the surfaces or rock discontinuity are discussed in section 3.3.4. A commonly used method of calculating void geometry from the surface geometry of the two walls of the discontinuity is

$$a_c(x, y) = a_1(x, y) + a_2(x, y) \tag{3.18}$$

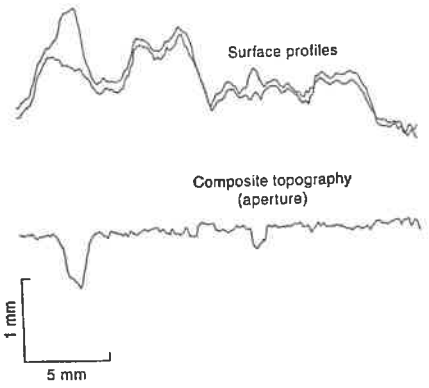

Figure 3.12: Composite topography of surfaces of a rock discontinuity

where $a_c(x, y)$ *composite topography* and $a_1(x, y)$ and $a_2(x, y)$ are heights of the surfaces of the discontinuity above their mean surfaces. This method is shown graphically in Figure 3.3.3.

Gale (1987) investigated the aperture variation within a natural discontinuity by measuring the thickness of the resin injected into the discontinuity. Hakami and Barton (1990) cast transparent replica of two sides of a discontinuity. They measured the aperture at grid points within the discontinuity by injecting a known volume of water into the discontinuity. The size of the aperture was calculated from the volume of water injected and the area covered by the water. Piggott and Elsworth (1993) measured the aperture variation within a natural discontinuity of size 320 mm x 190 mm. Twenty sampling points were drilled into the discontinuity for sampling pressure and electric voltage. On the assumption that the pressure and voltage variation within the discontinuity depend on the aperture, they calculated the distribution of the aperture from the head and voltage measured using the simultaneous inversion method. Keller et al. (1995) used the high technology of Computed Tomography (CT) X-ray to measure the aperture variation within a discontinuity and got the void geometry distribution shown in Figure 3.13 . Gale (1987) is an example of the method based on casting replica of the void geometry while Piggott and Elsworth (1993) and Keller et al. (1995) are examples of direct measurement of the void geometry.

Hakami and Barton (1990), Gale (1987) and Gentier as referenced in Tsang and Tsang (1989) reported a log-normal distribution from their measurement of void geometry in the laboratory. Some workers, for example, Neuzil and Tracy (1981), Brown (1987) and Tsang and Tsang (1989) have incorporated the variation of the void geometry within the rock discontinuity into their modeling of the flow of groundwater in rock masses— they applied the cubic flow law on the mi-

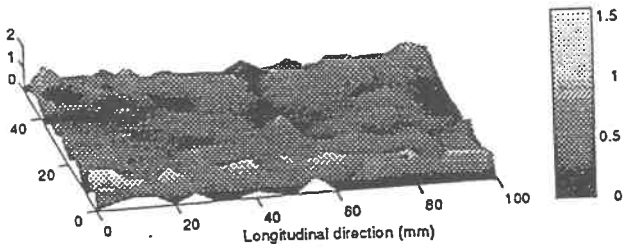

Figure 3.13: Void geometry obtained with CT scan (after Keller et al. 1995)

croscopic scale by dividing the discontinuity into segments; the distance between the walls of the discontinuities within the segments is assumed constant and the cubic law is then valid locally only.

3.3.4 Description of Surface Roughness

The commonest method of characterizing surface roughness in rock mechanics was developed by Barton and Choubey (1977). The method involves the determination of *Joint Roughness Coefficient* (JRC) using either tilt or push test or by visual comparison of the surface profile with a set of standard profiles (Figure 3.14 of known JRC). This method is not used in this work because it is highly subjective. The current trend in research on rock surface roughness characterization is the direct measurement of the topography of the surface (see Brown and Scholz, (1985), Huang et al. (1992) and Odling, (1994)). This method was originally developed in metallurgy for characterizing surface roughness of machined metal surfaces. It involves obtaining profiles along a line on the surface using mechanical or optical profilometers. The roughness of machined surface is expected to be relatively smooth in comparison with that of rocks. Consequently equipment used for characterizing metal surfaces have to be modified for rock surface. Such equipment modification have been carried out by Keller and Bonner (1985) and Poon et al. (1992). Aydan et al. (1996) have gone further to design a portable profilometer for field use.

A summary of the commonly used parameters in characterizing surface roughness was described in Aydan et al. (1996). These parameters are given in Table 3.3.4 where:

$L = L_p + Ln$ = total length of the sample,

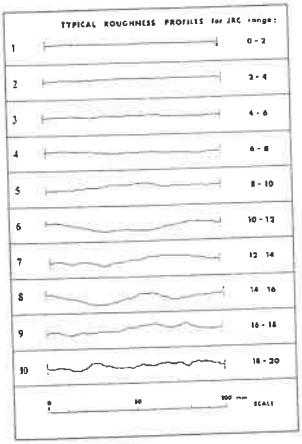

Figure 3.14: JRC table (after ISRM)

$L_{\overline{y}}$= total length where profile height is negative (below reference baseline),
$L_{\overline{n}}$= total length where profile height is positive (above reference baseline),
l = distance from the origin, and
e = height of the profile from the reference baseline.

The parameters are usually calculated for a surface on the assumption that the surface roughness is isotropic. Aydan et al. 1996 demonstrated that roughness of rock surface is anisotropic and used Equation 3.19 to calculate the surface parameter from two perpendicular profiles. One of the profiles is along the ridge axis.

$$F(\theta) = a_1 cos\theta + a_2 cos^2\theta + b_1 sin\theta + b_2 sin^2\theta \tag{3.19}$$

where $F(\theta)$ is the parameter of profile along angle θ and

$$a_1 = \frac{F(0) - F(180)}{2},\ a_2 = \frac{F(0) + F(180)}{2}$$
$$b_1 = \frac{F(90) - F(270)}{2},\ b_2 = \frac{F(900) + F(270)}{2}$$

A common deficiency of all parameters in the Table 3.3.4 with the exception of fractal dimension is that they all depend on the scale of measurement. This means that measurement of the same surface roughness using equipment with different

Center Line Average Height	$\frac{1}{L}\int_0^L \lvert e \rvert dl$
Mean standard Variation of Height	$\frac{1}{L}\int_0^L e^2 dl$
Root Mean Square of Height	$\left[\frac{1}{L}\int_0^L e^2 dl\right]^{\frac{1}{2}}$
Ratio of Profile Length	$\frac{1}{L}\int_0^L \left(1+\frac{de}{dl}\right)^{\frac{1}{2}} dl$
Weighted Asperity Inclination	$\tan^{-1}\left(\frac{1}{L}\int_0^L \left\lvert\frac{de}{dl}\right\rvert dl\right)$
Weighted Asperity Inclination Difference	$\tan^{-1}(\frac{1}{L_p}\int_0^{L_p} \left\lvert\frac{de}{dl}\right\rvert_p dl$ $-\frac{1}{L_n}\int_0^{L_n} \left\lvert\frac{de}{dl}\right\rvert_n dl)$
Mean Standard Variation of Inclination	$\frac{1}{L}\int_0^L \left(\frac{de}{dl}\right)^2 dl$
Root Mean Square of Inclination	$\left[\frac{1}{L}\int_0^L \left(\frac{de}{dl}\right)^2 dl\right]^{\frac{1}{2}}$
Autocorrelation Function	$\frac{1}{L}\int_0^L e(l)e(l+k)dl$
Structure Function (SF)	$\frac{1}{L}\int_0^L (e(l)-e(l+k))^2 dl$
Fractal Dimension	see 3.3.5

Table 3.1: Common parameters for characterizing surface geometry (after (Aydan et al. 1996)

resolutions leads to different values of the same parameters. A relatively new method of surface roughness characterization is based on the fractal geometry. The fractal geometry approach incorporates scaling into its scheme. Theoretically, the fractal dimension is independent of the scale of measurement.

3.3.5 Fractal Geometry

With respect to surface roughness characterization, a fractal can be defined as geometrical shape which maintains statistical similarity irrespective of the scale of observation. There are two commonly used fractal models—the self-similar and self-affine. A self-similar fractal appears similar in all scales when uniformly scaled in all directions and the fractal dimension is sufficient to characterize it. A self-affine on the other hand, has to be scaled differently in two directions for self-similarity condition to be maintained. Consequently, for self-affine fractals there exits a critical scale of measurement below which the surface appears essentially smooth; roughness information can only be obtained above critical scale. This critical scale is called the *crossover length*. Power and Tullis (1991) provided two definitions of the crossover length. The first due to Wong defines the crossover

length as the length, l_c, along the profile which is equal to the root mean square value of the profile within it(see equation 3.20). The second definition due to Mandelbrot is defined in equation 3.21.

$$l_c = l = \sigma_e = \left[\frac{1}{l}\int_0^l (e - E\{e\})^2 dl\right]^{\frac{1}{2}} \tag{3.20}$$

where l is the distance along the profile, σ_e is the root mean square of profile within length, l, e is the height and $E\{e\}$ is the average or expected value of e.

$$\frac{E\{|e(l+b) - e(l)|\}}{b} = 1 \tag{3.21}$$

It is important to measure surface roughness at a scale above the critical length. According to Poon et al. (1992) roughness of rock surfaces are better modeled using the self-affine fractal. There are different methods of obtaining the fractal dimension from the surface profile. Available methods of fractal analysis are: divider method and spectral analysis (Power and Tullis, (1991)) variogram method (Wang and Narasimhan, (1988)), Box Method (Roach and Fowler, (1993)), patchwork method (Brown et al. (1993)). As an example, the divider method is described below.

For a given roughness profile, the divider method can be visualized as follows: Set a divider to length r and walk it along the profile from one end to the other. The total length $L(r)$ of the profile is given by equation 3.22

$$L(r) = Nr \tag{3.22}$$

in which N is the count of walk step, r, which spans the profile. Repeat the measurement with different values of r. The fractal model for characterizing profiles is given by equation 3.23 below

$$L(r) = Ar^{1-\mathcal{D}} \tag{3.23}$$

where A is a constant and $\mathcal{D}$ is the fractal dimension. A comparison of equations 3.23 and 3.22 shows that $N = A/r^{\mathcal{D}}$. A plot of $\log L(r)$ against $\log(r)$ leads to a straight line. The fractal dimension is obtained from the slope of the plot which is equal to $(1 - \mathcal{D})$ and A is obtained from the intercept of the graph. Both A and $\mathcal{D}$ characterize completely the profile— $\mathcal{D}$, the fractal dimension describes the change of roughness with scale of observation and A quantifies the steepness of the topography or total profile variance.

Obviously, the methods of direct measurement of aperture discussed above are feasible only in the laboratory. Moreover, from the work of Iwai (1976) and Barton and Choubey (1977) the aperture measured in the laboratory using small

samples depends on the applied load and loading history. The basic philosophy underlying the current research is the use of methods which can be easily adapted to the field environment. In next the chapter, a new approach of characterizing rock discontinuities using water pressure test will be discussed. The characterization method developed is suitable for the subsequent analysis of the flow of grout in rock discontinuities.

Chapter 4

A new Method of Analysis of Fluid Flow in Rock Discontinuities

The injection of fluid into the rock discontinuity during water pressure test is an unsteady state problem. The solution to this type of problem involves finding the distribution of pressure and velocity within the flow boundaries at all times. For the development of the required relationship between pressure and velocity as a function of time, the fundamental equations of state[1] are combined with the constitutive equation of fluid. In this chapter, the general equations required for the analysis of fluid flow in rock discontinuities are developed. A particular form of the developed equation for water is derived.

4.1 Equations of Change

The analysis of all fluid flow problems is based on the following fundamental physical laws:

1. Law of conservation of mass
2. Law of conservation of momentum
3. Law of conservation of energy

These laws lead directly to the *Navier-Stokes equations*. A detailed discussion of the general Navier-Stokes equations and their derivation can be found in Anderson (1995). The Navier-Stokes equations are systems of nonlinear partial differential equations and hence are difficult to solve analytically. Analytical solutions exist only for a small number of flow problems within simple geometries. At present no general closed-form solution exists. Application of the Navier-Stokes equations

[1] Also called balance equations or conservation equations

to a flow within irregular boundary which is not stationary and not clearly defined, is very difficult. Consequently, conservative laws are directly applied to the flow of fluid in the rock discontinuity to obtain simplified equations of change.

In developing the equations of change the following assumptions are made:

1. The surfaces of the discontinuities are rough.
2. The density of the fluid is constant.
3. The flow is one dimensional.
4. The change in the average cross sectional S_s is a function of pressure alone.
5. The average velocity of flow is low enough for convective term and quadratic or second order terms to be negligible.
6. The gradient of the average cross-sectional area through which flow takes place is small.
7. Injection is an isothermal process, hence energy equation will not be considered.

Assumption 6 is an adaptation of the basic assumption in the lubrication approximation. It implies that the local flow can be approximated by uniform flow between parallel plates separated by the local distance between the walls of the discontinuity (see Pearson, 1994).

4.2 Model of the Geometry of the Flow Path

The description of the geometry of the flow path is a basic pre-requisite in all flow analyses. Unfortunately, the flow path within rock discontinuities is tortuous and is not easily described using analytical methods. A commonly used model of the geometry of the flow path in rock discontinuities is based on the comparison between Darcy's equation and the cubic flow law discussed in Chapter 3. This approach is discussed in subsequent paragraphs.

The one dimensional Darcy's equation is

$$\overline{v} = \frac{k}{\mu}\frac{\Delta p}{L} \tag{4.1}$$

in which $\overline{v}$ is the average superficial velocity, k the intrinsic permeability, μ the dynamic viscosity of the fluid and Δp the pressure difference between length L. From equation 3.5 in Chapter 3, the cubic flow law is

$$\overline{v} = \frac{a^2}{12\mu L}\Delta p$$

Comparison of equations 4.1 and 3.5 yields

$$k = \frac{a^2}{12}$$

k is the permeability of the porous media which is hydraulically equivalent to the discontinuity, provided that the conditions for the validity of Darcy's equations are met. According to Alvarado and Marsden (1979), the Dupuit-Forchheimer assumption is

$$\overline{v}_p = \frac{v}{\eta_p}$$

in which $\overline{v}_p$ is the average pore flow velocity and η_p is the porosity. Substitution of $\overline{v}_p$ in equation 4.1 yields

$$v_p = \frac{k}{\mu} \frac{\Delta p}{L \eta_p} \tag{4.2}$$

The permeability, k in above equations is used to hydraulically characterize the discontinuity.

As pointed out in Chapter 3, the cubic flow law is not valid for flow within rock discontinuities. Furthermore, the validity of Darcy's equation for flow conditions in water pressure test is doubtful— the pressure range ($> 10^5 N/m^2$) commonly used in water pressure test is sufficient to cause considerable deformation of the rock mass. This deformation was not built into Darcy's equation. On the basis of the above elucidated points, the description of flow geometry of rock discontinuity based on the Darcy's equation is not used in this work. In what follows the averaging approach on which subsequent developments are based is explained.

4.2.1 Averaging Process

The geometry of the flow path within the rock discontinuity is not regular. Two scales of irregularities can be identified—the waviness and the surface roughness. In figure 4.1 the local distance between the walls of the discontinuity is

$$a(l, y) = a_w(l, y) + \alpha_1(l, y) + \alpha_2(l, y) \tag{4.3}$$

where a_w is the distance between the two wavy surfaces of the discontinuity and α_1 and α_3 are the roughness heights above the wavy surfaces respectively. An alternative description of the distance between the walls of the discontinuity as discussed in section 3.3.3 is equation 3.18. The latter description is used in this work.

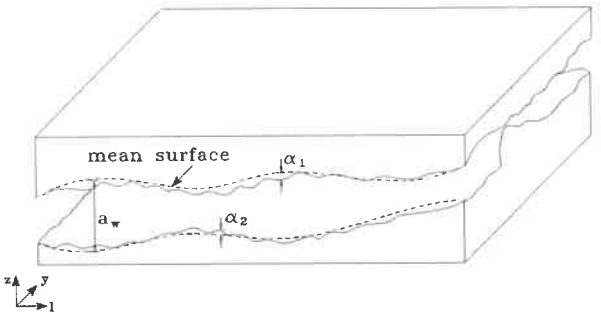

Figure 4.1: Surface geometry of rock discontinuity

Let <> denotes an averaging process within the conduction voids. The average distance between the two walls of the discontinuity within a conducting void i at a cross section is

$$< a_i >= \frac{1}{n} \sum_{j=1}^{n} a_c(l, y)|_{l=constant} \tag{4.4}$$

where n is the number of measured values of $a(l, y)|_{l=constant}$ within the conducting void at that section (see Figure 4.2.1). The cross sectional area, S_i, of a conducting void at a section is

$$S_i = b_i < a_i >$$

where b_i is the width of the conducting void. The average velocity of the fluid within area S_i in the direction of flow is

$$< u_i >= \frac{1}{S_i} \int u dS$$

If m is the number of conducting channels at a section, then the average distance between the walls of the discontinuity within conducting voids at a section is

$$< a_s >= \frac{1}{m} \sum_{i=1}^{m} < a_i > \tag{4.5}$$

and the average conducting area at a section is

$$< S_s >= \frac{1}{m} \sum_{i=1}^{m} S_i \tag{4.6}$$

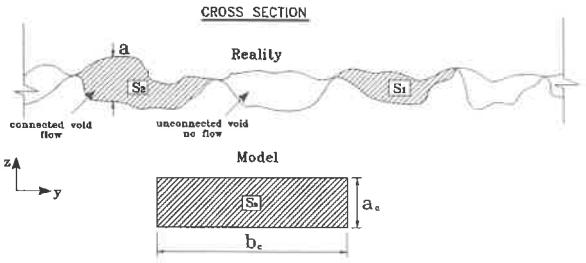

Figure 4.2: Void geometric description at a section for linear flow

It is assumed that the average width of the cross section, b_s, defined as $b_s = S_s/a_s$ is constant. The average velocity at a cross-section is

$$< u_s >= \frac{1}{m}\sum_{i=1}^{m} u_i \tag{4.7}$$

The averaging process is assumed to satisfy the following rules:

$$\left\langle \frac{\partial f}{\partial t} \right\rangle = \frac{\partial}{\partial t} < f > \tag{4.8}$$

$$\left\langle \frac{\partial f}{\partial l} \right\rangle = \frac{\partial}{\partial l} < f > \tag{4.9}$$

$$\tag{4.10}$$

where $u_s(l,t)$ and $a_s(l,t)$ can replace the arbitrary function f. The averaging sign <> will be left out in subsequent development to simplify notation.

4.2.2 The Control Volume Approach

The *control volume* approach to flow analysis is used for developing the basic flow equations. The control volume concept is based on the application of laws of

conservation of mass, momentum and energy to the interaction between a system and its surroundings. With respect to fluid flow, a system is an arbitrary volume of fluid occupying a control volume at an instant of time. The control volume is bounded by the *control surface*. All other things outside the control volume are called the *surroundings* of the system.

According to the *Reynolds transport theorem*, if dA is an infinitesimal area of the control surface, $d\mathcal{V}$ the volumetric element of the control volume, ρ the density of the fluid, $\mathbf{V}$ the velocity vector of flow and η the quantity of a property N of the fluid (mass momentum and energy) per unit mass within the control volume, then

$$\frac{dN}{dt} = \frac{\partial}{\partial t}\left(\int_{cv} \eta\rho d\mathcal{V}\right) + \left(\int_{cs} \eta\rho \mathbf{V}\cdot\mathbf{n}dA\right)_{out} - \left(\int_{cs} \eta\rho \mathbf{V}\cdot\mathbf{n}dA\right)_{in}$$

where $\mathbf{n}$ is the unit vector perpendicular to the infinitesimal element dA of the control surface. The first, second and third terms on the right hand side of Equation 4.2.2 are respectively:

1. The rate of change of N within the control volume
2. The flux of N out of the control surface
3. The flux of N into the control surface

The last two terms can be combined into a single term which represents the net flux, hence Equation 4.2.2 can also be written as

$$\frac{dN}{dt} = \frac{\partial}{\partial t}\left(\int_{cv} \eta\rho d\mathcal{V}\right) + \int_{cs} \eta\rho \mathbf{V}\cdot\mathbf{n}dA \tag{4.11}$$

4.2.3 Mass Balance Equation

The law of conservation of mass states that the mass of a system remains constant with respect to time. If m is the mass of the fluid within the control volume at an instant of time, then $N = m$ and $\eta = 1$ in Equation 4.11. Application of the law of conservation of mass to Equation 4.11 leads to

$$\frac{dm}{dt} = 0 = \frac{\partial}{\partial t}\left(\int_{cv} \rho d\mathcal{V}\right) + \int_{cs} \rho \mathbf{V}\cdot\mathbf{n}dA \tag{4.12}$$

For the one dimensional flow situation (assumption 3) $\mathbf{V} = u$ and $\mathbf{n}$ is along the direction of flow. Here, u is the average flow velocity in the direction of flow. Imposition of the one dimensional flow condition on Equation 4.12 yields

$$\boxed{\frac{\partial}{\partial t}\int_{cv} \rho d\mathcal{V} + \int_{cs} \rho u dA = 0} \tag{4.13}$$

From assumption 2, the density ρ = constant so that Equation 4.13 becomes

$$\frac{\partial}{\partial t}\int_{cv} d\mathcal{V} + \int_{cs} udA = 0 \tag{4.14}$$

For the control volume within a rock discontinuity shown in Figure 4.3 the cross sectional area, S_s, at a point along the flow direction, before the injection of fluid is given in Equation 4.5. The first term of equation 4.14 can be written as

$$\frac{\partial}{\partial t}\int_{cv} d\mathcal{V} = \frac{\partial}{\partial t}\left[\frac{1}{2}\left(S_s + (S_s + \frac{\partial S_s}{\partial l}\delta l)\right)\delta l\right] \tag{4.15}$$

From assumption 6 $\frac{\partial S_s}{\partial l}$ is small, therefore $\frac{\partial S_s}{\partial l}\delta l \delta l$ is small of the second order, hence the last term of the above equation can be neglected. Equation 4.15 then becomes

$$\frac{\partial}{\partial t}\int_{cv} d\mathcal{V} = \underbrace{\frac{\partial S_s}{\partial t}\delta l}_{\text{change in volume due to pressure}} \tag{4.16}$$

The second term of Equation 4.14 can be written as

$$\int udA = \underbrace{-u_s S_s}_{\substack{\text{inflow through}\\ \text{discontinuity}}} + \underbrace{(u_s S_s + \frac{\partial}{\partial l}(u_s S_s)\delta l)}_{\text{outflow through discontinuity}} + \underbrace{\chi p S_s \delta l}_{\substack{\text{outflow through}\\ \text{rock mass}}} \tag{4.17}$$

where χ is the outflow per unit volume per unit pressure into the rock mass.

Substitution of equations 4.16 and 4.17 in equation 4.13 with simplification yields

$$\frac{\partial S_s}{\partial t} + \chi p S_s + S_s\frac{\partial u_s}{\partial l} + u_s\frac{\partial S_s}{\partial l} = 0 \tag{4.18}$$

Equation 4.18 is the expression of the law of conservation of mass. From assumption 4

$$\frac{\partial S_s}{\partial t} = \frac{dS_s}{dp}\frac{\partial p}{\partial t} \tag{4.19}$$

Substitution of Equation 4.19 in Equation 4.18 yields

$$\frac{1}{S_s}\frac{dS_s}{dp}\frac{\partial p}{\partial t} + \chi p + \frac{\partial u_s}{\partial l} + \frac{u}{S_s}\frac{\partial S_s}{\partial l} = 0 \tag{4.20}$$

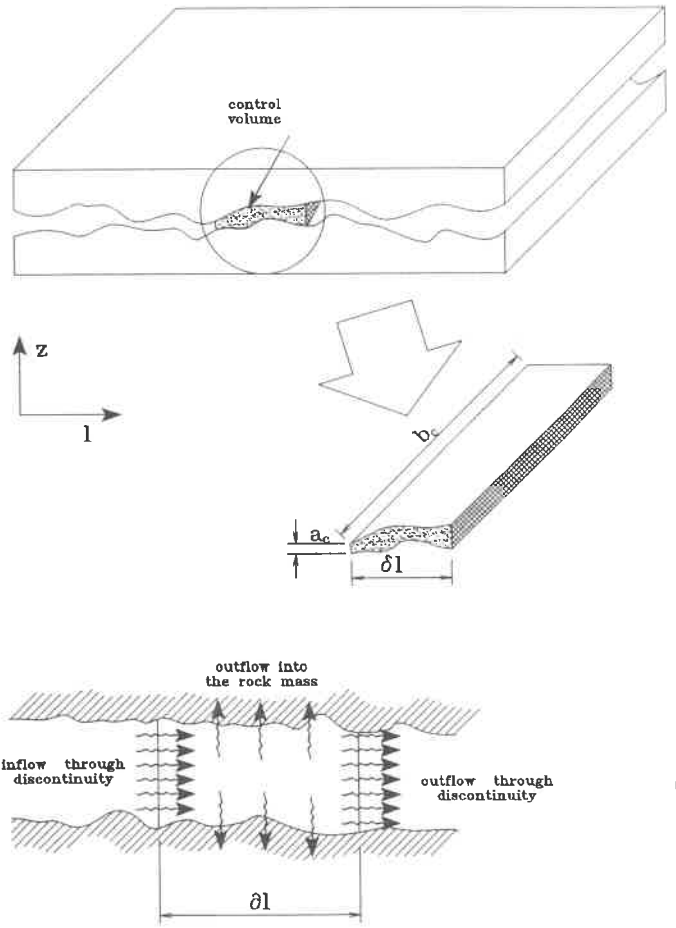

Figure 4.3: Law of conservation of mass— control volume

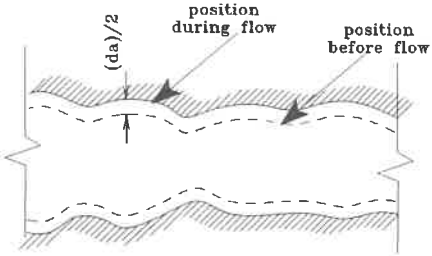

Figure 4.4: Section through a conducting discontinuity

Applying assumption 5 to Equation 4.20 yields

$$\boxed{\beta\frac{\partial p}{\partial t} + \chi p + \frac{\partial u_s}{\partial l} = 0} \tag{4.21}$$

where

$$\beta = \frac{1}{S_s}\frac{dS_s}{dp}$$

β is a function of the compressibility of the rock mass and a_s. Consider a section through a discontinuity as shown in Figure 4.4

Assuming the rock mass is elastic and isotropic, then the average deformation da_s due to the water pressure increase, dp, at a cross section is given by (Wylie, 1992):

$$da_s = 2\frac{C_d\mathcal{L}(1-\nu^2)}{E}dp \tag{4.22}$$

where $\mathcal{L}$ is the characteristic dimensions of the loaded area; C_d is a factor which depends on the dimensions of the loaded area; E is the Young's Modulus; and ν is the Poisson's ratio of the rock mass. From assumption 4

$$\beta = \frac{1}{S_s}\frac{dS_s}{dp} = \frac{1}{a_s}\frac{da_s}{dp}$$

substitution of equation 4.22 yields

$$\frac{da_s}{dp} = 2\frac{C_d\mathcal{L}(1-\nu^2)}{E}$$

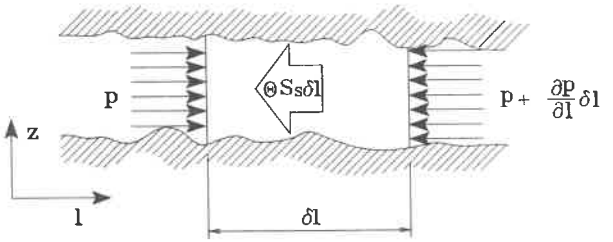

Figure 4.5: Force balancing for law of conservation of momemtum

consequently

$$\boxed{\beta = \frac{1}{a_s}\frac{da_s}{dp} = 2\frac{C_d\mathcal{L}(1-\nu^2)}{Ea_s}} \tag{4.23}$$

For the current problem, the range of the value of C_d is 5.15 – 6.60. The value of C_d used for a particular problem depends on the degree of discretization.

4.2.4 Momentum Balance Equations

The law of conservation of momentum states that the rate of change of momentum of a system with respect to time is equal to the resultant force acting on the system. If $\sum \mathbf{F}$ is the resultant force acting on the system, m the mass of the system and $\mathbf{V}$ the velocity, then $N = m\mathbf{V}$ and $\eta = \mathbf{V}$ in Equation 4.11. Equation 4.11 becomes Equation 4.24 after substitution of the above values

$$\frac{d}{dt}(m\mathbf{V}) = \sum \mathbf{F} = \frac{\partial}{\partial t}\int_{cv} \mathbf{V}\rho d\mathcal{V} + \int_{cs} \mathbf{V}\rho(\mathbf{V}\cdot\mathbf{n})dA \tag{4.24}$$

For the one dimensional case, Equation 4.24 reduces to

$$\boxed{\sum \mathbf{F} = \frac{\partial}{\partial t}\int_{cv} u\rho d\mathcal{V} + \int_{cs} u^2\rho dA} \tag{4.25}$$

Considering the control volume shown in Figure 4.5, the resultant force acting on the control volume is given by

$$\sum \mathbf{F} = pS_s - (pS_s + \frac{\partial}{\partial l}(pS_s)\delta l) - \theta S_s\delta l$$

which on simplification yields

$$\sum \mathbf{F} = -\frac{\partial}{\partial l}(pS_s)\delta l - \theta S_s \delta l \tag{4.26}$$

where θ the viscous resistance per unit volume and p the pressure.
The first term on the right hand side of Equation 4.25 can be written as (assumption 6)

$$\frac{\partial}{\partial t}\int_{cv} u\rho d\mathcal{V} = \rho\frac{\partial}{\partial t}\int_{cv} u d\mathcal{V} = \rho\frac{\partial}{\partial t}(u_s S_s \delta l) \tag{4.27}$$

The second term on the right hand side of Equation 4.25 can be written as

$$\int_{cv} u^2 \rho dA = \rho\left[-u_s^2 S_s + (u_s^2 S_s + \frac{\partial}{\partial l}(u_s^2 S_s)\delta l)\right] \tag{4.28}$$

Equation 4.28 then becomes

$$\int_{cv} u^2 \rho dA = \rho\frac{\partial}{\partial l}(u_s^2 S_s)\delta l \tag{4.29}$$

Substitution of Equations 4.26, 4.27 and 4.29 in Equation 4.25 yields

$$\frac{\partial}{\partial l}(pS_s) + \theta S_s + \rho\frac{\partial}{\partial t}(u_s S_s) + \rho\frac{\partial}{\partial l}(u_s^2 S_s) = 0 \tag{4.30}$$

which simplifies to

$$p\frac{\partial S_s}{\partial l} + S_s\frac{\partial p}{\partial l} + \theta S_s + \rho S_s\frac{\partial u_s}{\partial t} + \rho u_s\frac{\partial S_s}{\partial t} + \rho\frac{\partial}{\partial l}(u_s^2 S_s) = 0 \tag{4.31}$$

Applying assumption 5, Equation 4.31 yields

$$\boxed{p\frac{\partial S_s}{\partial l} + S_s\frac{\partial p}{\partial l} + \theta S_s + \rho S_s\frac{\partial u_s}{\partial t} = 0} \tag{4.32}$$

Equation 4.32 is the expression of the law of conservation of momentum.
From assumption 4

$$\frac{\partial S_s}{\partial l} = \frac{dS_s}{dp}\frac{\partial p}{\partial l} \tag{4.33}$$

Substitution of Equation 4.33 in Equation 4.32 yields

$$\frac{\partial p}{\partial l} + \frac{p}{S_s}\frac{dS_s}{dp}\frac{\partial p}{\partial l} + \theta + \rho\frac{\partial u_s}{\partial t} = 0 \tag{4.34}$$

On the application of assumption 5, the second term in Equation 4.34 can be neglected and it can be written as

$$\boxed{\frac{\partial p}{\partial l} + \theta + \rho\frac{\partial u_s}{\partial t} = 0} \tag{4.35}$$

Up to this stage, the flow characteristics of the fluid have not been mentioned. In the subsequent section, the equations developed in this section will be applied to water.

4.3 Constitutive Equation

The constitutive equation for water, a Newtonian fluid, is

$$\tau = \mu\dot{\gamma}$$

With assumption 6, the rheology of water dictates that the viscous resistance per unit volume equals

$$\theta = \frac{12\mu}{a_s^2}u_s \tag{4.36}$$

Substitution of θ in Equation 4.35 yields

$$\frac{\partial p}{\partial l} + \frac{12\mu u_s}{a_s^2} + \rho\frac{\partial u_s}{\partial t} = 0$$

which can be written as

$$\frac{\partial p}{\partial l} + \zeta u_s + \rho\frac{\partial u_s}{\partial t} = 0 \tag{4.37}$$

where

$$\zeta = \frac{12\mu}{a_s^2}$$

Differentiation of Equation 4.37 with respect to t yields

$$\frac{\partial^2 p}{\partial t\partial l} + \zeta\frac{\partial u_s}{\partial t} + \rho\frac{\partial^2 u_s}{\partial t^2} = 0 \tag{4.38}$$

Differentiation of Equation 4.21 with respect to l yields

$$\beta\frac{\partial^2 p}{\partial t\partial l} + \chi\frac{\partial p}{\partial l} + \frac{\partial^2 u_s}{\partial l^2} = 0 \tag{4.39}$$

Multiplication of Equation 4.38 by β and subtraction of Equation 4.39 from the result, yields

$$\beta\zeta\frac{\partial u_s}{\partial t}+\beta\rho\frac{\partial^2 u_s}{\partial t^2}-\chi\frac{\partial p}{\partial l}-\frac{\partial^2 u_s}{\partial l^2}=0 \tag{4.40}$$

Substitution of $\partial p/\partial l$ from Equation 4.37 in Equation 4.40 and rearranging leads to

$$\boxed{(\beta\zeta+\chi\rho)\frac{\partial u_s}{\partial t}+\beta\rho\frac{\partial^2 u_s}{\partial t^2}+\chi\zeta u_s=\frac{\partial^2 u_s}{\partial l^2}} \tag{4.41}$$

Similarly the differentiation of Equation 4.37 with respect to l and Equation 4.21 with respect to t and elimination of $\partial^2 u_s/(\partial t\partial l)$ and substitution of the value of $\partial u_s/\partial l$ from Equation 4.21 in the resulting equation yields

$$\boxed{(\beta\zeta+\chi\rho)\frac{\partial p}{\partial t}+\beta\rho\frac{\partial^2 p}{\partial t^2}+\chi\zeta p=\frac{\partial^2 p}{\partial l^2}} \tag{4.42}$$

4.3.1 Transmission Line Equation

Transmission lines are used in electric power and communication industries for the conduction of power and signals between locations. The simplest transmission line consists of two conductors as shown in Figure 4.6(a). The transmission line is characterized electrically using four parameters—L_l, the distributed inductance in henrys per unit length; R_l, the distributed resistance in ohms per unit length; C_l, the distributed capacitance in farads per unit length; and G_l the distributed shunt conductance in siemens per unit length. These parameters are shown in Figure 4.6(b) using equivalent lumped parameters. If $I(l,t)$ is the current through the wire and $V(l,t)$ is the voltage at position l and time t with respect to a reference point, then the voltage across the resistor is $irdl$ and the voltage across the inductor is

$$\frac{\partial I}{\partial t}L_l dl$$

The difference in voltage, dv between the ends of the wires is

$$dv=-IR_l dl-\frac{\partial I}{\partial t}L_l dl \tag{4.43}$$

There is current loss from the circuit because of the shunting and capacitive effects of the conductors. The total current loss between the ends of a wire of length dl is

$$dI=-VG_l dl-\frac{\partial V}{\partial t}C_l dl \tag{4.44}$$

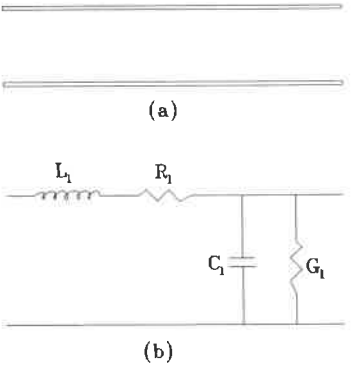

Figure 4.6: (a) Transmission line (b) Equivalent lumped parameter circuit

Dividing Equations 4.43 and 4.44 by dl and taking the limit as $dl \rightarrow 0$ leads to

$$\frac{\partial V}{\partial l} + R_l I + L_l \frac{\partial I}{\partial t} = 0 \tag{4.45}$$

$$C_l \frac{\partial V}{\partial t} + G_l V + \frac{\partial I}{\partial l} = 0 \tag{4.46}$$

Differentiation of Equation 4.45 with respect to t yields

$$\frac{\partial^2 V}{\partial t \partial l} + R_l \frac{\partial I}{\partial t} + L_l \frac{\partial^2 I}{\partial t^2} = 0 \tag{4.47}$$

Differentiation of Equation 4.46 with respect to l yields

$$C_l \frac{\partial^2 V}{\partial t \partial l} + G_l \frac{\partial V}{\partial l} + \frac{\partial^2 I}{\partial l^2} = 0 \tag{4.48}$$

Multiplication of Equation 4.47 by C_l and subtraction of Equation 4.48 from the result, yields

$$C_l R_l \frac{\partial I}{\partial t} + C_l L_l \frac{\partial^2 I}{\partial t^2} - G_l \frac{\partial V}{\partial l} - \frac{\partial^2 I}{\partial l^2} \tag{4.49}$$

from Equation 4.45

$$\frac{\partial V}{\partial l} = -L_l \frac{\partial I}{\partial t} - R_l I$$

Electric Parameters	Hydraulic Analogies
voltage(V)	pressure (p)
current (I)	velocity (u_s)
capacitance (C_l)	Parameter (β)
inductance (L_l)	density (ρ)
conductance(G_l)	parameter χ
electrical resistance (R_l)	viscous resistance term (ζ)

Table 4.1: Electrical and hydraulic analogies

Substitution for $\partial v/\partial l$ in Equation 4.49 and rearranging leads to

$$\boxed{(C_l R_l + G_l L_l)\frac{\partial I}{\partial t} + C_l L_l \frac{\partial^2 I}{\partial t^2} + G_l R_l I = \frac{\partial^2 I}{\partial l^2}} \tag{4.50}$$

Similarly, the differentiation of Equation 4.45 with respect to l and Equation 4.46 with respect to t and elimination of $\partial^2 i/(\partial t \partial l)$ and substitution of the value of $\partial i/\partial l$ from Equation 4.46 in the resulting equation yields

$$\boxed{(C_l R_l + G_l L_l)\frac{\partial V}{\partial t} + C_l L_l \frac{\partial^2 V}{\partial t^2} + G_l R_l V = \frac{\partial^2 V}{\partial l^2}} \tag{4.51}$$

A close look at Equations 4.41 and 4.42 shows that they have the same form as Equations 4.50 and 4.51 respectively. Therefore there exist hydraulic analogies to electrical parameters. These analogies are shown in Table 4.1. In analyzing the result of water pressure test, the a_s in β in Equation 4.21 and ζ in Equation 4.37 characterizes the geometry of the flow path. It is important to note that $a_s = a_s(l)$.

4.3.2 Background Information on Transmission Line Modeling

The transmission line modeling is based on three basic circuit elements—resistor, capacitor and inductor. In this section, the characteristics of these elements are discussed with other basic electrical engineering theorems which are used in explaining TLM.

4.3.3 Resistor

The resistor is an electrical component characterized by

$$\Delta V = IR \tag{4.52}$$

in which ΔV is the voltage across the resistor, i the current through the resistor and R the resistance of the resistor. The unit of resistance is Ohm (Ω). A more fundamental form of equation 4.52 is

$$I = \Delta V \frac{\sigma A}{l} \tag{4.53}$$

where σ is the *electric conductivity*, l the length and A the cross sectional area of the resistor. Comparison of equations 4.52 and 4.53 yields

$$R = \frac{\sigma A}{l}$$

The resistance per unit length, R_l, equals σA. The electrical symbol of a resistor is

4.3.4 Capacitor

The capacitor is an electrical component which stores electric charges. In a capacitor, the quantity of electric charge stored, ΔQ, has a constant ratio to the voltage, ΔV across the capacitor, thus

$$C = \frac{\Delta Q}{\Delta V} \tag{4.54}$$

in which C is the capacitance. The unit of capacitance is farad. The above relationship, although fundamental is not very useful in network analysis which uses voltage and current. The relationship between voltage and current for a capacitor is derived below. The current is the rate of flow of electric charge with respect to time, hence the formula for current is

$$I = \frac{\Delta Q}{\Delta t} \tag{4.55}$$

Substitution for ΔQ in equation 4.54 yields

$$I = C\frac{\Delta V}{\Delta t} = C\frac{dV}{dt} \tag{4.56}$$

Equation 4.56 describes the $i - v$ characteristics of the capacitor. The capacitance per unit length, C_l, can replace C in equation 4.56 if ΔV is defined as the voltage across unit length. The electrical symbol for a capacitor is

4.3.5 Inductor

The inductor is also an electrical component which stores energy in form of magnetic field. There is no fundamental equation (similar to equation 4.54) for an inductor, but it is know experimentally that it has the electrical characteristics of

$$\Delta V = L\frac{dI}{dt} \tag{4.57}$$

in which L is the inductance. The unit of inductance is henry. The electrical symbol for inductors is

There are different methods of solving equations 4.50 and 4.51. The two most commonly used methods in a non-uniform field are the Finite Difference Time Domain (FDTD) and the Transmission Line Matrix (TLM). Chapter 6 contains comprehensive information on the TLM procedure. The TLM approach has been selected for use in this work because of its simplicity and robustness. According to Pomeroy (1991), the TLM is "simple, explicit, and unconditionally stable". Furthermore, a TLM model can be developed for and tested for a small model and scaled to accommodate larger problems without becoming unstable or invalid.

4.4 Inversion Procedure for Water Pressure Test

The geometric information on the flow path within the rock discontinuities can be obtained through the inversion of the flowrate-time curve during the transient phase. If the injection pressure is kept constant (see experimental details in Chapter 7) typical transient flow curve is sown in Figure 4.7. For the one dimensional flow situation, the relationship between the transient flowrate $q(t)$ and the geometry of the flow path can be symbolically represented as

$$q(t) = f(\mathbf{a}_s) \tag{4.58}$$

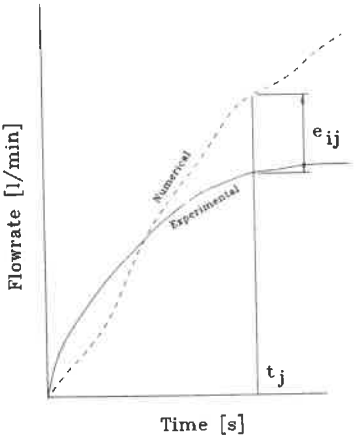

Figure 4.7: Inversion process — Comparison of experimental and synthesized flowrate-time curve for the transient Water Pressure Test for injection pressure, p_i

where $\mathbf{a}_s$ is the vector of the average distance between the walls of the discontinuities at cross sections along the flow path and can be written as

$$\mathbf{a}_s = [a_{s1}, a_{s2}, a_{s3}, \ldots, a_{sn}]^T \tag{4.59}$$

where n is the number of points along the discontinuity at which the average distance between the walls of the discontinuity are to be determined. T indicates vector transpose. When the fluid injection is carried out at different constant pressure we have a family of flow rate curves. The general relationship is then

$$q(t,p) = g(\mathbf{a}_s) \tag{4.60}$$

4.4.1 Fundamentals

The inversion process can be symbolically represented as

$$\mathbf{a}_s = g^{-1}(q(t,p)) \tag{4.61}$$

The inversion process is based on guessing a solution. For this particular case, a guess of the vector $\mathbf{a}_{sf}$ is made. The guessed vector is used to numerically solve the flow equations 4.50 and 4.51. In general the flowrate-time curve, $q_{nu}(t,p)$ obtained from the numerical simulation will be different from the experimental results. Obviously, $q_{nu}(t,p)$ is a function of the guessed vector, $\mathbf{a}_{sf}$.

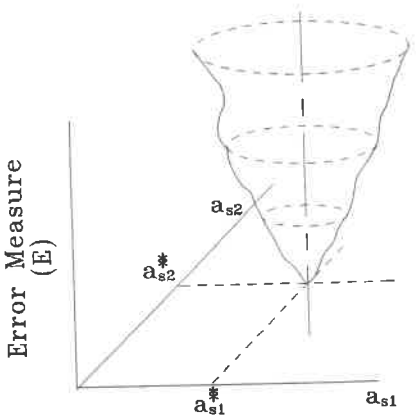

Figure 4.8: Graphical description of error measure minimization

For a given time t_j and pressure p_i (see figure 4.7), the error measure can be defined as

$$E = \sum e_{ij} = \sum [(q(t_j, p_i) - q_{nu}(t_j, p_i))]^2 \tag{4.62}$$

The inversion process is a successive iteration method of minimizing E. For example, if $\mathbf{a}_s = [a_{s1}, a_{s2}]$, the inversion process is a means of finding the values of $[a^*_{s1}, a^*_{s2}]$ which minimize E see figure 4.8.

Differentiation is the classical means of finding the vector $\mathbf{a}_{sf}$ which minimizes E in equation 4.62. However, the computational time increases as the size of $\mathbf{a}_{sf}$ increases. Consequently, researchers have come up with different schemes of error minimization which are not based on differentiation. Details of minimization (also called optimization) algorithms (with and without differentiation) can be found in Press et al. (1992). Computational Science Foundation (1995) provides a general overview of optimization methods. In this work, the Powell's method (Powell, 1964) was used because its algorithm is relatively fast as it does not require differentiation.

The inversion process can be summarized as follows:

1. Establish acceptable error tolerance.

2. Make a first guess of vector, $\mathbf{a}_s$.

3. Use the guessed data to solve equations 4.50 and 4.51.

4. Compare numerical solution to experimental results and calculate the resulting error. If the error falls within the tolerance, the iteration ends, otherwise the error is optimized to obtain a new set of values of $\mathbf{a}_s$.

5. Steps, 3,4 and 5 are repeated until the desired error falls within the specified limit.

Chapter 5

The Blockage and Flow Mechanisms of Cement Grout in Rock Discontinuities—A new Explanation

An understanding of the process through which rock discontinuities are blocked with cement grout injected into them is fundamental to the development of the theory of rock grouting. In this chapter, the constitutive equation[1] of cement grout is discussed with the implication of this type of constitutive equation for the blockage mechanism of cement grout in rock discontinuities. The model of blockage mechanism of rock discontinuities currently in use is also discussed with its inability to predict blockage of real rock discontinuities. In addition, a new blockage mechanism is presented with limitations to its applications. Finally, a model of the flow of cement grout in rock discontinuities which takes into consideration progressive blockage is developed.

5.1 Constitutive Equation Of Cement Grout

The constitutive equation relates shear stress (τ) to shear rate ($\dot{\gamma}$). The general constitutive equation is of the form

$$\tau = f(\dot{\gamma}) \tag{5.1}$$

According to Whorlow (1980) some of the factors which may influence the choice of an constitutive model for a particular application include:

1. The close fit of experimental data.
2. Use of the smallest number of disposable constants.

[1]Also called flow equation or rheological model

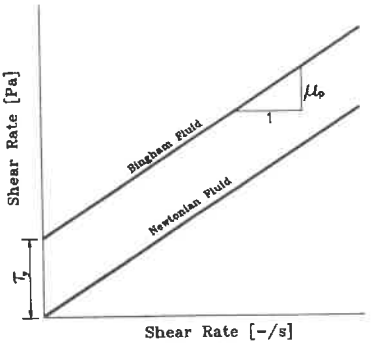

Figure 5.1: Graphical representation of Newtonian and Bingham constitutive equations

3. Mathematical analysis leading to a straight-forward analysis of different shear flow and
4. Possibility of generalizing the equations, into tensor form for use with more general type of flow.

Newtonian fluids have the simplest constitutive equation:

$$\tau = \dot{\gamma}\mu \tag{5.2}$$

where

τ = shear stress
$\dot{\gamma}$ = shear rate
μ = dynamic viscosity

This model is depicted graphically in Figure 5.1. Unfortunately, cement suspension within the mix ratio employed in grouting (water/cement < 2, by weight) exhibits a more complex behaviour than the Newtonian fluid. Some workers (e.g. Ashikmen and Pronina, (1986); Murata and Kikukawa, (1992)) have reported that cement suspension with mix ratio used in grouting can be modeled using Bingham's equation

$$\begin{aligned} \tau &= 0, \quad \tau < \tau_y \\ \tau &= \tau_y + \mu_p\dot{\gamma}, \quad \tau \geq \tau_y \end{aligned} \tag{5.3}$$

in which μ_y and τ_y are the *plastic viscosity* and *yield stress* respectively. Equation 5.3 is also depicted graphically in Figure 5.1. Other workers e.g Umlauf (1993) have reported that cement suspension within the concentration used in rock grouting has Herschel-Bulkley characteristics. The Herschel-Bulkley equation which is a generalized form of Bingham equation is

$$\tau = \tau_y + k\dot{\gamma}_n \tag{5.4}$$

The constants k and n in Equation 5.4 are determined experimentally.

5.2 The Blockage Mechanism based on the Flow of Bingham's Fluid Within Parallel Plates

All previously published work on the flow of grout within rock discontinuities— Wittke (1968), Wallner (1976), Lombardi (1985), Hässler, (1991) etc are based on the idealization of rock discontinuities as parallel plates. This idealization is discussed in this section.

Consider Figure 2.14, the pressure across the fluid segment of length Δl is Δp, and a is the distance between the parallel plates. Assuming steady state flow condition. The balance of the forces acting on the fluid element yields

$$\tau_w = \frac{a}{2}\frac{\Delta p}{\Delta l} = \frac{a}{2}\mathcal{J} \tag{5.5}$$

where τ_w is the shear stress at the walls of the discontinuity and $\mathcal{J}$ is the pressure gradient. The shear stress within the fluid element varies from zero at the center of the discontinuity to maximum at the walls as shown in Figure 2.14. The fluid starts flowing only if the shear stress at the walls of the discontinuity, τ_w is greater than the yield stress of the fluid, τ_y. The fluid stops flowing if τ_w falls below τ_y and the surface of the walls are rough (if the surface is smooth, extrusion—flow of unyielded fluid— occurs). As a result of the distribution of shear stress within the fluid, it is possible that a central core of thickness

$$\xi = \frac{\tau_y}{\mathcal{J}}$$

may remain unyielded. The average flow velocity is given in Equation 2.4. and the minimum pressure gradient, $\mathcal{J}_{min}$ required to cause flow is

$$\mathcal{J}_{min} = \frac{2\tau_y}{a} \tag{5.6}$$

From Equation 5.6, it appears that $\mathcal{J}_{min}$ is a function of both τ_y, the yield stress and a, the distance between the walls of the discontinuity.

By assuming a linear flow (see section 3.3.2) the macroscopic pressure gradient across the parallel plate remains constant. Frictional losses occur as the Bingham's fluid flows within the parallel plates. If the plates are long enough, at a particular distance l_R from the point of injection of the fluid, the available head is no more sufficient to overcome the yield stress. At this stage, the grout stops flowing and the flow channel is blocked. If the pressure gradient is increased beyond that required to overcome the yield stress, the fluid starts flowing again.

The distance l_R is called the reach of the grout under the prevailing injection condition. On the basis of equilibrium approach, it can be calculated from

$$l_R = \frac{a\Delta p}{2\tau_y} \tag{5.7}$$

If the plate is shorter than l_R, blockage of flow channel will never occur and there will be continuous flow as long as the pressure gradient is maintained. When this situation occurs, there are two possibilities of blocking the flow channel under this condition—The injection pressure can be reduced or the yield of the grout increased. This is because the blockage of the flow channel is attributed entirely to the yield stress of the cement grout. Published reports on blockage mechanism of a rock discontinuity— Wittke (1968), Lombardi (1985) and Lombardi and Deere (1993)— known to the author are based on the blockage mechanism discussed above.

5.3 Flow of Cement Grout in Real Rock Discontinuity

Consider a rock sample with discontinuity shown in Figure 5.2. If pressure gradient, $\mathcal{J}$ across the sample is sufficient to cause the flow of grout through it continuously, then on the basis of flow of Bingham's fluid between parallel plates, the length of the sample is shorter than l_R, the length from the injection point at which available pressure gradient equals that required to bring the stress at the walls of the discontinuity to yield level. Therefore flow through the discontinuity will continue as long as the pressure gradient is maintained. However, laboratory results (see Chapter 8) showed that flow within the discontinuity increased to a maximum and subsequently decreased to zero as shown in Figure 5.3. The blocked channel did not open up when the pressure gradient was increased. These observations are contrary to the prediction of the blockage mechanism discussed in the last section. The failure of the blockage mechanism based on the flow of Bingham fluid between parallel plate in explaining the reality of flow within rock discontinuity can be attributed to variation of the geometry of the flow path within

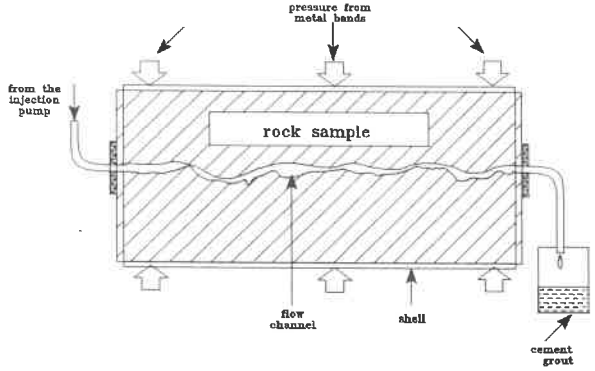

Figure 5.2: Flow of cement grout through rock discontinuity

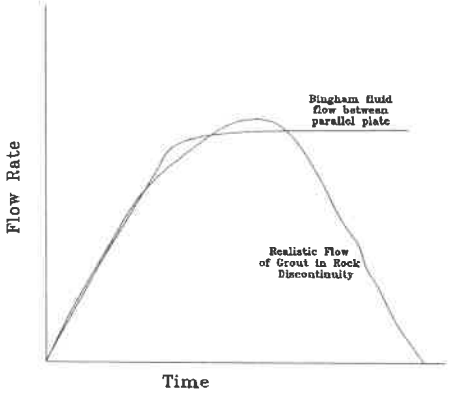

Figure 5.3: Flow rate- time curve for flow of cement grout in a rock discontinuity

the rock discontinuities and the size of grains in the cement suspension which it ignores. In subsequent section, a more realistic model of blockage mechanism of cement grout in rock discontinuities is presented.

5.4 Progressive Blockage Mechanism of Rock Discontinuities During Grouting

The presence of a discontinuity in the rock mass does not guarantee that it will serve as a conduit in which flow of fluid can take place. A precondition for a discontinuity to serve as a conduit is the interconnection of voids within it. Consequently, only interconnected voids within the discontinuity serve as conduit. This means, some of the available voids which are isolated (not connected) will not serve as conduit. Therefore the flow of fluid within the discontinuity takes place in channels which may not cover all available voids. This phenomenon is usually referred to in literatures as *flow channelization*. Flow channelization occurs because of irregularities on the surface of the walls of the discontinuities which lead to variation in the distance between the walls of the discontinuities. The concept of the progressive blockage mechanism of rock discontinuities during grouting is based on the assumptions that blockage of the rock discontinuity is:

1. A continuous process which occurs as grouting proceeds. Consequently transient analysis of flow must be used.
2. It can be attributed completely to the following factors which act together
   - Yield stress of the grout.
   - Grains of the cement grout.
   - Obstructions within the discontinuity.
   - Dead ends within the discontinuity.
   - Van der Waals forces.
3. Increase in grouting pressure does not necessarily open blocked flow channels.

Obstructions within the rock discontinuities occur at points where the body of the rock mass protrudes into the flow channel but the grout can still flow around it. Obstructions essentially act to reduce the distance between the walls of the discontinuity. Only partial blockage of the discontinuity occur at obstructions as shown in figure 5.4. Dead ends occur at points when the grout stops flowing. The occurrence a of dead end may be due to:

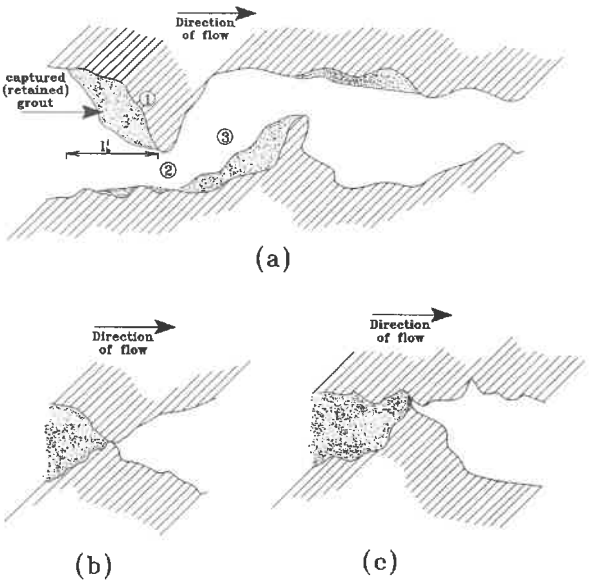

Figure 5.4: Blockage Mechanisms in Rock Discontinuities, (a) Partial blockage at obstructions, (b) total blocakge when the distance between the walls equals 0 (c) Blockage due to cement particle.

1. The distance between the walls of the continuity is zero— absence of conducting void and

2. The distance between the walls discontinuity is too small to allow the passage of the grains within the cement suspension.

3. Available pressure gradient is not sufficient to overcome the yield stress of the grout.

To illustrate the concept of progressive blockage mechanism of rock discontinuities by cement grout, consider the discontinuity shown in Figure 5.4 (a). As the grout front arrives at the obstruction — surface 1, a fraction of it is reflected backwards while the remaining fraction continues to flow through gap 2. If the pressure gradient due to reflection, $\mathcal{J}_r$ is less than $\mathcal{J}_{crit}$, then blockage will occur, otherwise it will be reflected towards the injection point. Meanwhile a fraction of the grout that passed through gap 2 would bave encountered another obstruction at 3. The reflected grout from 3 will also encounter the obstruction above gap 2 and a local oscillatory flow is set up. This is always the case whether or not the injection pressure is oscillatory. While all these are happening, the rock mass deforms due to the flow pressure. With time the grout looses its energy to friction and local local blockage occurs. The above process is formalized in transmission line method which is used to simulate the flow of water and grout. The length, l_b^i and shape of the grout retained by the obstruction depends mainly on:

1. The yield stress of the grout.

2. The pressure gradient across the obstruction.

3. The extend to which the obstruction protrudes into the flow channel.

4. The geometry of the surface of the discontinuity.

The reduction of the size of flow channel leads to the conversion of pressure head to velocity head which is accompanied with head loss. Furthermore, head loss also occurs as the grout flows from point 2 to point 3 due to expansion of the flow channel. These losses are in addition to the frictional loss which occurs because of the viscosity of the fluid. The process illustrated above occurs at all obstructions. The rate of head loss as function of distance from the source of injection depends on the size and occurrence of obstructions and the viscosity of the grout. If the grout does not flow into a physical barrier which totally prevents further flow, eventually, a length, l_R will be reached at which available head is not sufficient to overcome the yield of the grout and the grout stops flowing. In addition, blockage of the flow channel can also occur if the grout retained at one obstruction (e.g point 3) extends to preceding obstruction (point 2) as shown in Figure 5.4(a).

As the grout flows along the discontinuity, if at any point along the flow channel, the distance between the walls of the discontinuity is smaller than that necessary to allow the passage of some of the grains in the cement grout partial blockage of the flow channel also occurs. According to Lau and Crawford (1986), if D_{max} is the maximum size of grain in the cement suspension and a_i is the local distance between the walls of the discontinuity, then

$$\frac{a_i}{D_{max}} > 3$$

is required to guarantee the continuous flow of grout through that point in the discontinuity. The van der Waals force also enhances blockage as mobile particles are attracted to captured ones.

Although the yield stress plays an important role in the flow of grout within the rock discontinuities as pointed out by Wittke (1968) and echoed by Lombardi, (1985), however the geometry of the flow path is also equally important. Obviously, the parallel plate assumption made in earlier work cannot be used to explain the progressive blockage observed both in the laboratory and on the field.

It is impossible to incorporate mathematically all the above factors influencing the flow of grout within the rock discontinuities. In the analysis that follows, it is assumed that the effects of the van der Waals forces are negligible.

5.5 Mathematical Analysis of the Flow of Grout in Rock Discontinuity

In this section, the analysis of the flow of fluid in rock discontinuities developed in chapter 4 is extended to cover the flow of grout in rock discontinuities. The constitutive equation of a cement grout — a Bingham fluid (Equation 5.3) is

$$\begin{aligned} \tau &= 0, \quad \tau < \tau_y \\ \tau &= \tau_y + \mu_p \dot{\gamma}, \quad \tau \geq \tau_y \end{aligned}$$

This equation is difficult to use in numerical simulation because of the need to track the yield surface in equation 5.3. To overcome this difficulty, the modified Bingham's model (Equation 5.8) proposed by Papanastasiou, (1987) will be used. This model has previously been used by Abdali et al. (1992) and Donier and Tichy (1992) in analysing the flow of Bingham fluid.

$$\tau = \left[\mu_p + \frac{\tau_y(1 - e^{-m|\dot{\gamma}|})}{|\dot{\gamma}|}\right]\dot{\gamma} = \mu_m \dot{\gamma} \tag{5.8}$$

Equation 5.8 is a continuous equation which holds within both the yielded and

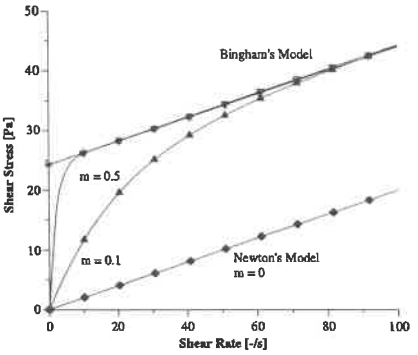

Figure 5.5: Graphic representation of constitutive equations

unyielded regions. With the appropriate value of m, called the growth exponential, Equation 5.8 can replace equation 5.3. The major advantage of using equation 5.8 is that tracking of the yield surface is eliminated. A further advantage is that flow equations developed for Newtonian fluid can easily be adapted with minimum modifications — the μ in $\zeta = \frac{12\mu}{a_s^2}$ of equation 4.37 is replaced with μ_m given by

$$\mu_m = \mu_p + \frac{\tau_y(1 - e^{-m|\dot{\gamma}|})}{|\dot{\gamma}|} \tag{5.9}$$

in which μ_p and τ_y are the plastic viscosity and yield stress of the grout respectively and m a constant called growth exponential. The blockage of the flow path is assumed to occur at any time if the local pressure gradient falls below $\mathcal{J}_{crit}$.

Chapter 6

Transmission Line Modeling

6.1 Introduction

The use of electrical analogy in solving groundwater flow problems was popular. The method lost its popularity as digital computers became widely available. Rushston and Redshaw (1979) cited the work of Skibitzke of 1960 as one of the earliest references on the use of electrical analogy in solving groundwater flow problems. In the past, the use of electrical analogy meant the coupling together of electrical components representing the flow system to be investigated. Current and(or) voltage were(was) measured at desirable location on the electrical network. Today, electrical engineers use digital computers to analyse electrical network. Consequently, the method of electrical analogy can be used through computer simulation of electrical networks. If the coupling of electrical components is desirable, the computer can still be used to control and take measurement within the network. From the above, it is clear that the computer is a useful tool for electrical analogy methods.

Within the framework of this research, the transmission line modeling (TLM) is an electrical analogy method. It is based on the numerical simulation of the propagation of wave using Huygens's wave propagation model(Johns, 1974). It was originally developed for solving problems of propagation of electromagnetic waves by Johns and Beurle (1971). According to Hoefer (1985), it has also been used to solve both linear and non-linear lumped network problems and diffusion problems. TLM, a powerful and versatile method has been extensively studied and its maturity was confirmed recently with the First International Workshop on TLM held in Canada at the University of Victoria (Trenkić, 1995). In this research, the transmission line modeling is being used in solving the problem of flow of fluid within rock discontinuities for the first time.

6.2 Basic Laws and Theorem

The fundamental laws used in network analysis are the *Kirchhoff's voltage law* and the *Kirchhoff's current law*. Kirchhoff's voltage law states that at any instant of time, the algebraic sum of all voltages across elements in any closed loop of a network equals zero. The Kirchhoff's current law states that at any instant of time , the algebraic sum of currents entering a node and currents leaving a node equals zero (Johnson, 1984). For relatively simple network, the *Thévenin equivalent circuit law* can be used as alternative to the Kirchhoff's laws. The Thévenin equivalent circuit law states that a network can be replaced by a single voltage source V_{TH} in series with a single impedance, Z_{TH} as shown in figure 6.1(c). The single voltage source V_{TH} is the open circuit voltage at the port of the network—ab—and Z_{TH} is the impedance of the port of the network. For example, in figure 6.1

$$V_{TH} = \frac{Z_2}{Z_1 + Z_2} V_1$$

and

$$Z_{TH} = \frac{Z_1 + Z_2}{Z_1 Z_2}$$

A basic theorem that is used in explaining TLM is the parallel generator theorem (Millman's theorem). According to this theorem, the node voltage, V_B at the point B in Figure 6.2 is given by

$$V_B = \frac{\frac{V_1}{Z_1} + \frac{V_2}{Z_2} + \frac{V_3}{Z_3}}{\frac{1}{Z_1} + \frac{1}{Z_2} + \frac{1}{Z_3}} \tag{6.1}$$

6.3 Fundamentals of Transmission Line Modeling

The theory of transmission line is discussed in almost all basic books on antenna, telephone network and electric power transmission. There are also books devoted entirely to transmission line theory e.g. Magnusson (1965). The only available book on TLM is Christopoulos (1995). The basics of TLM are discussed in Johns and Beurle (1971) and Hoefer (1985). In addition, there are hundreds of journal publications on TLM in electrical/electronics specialist literature.

A lossless transmission line does not attenuate a signal propagating through it. This means that $R_l = G_l = 0$ in Equation 4.51. A frictionless fluid flowing through a conduit with deformable and impermeable wall is the hydraulic analogy to lossless transmission line.

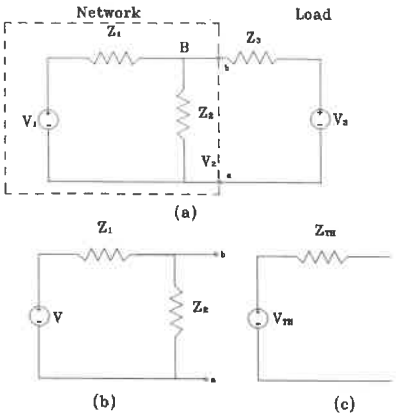

Figure 6.1: (a) An electric circuit to be analysed (b) Circuit to be Thévenized (c) Thévenin Equivalent

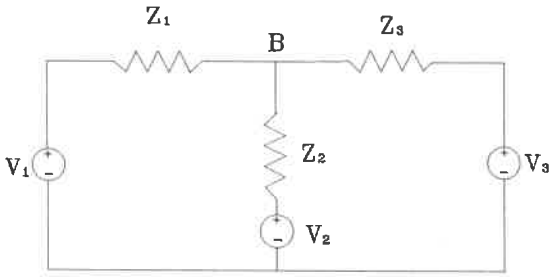

Figure 6.2: Parallel Generator (Millman's) Theorem

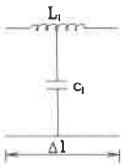

Figure 6.3: Transient charging of a lossless transmission line

Consider a lossless transmission line. If a direct voltage source, V is connected to the line at time $t = 0$, at $t = \Delta t$ the voltage has traveled a distant Δl into the line. The capacitance, $C_l \Delta l$ of the section of line which the voltage has traveled has charged to the source voltage V. The quantity of charge, ΔQ transfered within the time Δt into the energized segment of the line equals $C_l V \Delta l$. The rate of flow of charges, which is the current, I equals:

$$I = \frac{\Delta Q}{\Delta t} = C_l V \frac{\Delta l}{\Delta t} = C_l V U_p \tag{6.2}$$

in which U_p is the *propagation velocity* . As a result of the flow of current, i, a magnetic flux , Φ, associated with the line inductance is created. The magnetic flux has the value

$$\Phi = L_l \Delta l I = L_l \Delta l C_l V U_p \tag{6.3}$$

in which L_l is the line inductance per unit length.

According to Faraday's Law:

$$V = \frac{\Delta \Phi}{\Delta t} = L_l C_l V U_p^2 \tag{6.4}$$

From equation 6.4

$$\boxed{U_p = \frac{1}{\sqrt{L_l C_l}}} \tag{6.5}$$

Substitution of equation 6.5 in equation 6.2 yields

$$I = \frac{V}{\sqrt{\frac{L_l}{C_l}}} \tag{6.6}$$

The *line impedance* is defined as

$$Z = V/I$$

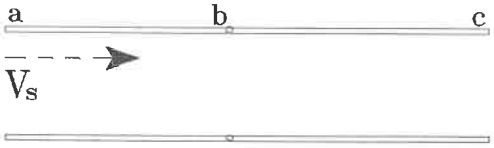

Figure 6.4: Propagation of voltage along lossless transmission line

From equation 6.6

$$\boxed{Z = \sqrt{\frac{L_l}{C_l}}} \tag{6.7}$$

6.4 Propagation of Impulse Through Transmission Lines

In solving the problem of propagation of impulse through transmission line, the line is usually divided into segments with the same propagation velocity. The transmission behaviour of the line is then observed at nodes of interest at discrete time intervals. The time intervals, Δt, is the time required for the impulse to travel from one node to another.

If a lossless transmission line with propagation velocity, U_p, and impedance Z_o is excited with a dc — direct current — voltage of magnitude V at time $t = 0$, the voltage will travel along the line with velocity U_p and magnitude V as long as the impedance of the transmission line remains the same. If the voltage encounters a change in impedance, reflection will occur. The reflection characteristics at the point of change in impedance is a function of the impedance of the transmission lines meeting at that point.

Consider a lossless transmission line ab with impedance Z_{ab} which is connected to another lossless transmission line bc with impedance Z_{bc} at node b (see figure 6.4). For the first time step, $k = 1$, if a dc voltage pulse, V_s is lunched into line ab as shown in figure 6.4 from end a towards b at time $t = 0$. The incident voltage from the left of node b, for the time step $k = 1$, ${}_1V_{lb}^{i} = V_s$, arrives at node b

at time $t = t_1 = 1/\sqrt{L_{ab}C_{ab}}$ in which L_{ab} and C_{ab} are inductance and capacitance of line ab respectively. The followings are the different possibilities at node b.

- If $Z_{ab} \neq Z_{bc}$:
  Because of the change in impedance at node b, a component of ${}_1V_{lb}^i$ will be reflected by into line ab during the second time step, $k = 2$ as ${}_2V_{lb}^r$. The magnitude of ${}_2V_{lb}^r$ is

  $$ {}_2V_{lb}^r = \frac{Z_{bc} - Z_{ab}}{Z_{bc} + Z_{ab\,1}} V_{lb}^i = \Gamma_1 V_{lb}^i = \Gamma V_s $$

  in which

  $$ \Gamma = \frac{Z_{ab} - Z_{bc}}{Z_{ab} + Z_{bc}} $$

  is called the *reflection coefficient*. The remaining component of ${}_1V_{lb}^i$, ${}_2V_{rb}^r = {}_1V_{lb}^i - {}_2V_{lb}^r$ will be lunched into the right of node b (transmission line line bc).

- If $Z_{ab} = Z_{bc}$:
  $\Gamma = 0$ and ${}_2V_{lb}^r = 0$ and ${}_2V_{rb}^r = V_s$. This means all the energy of V_s in line ab is completely transferred to line bc.

- If $Z_{bc} = 0$:
  This is equivalent to saying that the line ab is shunted at node b. For this situation, $\Gamma = -1$ and ${}_2V_{lb}^r = V_s$ and ${}_2V_{rb}^r = 0$.

- If $Z_{bc} = \infty$:
  This is equivalent to saying that ab is opened at node b, then $\Gamma = 1$ and ${}_2V_{lb}^r = V_s$. Therefore, the resultant voltage at node b equals 2 V_s (see figure 6.5)

The last case is of particular importance. It implies that an open ended transmission line can be replaced with the Thévenin equivalent circuit with $V_{TH} = 2\ {}_1V_{lb}^i$ and $Z_{TH} = Z_{ab}$ for a time interval as shown in Figure 6.5.

6.5 Analysis of Transmission Lines Connected in Series

In chapter 4 it was shown that linear flow of fluid in rock discontinuities can be modeled using transmission line equation. The analogies between flow parameters in rock and transmission line are shown in Table 4.1. To model the linear flow

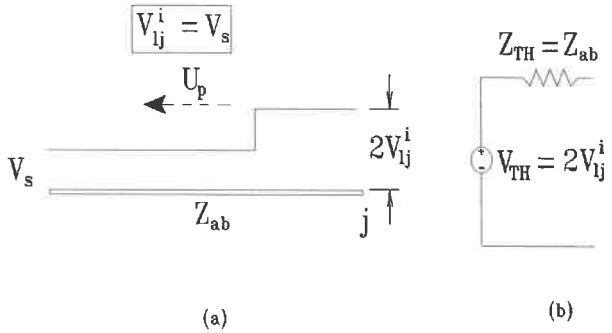

Figure 6.5: (a) A transmission line with open end (b) Its Thévenin Equivalent Circuit

in rock discontinuities, transmission lines are connected in series. In general, the parameters of the transmission lines—resistance, inductance, capacitance and conductance are different for all the lines. In subsequent paragraphs the method of analysis of transmission lines connected in series are discussed. The discussion starts with a special situation in which the parameters of all the lines are equal. Subsequently, the discussion is extended to cover the general case in which there is variation in the line parameters.

Consider the series of transmission lines connected as shown in figure 6.6(a). The lumped component equivalent of one of the transmission lines is shown in figure 6.6(b). For the time being, it is assumed that the lines have the same electrical parameters. The nodes are labeled $j = 1 \ldots n$. The problem is the determination of voltage (analogy to pressure) of current (analogy to velocity) as a function of time, t, and length, l, when the source voltage, $V_s(t)$, is given.

A lossy transmission line can be modeled as a combination of a lossless transmission having impedance z_o with the circuit elements R_l and G_l connected as shown in figure 6.6 (c). A node of a lossy transmission line is shown in figure 6.7(a). The node j is also shown in figure 6.7(b) with the transmission line replaced with its Thevenis equivalent.

The circuit shown in figure 6.7(b) can be used for the analysis at nodes $j = 2 \ldots n-1$. For these nodes and time step k, the node voltage, ${}_kV_j$ can be calculated from the incident voltages—${}_kV_{lj}^{i}$ and ${}_kV_{rj}^{i}$ using Millman's theorem

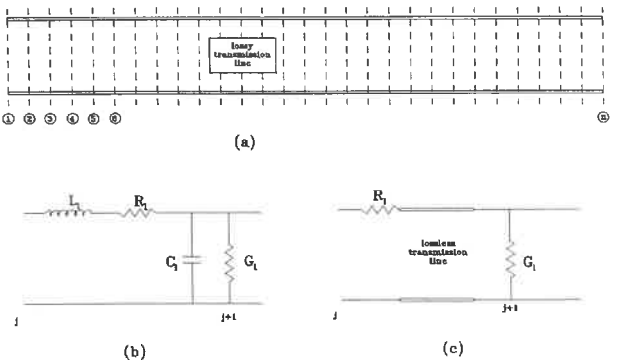

Figure 6.6: Series connection of transmission lines

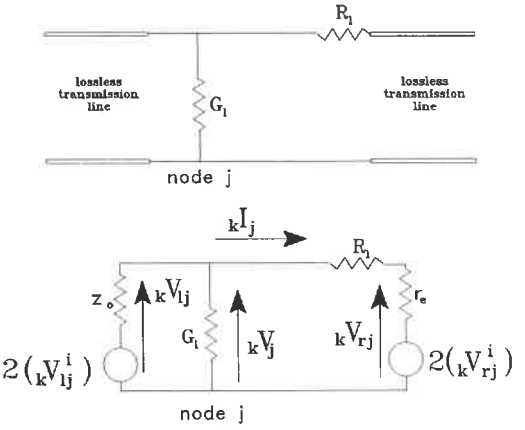

Figure 6.7: (a) A node with transmission line (b) transmission line replaced with its thevenin equivalent

hence

$$ {}_kV_j = \frac{\frac{2({}_kV_{lj}^i)}{z_o} + \frac{2({}_kV_{rj}^i)}{z_o+R_l}}{\frac{1}{z_o} + \frac{1}{R_l+z_o} + G_l} \tag{6.8} $$

The associated current is

$$ {}_kI_j = \frac{{}_kV_j - 2({}_kV_{rj}^i)}{R_l + z_o} \tag{6.9} $$

The voltage at the input to the transmission line on the left of node j is

$$ {}_kV_{lj} =_k V_j \tag{6.10} $$

The voltage to the input to the transmission line on the right of node j is

$$ {}_kV_{rj} = 2({}_kV_{rj}^i) +_k I_j z_o \tag{6.11} $$

Because of the difference in electrical characteristic at the node, the voltage

$$ {}_kV_{lj}^r =_k V_{lj} -_k V_{lj}^i \tag{6.12} $$

is reflected into the transmission line on the left while the voltage

$$ {}_kV_{rj}^r =_k V_{rj} -_k V_{rj}^i \tag{6.13} $$

is reflected into the transmission line on the right. The voltage reflected from node j end of the transmission line $j-1, j$ during time step k is the voltage which incidents at node $j-1$ end of the same transmission line at time step $k+1$.

$$ {}_{k+1}V_{lj}^i =_k V_{r(j-1)}^r \tag{6.14} $$

Also, the voltage reflected from node j end of the transmission line $j, j+1$ during time step k is the voltage which incidents at node $j+1$ end of the same transmission line at time step $k+1$ hence

$$ {}_{k+1}V_{rj}^i =_k V_{r(j+1)}^r \tag{6.15} $$

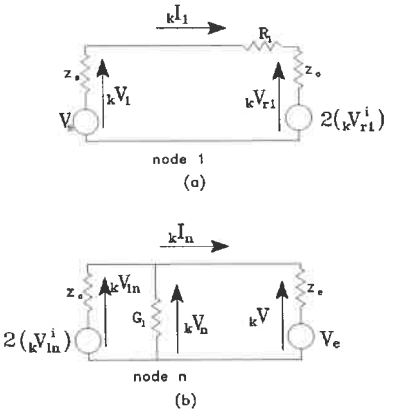

Figure 6.8: (a) Circuit diagram for node 1 (b) Circuit diagram for node n

6.5.1 Boundary Conditions

The circuit shown in figure 6.8(a) represents the situation at node 1. For this case, the node voltage equals

$$ {}_kV_1 = \frac{\frac{{}_kV_s}{r_s} + \frac{2({}_kV_{r1}^i)}{R_1+z_o}}{\frac{1}{r_s} + \frac{1}{R_1+z_o}} \tag{6.16} $$

and current flowing into the transmission line is

$$ {}_kI_1 = \frac{{}_kV_1 - {}_kV_{rj}^i}{r + z_o} \tag{6.17} $$

The input voltage at the transmission line on the left of node 1 is

$$ {}_kV_{r1} = 2({}_kV_{r1}^i) + {}_kI_1 z_o \tag{6.18} $$

while the reflected voltage into the line is

$$ {}_kV_{r1}^r = {}_kV_{r1} - {}_kV_{r1}^i \tag{6.19} $$

The incident voltage on node 1 at time step $k+1$ is the reflected voltage from the right side of node s at time step k.

$$ {}_{k+1}V_{r1}^i = {}_kV_{l2}^r \tag{6.20} $$

The circuit shown in figure 6.8(b) represents the situation at node n. For this case, the node voltage is

$$ {}_kV_n = \frac{\frac{2_kV_{ln}}{z_o} + \frac{V_e}{r_e}}{\frac{1}{z_o} + \frac{1}{r_e} + G_l} \tag{6.21} $$

The current flowing from the node is

$$ {}_kI_n = \frac{{}_kV_n - V_e}{r_e} \tag{6.22} $$

The input voltage on the line left of n is

$$ {}_kV_{ln} =_k V_n \tag{6.23} $$

The voltage reflected into the line on the left is

$$ {}_kV^r_{ln} =_k V_{ln} -_k V^i_{ln} \tag{6.24} $$

The incident voltage on node n at the time step $k+1$ is the reflected voltage from the transmission line on the right of node $n-1$:

$$ {}_{k+1}V^i_{ln} =_k V^r_{r(n-1)} \tag{6.25} $$

6.6 Algorithm

The implementation of the procedure described above is shown in figure 6.9 below

6.7 Solutions to Problems with Variable Line Parameters

There are two approaches to solving problems with variable line parameters viz:

1. Variable length method, and
2. Constant length method.

6.7.1 Variable Length Method

The maintenance of the same travel time within all segments—synchronization– is of paramount importance in TLM analysis. To enforce synchronization, the length of the different segments are scaled according to their propagation velocities. With the selection of Δt, the length of the segments are calculated from

$$\Delta l_j = u_{pj}\Delta t$$

in which u_{pj} and Δl_j are the propagation velocity and length of the transmission line j respectively.

With the above modification, the solution method follows that for lines with uniform line parameters described earlier..

6.7.2 Constant Length Method

In the constant length method, the same Δt and Δl are maintained for all the segments. Variations in line parameters are introduced by connecting extra transmission line with open end— *a stub*— to the nodes. The length of the stubs at the nodes accounts for the variations in the line parameters. Obviously, the stub introduces the variation in the propagation velocity. The constant length method is used in this work.

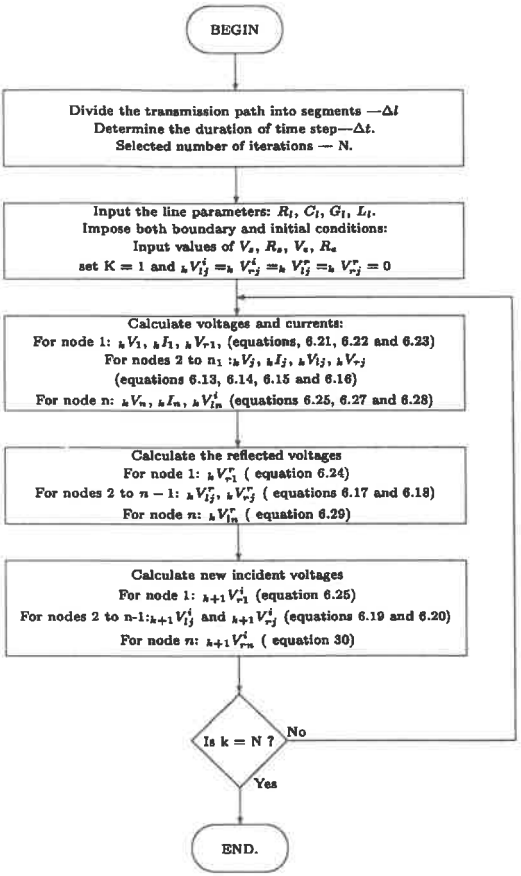

Figure 6.9: Flow Chart for TLM

Chapter 7

Laboratory Measurements

In this chapter, the different laboratory methods employed within this research programme are discussed. This methods are:

- Characterization of cement grout.
- Characterization of the void geometry using transient water pressure test.
- Characterization of the void geometry using surface geometry of the walls of the discontinuity.
- Physical simulation of rock grouting.
- Suitability test.

7.1 Characterization of Cement Grout

A good grout, besides being reasonably priced should possess the following characteristics:

1. It should be homogeneous.
2. It should be stable, i.e no tendency towards segregation.
3. The rheological parameters show be low enough for it to be easily pumped and they should be high enough to resist water pressure immediately after injection.
4. It should penetrate discontinuities easily.
5. It should be resistant to chemicals present in the rock and the groundwater.
6. It should provide adequate impermeability against water.

Preliminary test showed that the cement used in this research work is stable if the water/cement ratio is less than 1.5. Homogeneity of the grout was ensured by the use of a turbo-mixer. The resistance of the grout to chemicals present in the groundwater and rock was not investigated within the current research.

Two basic tests tests—rheology and density were used to characterize the cement grout.

7.1.1 Density Test

In flow analysis, the density of the fluid appears in the governing equations. For a successful numerical simulation, measurement of the density of the fluid is a necessity. The procedure for the measurement of density is as follows— The mass , M_e of each of the three 0.25 l empty measuring cylinders was noted. The cylinders were subsequently filled with known volume, V of cement suspension. The mass, M_f of each of the filled cylinders was measured. The density was calculated from the relationship $\rho = (M_f - M_e)/V$. The density for a mix is taken as the average of the three values calculated.

7.1.2 Rheological Test

The rheology of the grout is of central importance to both the experimental and the theoretical components of this work. Rheological measurements were necessary for

- the determination of the optimum dose of fluidizer for a given water/cement mix, and
- for the determination of the parameters in the constitutive equation which was required for the numerical simulation of grout flow.

A fluid being injected is subjected to shear stress. Roughly, the shear stress, τ, developed within a flowing fluid is a function of the geometry of the flow path and the pressure gradient, while the shear rate, $\dot{\gamma}$, is a function of velocity and the geometry of the flow path. The relationship between the shear stress and shear rate defines the constitutive equation for the material (see equation 5.1). Equation 5.1 can also be written as

$$\dot{\gamma} = g(\tau) \tag{7.1}$$

Experimental measurement of the rheological parameter involves the determination of shear stress as a function of shear rate. Determination of the optimum dose of fluidizer involves determining the minimum amount of fluidizer to minimize the flow parameters.

From section 5.1, the Bingham's equation:

$$\tau = 0, \quad \tau < \tau_y$$
$$\tau = \tau_y + \mu_p \dot{\gamma}, \quad \tau \geq \tau_y$$

approximates the flow behaviour of cement grout. The yield stress in both the Bingham's equation (equation 5.3) and Herschel-Bulkley's equation (equation 5.4) is defined as *the shear which must be exceeded before the commencement of flow*. The concept of yield stress is not universally accepted. According to Barnes and Walters (1985), yield stress is a result of inaccurate equipment used for the measurement of flow properties of materials and that there exists no yield stress when accurate equipment at low stresses is used. Cheng, as reported in Haimoini and Hannant, (1988) argued that yield stress is not a unique material property and that its magnitude depends on the time allowed to determine whether or not the material has stopped flowing under the action of a given stress. The above different views can be reconciled as follows— If a material is sheared slowly in such a way that it is allowed to respond fully under a given stress, it will not exhibit yield stress, however, the same material when sheared rapidly may exhibit yield stress.

It is therefore important to take rheological measurements for estimating flow parameters under experimental conditions, similar to those the material will be subjected to in the process being simulated. During injection process, the rate of shearing of the grout is rapid enough for the grout to exhibit yield stress (see Ashikmen and Pronina, 1985). Furthermore, the yield stress also depends on whether the material is being sheared under increasing shear rate or decreasing shear rate. The yield stress measured under increasing shear rate is called *static yield stress* while that measured under decreasing shear rate is called *dynamic yield stress*. Usually static yield stress is greater than dynamic yield stress. With respect to the constitutive equation, the dynamic yield stress is relevant in simulating injection because under injection, the material is being subjected to decreasing shear rate. The static yield stress is important in estimating the pressure required to re-start injection in a fissure which has been shut down (e.g. because of breakdown in the pipeline) while filled with injection material.

7.1.3 Equipment for Rheological Measurement

The equipment for measuring the flow properties of injection materials (cement suspension) can be classified into two. The first class is the equipment that yields single parameter (such as the time required for a given quantity of material to flow through a specified channel dimension). Examples of this type of equipment include Marsh Funnel, *Kasumeter* and Cohesion Plate Meter (Lombardi,1983) (see section 2.3.2). The other class of equipment are those suitable for measuring more

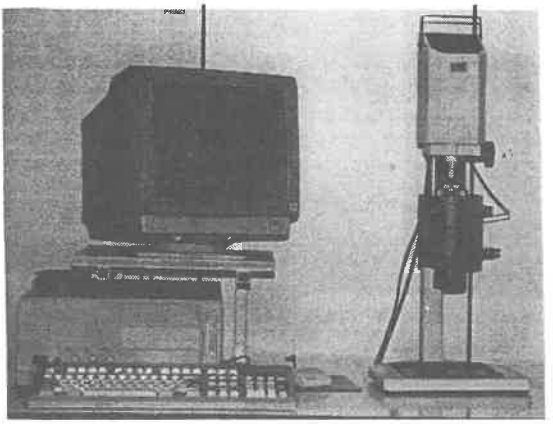

Figure 7.1: Rheometer MC1 from Paar Physica

than one flow parameter. Examples of this class include common laboratory viscometer e.g. Plate and Cone, Plate and Plate, Concentric Cylinder and Capillary viscometer. The earlier group are characterized by their simplicity and they can be used for rough and relative determination of the flow characteristics. Most of them are not standardized and this makes comparison of reported results very difficult. The latter group is available in various levels of sophistication.

As stated earlier, it is necessary to take rheological measurements at conditions similar to those in the process being modeled. Only a computer controlled viscometer meets this criterion. The cheapest computer controlled viscometer is the concentric cylinder type. Consequently, this type was adopted for the rheological measurements in this research.

7.2 The Concentric Cylinder Viscometer

The concentric cylinder viscometer used for this research is the Rheometer MC1 manufactured by Paar Physica (figure 7.1). The measuring system consists essentially a rotating inner cylinder (bob) in a hollow stationary cylinder (cup) in which the sample is placed (Figure 7.2).

7.2.1 Analysis of Result—Theory

The method of analysis discussed below is based on the following assumptions.

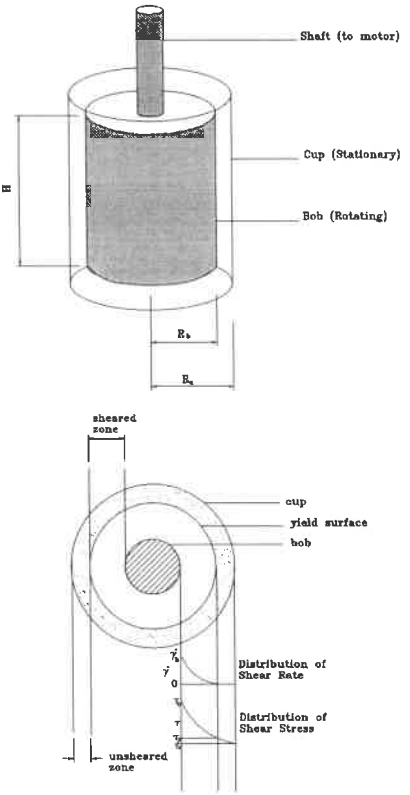

Figure 7.2: Measuring system of viscometer

1. the yield stress can be measured experimentally,
2. flow is steady, laminar and the fluid is incompressible,
3. there is no slippage at the fluid /cylinder interface,
4. the fluid flow is two dimensional

To determine the flow parameters of a material, the torque, T at the bob is measured as a function of its rotating speed, ω. The shear stress τ_r at distance r (see figure 7.2) within the annulus is calculated from the measured torque using the relationship given in Equation 7.2.

$$\tau = \frac{T}{2\pi r^2 H} \tag{7.2}$$

At the bob, $r = R_b$, therefore the shear stress at the bob, $\tau_b = T/(2\pi R_b^2 H)$ in which H is the height of the bob.

The shear rate, within the annulus is given by Equation 7.3.

$$\dot{\gamma} = r\frac{d\omega}{dr} = r\frac{d\omega}{d\tau}\frac{d\tau}{dr} \tag{7.3}$$

where ω is the instantaneous angular speed. To obtain the shear rate at the surface of the bob, Equation 7.3 has to be solved with the boundary conditions that at $r = R_b$, $\omega(R_b) = \Omega$.
From Equation 7.2, Equation 7.3 can be written as:

$$\boxed{\dot{\gamma} = -2\tau\frac{d\omega}{d\tau} = g(\tau)} \tag{7.4}$$

From Equations 7.4 and 7.3,

$$d\omega = \dot{\gamma}\frac{dr}{r} = -\frac{1}{2}\frac{g(\tau)d\tau}{\tau} \tag{7.5}$$

The integration of equation 7.5 yields:

$$\boxed{\Omega = \int_{R_b}^{R_c} \dot{\gamma}\frac{dr}{r} = -\frac{1}{2}\int_{\tau_b}^{\tau_c} \frac{g(\tau)d\tau}{\tau}} \tag{7.6}$$

Equation 7.6 can only be solved only if $g(\tau)$, the constitutive equation is known. With the Newton's equation:

$$g(\tau) = \frac{\tau}{\mu} \tag{7.7}$$

and substituting equation 7.7 in equation 7.6, yields the shear rate at the surface of the bob:

$$\dot{\gamma}_b = \frac{2\Omega R_b^2}{R_c^2 - R_b^2} \tag{7.8}$$

With the Bingham's equation:

$$g(\tau) = \frac{(\tau - \tau_y)}{\mu_p} \tag{7.9}$$

equation 7.6 after integration yields:

$$\Omega = \frac{T}{4\pi\mu}\left(\frac{R_c^2 - R_b^2}{R_b^2 R_c^2}\right) - \frac{\tau_y}{\mu}\ln(\frac{R_c}{R_b})^2 \tag{7.10}$$

From the slope of the graph of the angular velocity Ω against T the value of μ can be calculated provided the stress in the material within the annulus is greater than the yield stress. For the situation where the yield surface is within the annulus, the distance of the yield surface from the center of the bob can calculated using equation 7.11 below.

$$r = \sqrt{\frac{T}{2\pi\tau_y}} \tag{7.11}$$

Under this condition equation 7.6 yields

$$\Omega = \frac{T}{4\pi\mu}\left(\frac{T - 2\pi\tau_y R_b^2}{R_b^2 T}\right) - \frac{\tau_y}{\mu}\ln\frac{T}{2\pi\tau_y R_b^2} \tag{7.12}$$

Having discussed methods of analysis of results, it is important to highlight problems of measuring the flow parameter of cement suspension. The foregoing analysis assumed no slip condition (that is there is no relative movement between cement suspension at both the surfaces of the bob and the cup.) For this assumption to be valid special experimental precautions have to be taken. Mannheimer, (1983) demonstrated that slippage introduces large errors into the flow parameter obtained using a conventional smooth surfaced viscometer. The poor experimental data reported in Raffle, (1977) can also be attributed to slip at the suspension/wall interface. The problem of slippage can be handled in two ways:

- The first involves an analytical method for correcting the flow curve for slippage effect. This approach was pioneered by Mooney (1931) and a modification of the Mooney's classical work was proposed by Yoshimura and Prud'homme (1988).
- The second method is experimental and involves replacing the smooth surface of the measuring cylinders with a rough surface to prevent slippage. The experimental approach was used in this work.

7.2.2 Sample Preparation

The ultrafine cement (Microcem A), the fluidizer (*Injektion Hilfe 1 - IH 1*) and the high speed mixer used for this work were supplied as a complete package by the cement manufacturer— Heidelberger Baustofftechnik, Leimen. According to the material data supplied by the manufacturer, the specific surface of the cement is 11000 cm^2/g. For a given type of mixer, the physical properties of cement suspension produced are time dependent. In order to obtain comparable results it is very important to follow rigidly a defined sample preparation procedure. The sample preparation is as follows—Half the required dose of fluidizer for a given mix is mixed with water for 5 seconds. As mixing continues, the cement is added to the water/fluidizer mixture gradually within the next 2 minutes and 55 seconds. The remaining half of the fluidizer is added to the mixture as mixing continues for 2 minutes, thus bringing the total mixing time to 5 minutes. After mixing in the high speed mixer, the suspension is transferred to a slower mixer where it remains for 1 minute in order to remove entrained air. The quantity of the suspension required for the different tests was taken from the slower mixer. The water/cement ratios (by weight) used are: 1, 1.2, 1.3,1.4 and 1.5 with the following variation in fluidizer/cement (by weight) content : 0%, 1%, 2%, 3%.

7.2.3 Experimental Procedure

As stated previously laboratory measurement of rheological parameters must be made under situations similar to those on site during injection. Therefore the first step in laboratory rheological measurement the estimation of the range of shear rate on site. This was estimated to be between 0 to 100 -/s. On site, the injection material is subjected to the highest shear rate very close to the entry into the fissure and finally reduced to zero at the end of injection. Therefore, in the laboratory the specimen should be subjected to decreasing shear rate from the estimated 100 -/s. If injection stops for whatever reason and later continued the shear rate increases from zero to a maximum value after which it decreases to zero again. Under this condition the rheology measurement as stated above should be augmented with measurement under increasing shear rate. Rheological results are discussed in Chapter 8.

7.3 Suitability Test, Water Pressure Test and Physical Simulation of Grouting

The rock discontinuity was initially modeled with Plexiglas. The cylindrical model (figure 7.3) was 250 mm in diameter and 75mm high. It was cut into

six (6) sectors which are radially movable in order to define various sizes for the 3 intersecting vertical discontinuities. At the centre of the block is a hole which facilitates injection. The sectoral blocks are held together with three metal bands. The ends of the block are sealed with silicon rubber situated between the upper and the lower plates of the sample holder.

The suitability tests (see procedure below) with smooth surfaced Plexiglas (figure 7.4) showed that sufficient bond did not develop between the smooth surface of the Plexiglas and the hardened cement (see figure 7.4). Water resistant sand paper was subsequently gummed to the surface of the Plexiglas to simulate surface roughness. The bond between the grout and sand paper was good and the grout was uniformly distributed across the surface the sandpaper (figure 7.5). However, the surface roughness characteristics of sand paper are different from those of rock surfaces. This might eventually pose problems in adapting laboratory results to field work.

To solve this problem, it was decided that real rock samples should be used. The prohibitive price of obtaining rock specimens of the size and shape of the Plexiglas block forced the use of readily available rock specimens. This however meant that only one discontinuity instead of the three as originally planned can studied. The use of real rock samples however, posed the problem of defining the size of the discontinuity. As discussed in Chapter 3 and highlighted in Chapters 4 and 5, the common practice of using a water pressure test for the determination of a single valued size of discontinuity is not suitable for the analysis of the flow of fluid in rock discontinuities. The lack of a unique single valued size of discontinuity was demonstrated by injecting water into a laboratory sample. Curve AB in figure 7.6 is the flowrate-pressure curve when water was injected from end A of the sample and curve BA the corresponding curve when the water was injected from end B. Obviously, these two results are quite different. The problem—which of the curves should one use to calculate the size of discontinuity? Observation of the rock sample showed that the size of discontinuity at end B is larger than that at end A. From this test, it is clear that the size of the rock discontinuity at the injection point has a high influence on the flow rate through the discontinuity. A simple solution to the above problem might be the specification of direction of injection with the single valued size of discontinuity. However, as discussed in chapter 5, single valued size of discontinuity does not explain the progressive blockage observed during grouting.

As a final solution to the problems highlighted above it was decided that the discontinuity be characterized using variable void geometry. The major advantage of this method of characterization is that is is realist and it can be used to explain the concept of progressive blockage of the distribution. Unfortunately, it is well known that the void geometry within the rock discontinuities cannot be directly observed. Fortunately, water pressure test is routinely carried out on grouting sites

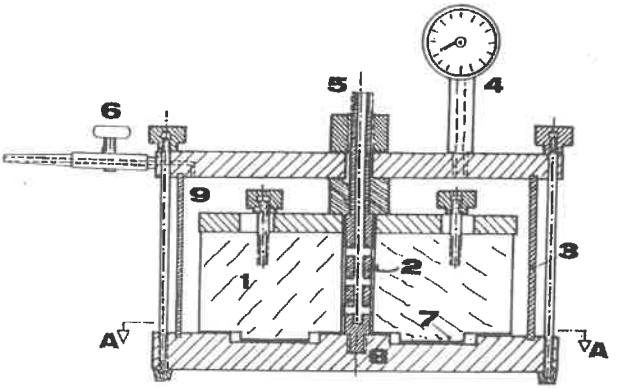

SECTION B - B

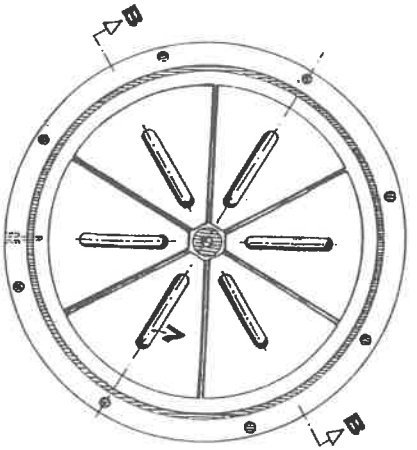

1. Sectorial Block
2. Injection Pipe
3. Cell wall
4. Manometer
5. Pump Connection
6. Overflow Pipe
7. Groove
8. Base Plate

SECTION A - A

Figure 7.3: Model of discontinuity made from Plexiglas (after Smoltczyk)

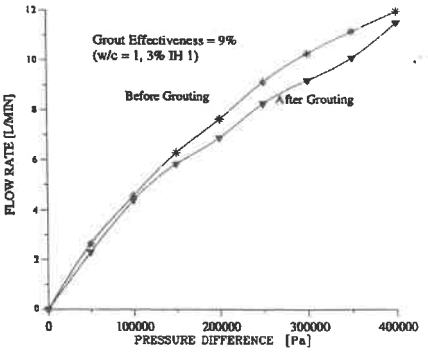

Figure 7.4: Result of suitability test for Plexiglas

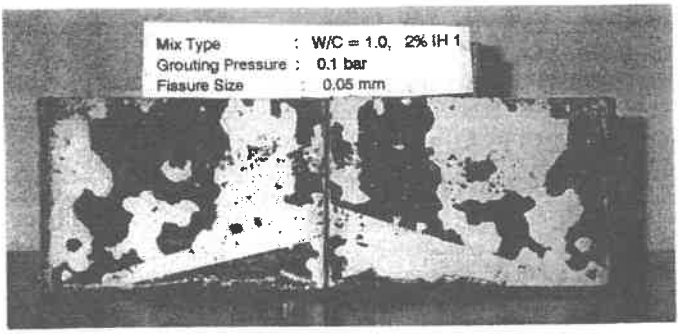

Figure 7.5: Distribution of cement grout within discontinuity simulated with Plexiglas and cement grout

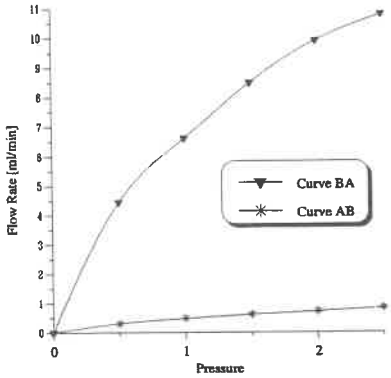

Figure 7.6: Water pressure test for the same rock sample injected from different ends

and the result during transient flow stage can be numerically inverted to obtain information on the geometry of the flow path. However, flow within rock discontinuities takes place only within interconnected voids which does not necessarily cover all available voids (see Chapter 3).

Numerical inversion of the result of transient water pressure test was chosen for the characterization of the void geometry of the flow path. The necessary theoretical base for the inversion process was developed in Chapter 4. It was also decided that the void geometry within the rock discontinuity be characterized using surface geometry of the walls of the discontinuity. The void geometry obtained from surface geometry measurement is used as check on that obtained from numerical inversion. It is here emphasized that the comparison of the results obtained from the two methods are comparable only on the laboratory scale.They are expected to be different in the field. Of course, large scale direct measurement of the geometry of the surfaces of the discontinuities is not feasible in the field. Further, the necessity of application of pressure to the samples to prevent leakage implies the occurrence of deformation of the two surfaces of the discontinuity. Consequently the void geometry obtained from the surface geometry can only be an estimate.

The injection of both water and cement grout was planned to be carried out in

the commercially available Hock's Cell so that the confining pressure for the samples could be quantified. Unfortunately, it was impossible to make the sample-cell interface water tight. This was due to the low degree of flexibility of the synthetic material used to transfer hydraulic pressure to the sample. As a consequence of this, a new sample holder was designed and used as described sections 7.3.2 and 7.6.

7.3.1 Rock Samples

Sandstone and granite samples were used for the test. The samples were cylindrically shaped and are 64 mm in diameter and 125 mm in length. A total of 10 samples were used — 6 granite and 4 sandstone. The granite were labeled G1 to G6 and the sandstones S1 to S4. Samples G1, G2 and G3 were obtained from a stone processing factory in Stuttgart while G4, G5, and G6 granite samples were obtained from a quarry in the Black Forest. All the sandstones samples were from the Rock Mechanics Laboratory at FMPA, Stuttgart. The samples were cored in the laboratory and splitted using the indirect tensile test — the Brazilian method. The modulus of elasticity, E and the poisson ratio, ν were estimated from the Brazilian test. The estimated modulus of elasticity and poisson ratio for samples G1, G2 and G3 are 73.24 GPa and 0.22 respectively while the corresponding values for samples G4, G5 and G6 are 65.4 GPa and 0.28. The E and ν for the sandstone samples are 24.20 GPa and 0.26 respectively. No attempt was made to glue splintered pieces. This however made some samples to have relatively large voids. The surfaces of samples G4 and S3 were scanned with the laser mapper for the estimation of void geometry. Samples G4, G5, G6, S3 and S4 were used for transient water pressure test without taking record of the blockage time. The *Grout Effectiveness* was calculated for all the 10 samples. For the suitability tests and water pressure tests, the samples were submerged in water for 24 hours before the test. This was done to prevent the absorption of water by the rock matrix during the tests.

7.3.2 Characterization of Void Geometry Using Transient Water Pressure Analysis and Simulation of Grouting

The experimental setup for the transient water pressure test is shown in figure 7.7. The flowmeter and the valve V3 were controlled by the computer. The sample holder is described in section 7.6. The injection piping system was filled with water and the pressure in the tank T1 was kept constant with the aid of a constant pressure valve (not shown) which connected it to the compressed air network. In-

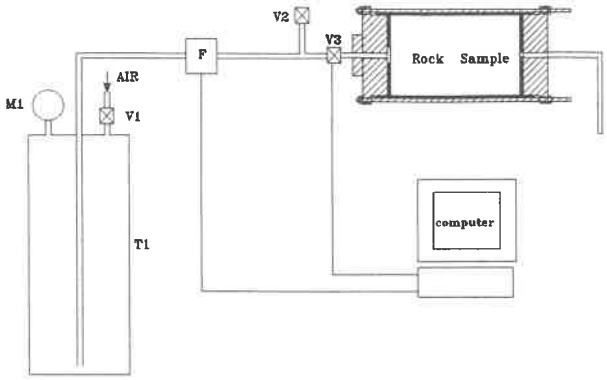

Figure 7.7: Experimental setup for transient water pressure test and grouting simulation

jection of water into the sample was initiated with the activation of valve V3 from the signal in the data acquisition program. The transient flowrate was automatically recorded. Valve V3 was deactivated as soon as the steady state was reached. The result of this test is used in inversion analysis to obtain the variation in the geometry of flow path. The experiment was carried out at 50 kPa, 100 kPa, 150 kPa, 200 kPa, 250 kPa. For all the tests steady state was reached within 6 secs. The setup discussed here was used for the simulation of grouting, except that the flowmeter and the valve V1 were removed and the grout flowrate of the grout measured as in the suitability test. The grouting pressure was 50 kPa for all the samples.

7.4 Characterization of Void Geometry Using Surface Geometry of the Walls of the Discontinuity

The importance of the geometry of the flow path in any flow analysis has been pointed out in different parts of this report. The impossibility of direct measurement of the geometry of the flow path (conducting void geometry) in rock discontinuities was also highlighted. In this section, the method of characterization

of the flow path using the surface geometry of the walls of the discontinuities is reported. The geometry of the two surfaces of a laboratory samples were directly measured by means of a new apparatus which uses laser beam. The void geometry within the rock discontinuity was calculated from the two surface geometries using equation 3.18. The average void at a section a_s is calculated from

$$a_s = \frac{\sum a_i(l, y)|_{y=constant}}{n}$$

in which n is the number of points at a cross-section. The flow path geometry obtained from this section will then be compared with that obtained from numerical inversion of the result of transient water pressure test.

7.5 Measurement of Surface Geometry of Rock Discontinuity using Laser Beam

The laser scanner used for the measurement of the surface roughness of the discontinuity was developed at the Institute of Navigation, University of Stuttgart. In addition to the geometry of the surface, the scanner also records the intensity of the reflected laser ray, hence it is called the *4D-Laser Mapper*.

7.5.1 Procedure

A block diagram of the 4D-Laser mapper is shown in figure 7.8. It consists 4 major components—signal processing unit, laser unit, scanning unit and the computer. The laser unit produces the laser beam which is modulated with sinusoidal signal from the signal processing unit. The beam is fed into a scanning unit which consists essentially of mirrors and a mechanical system for moving the modulated laser beam across the surface of the rock discontinuity. The motion of the laser beam across the surface of the rock discontinuity is as shown in figure 7.9 As the laser beam traverses the surface of the discontinuity, the detector of the reflected beam, whose movement is synchronized with the source of the incident beam, records the arrival of the reflected beam. The signal processing unit which is directly connected to the computer, processes the signal from the detector of the reflected beam. The computer coordinates the activities of the other components and produces the coordinates—(x,y,z), and reflection coefficient of points on the surface of the rock discontinuity.

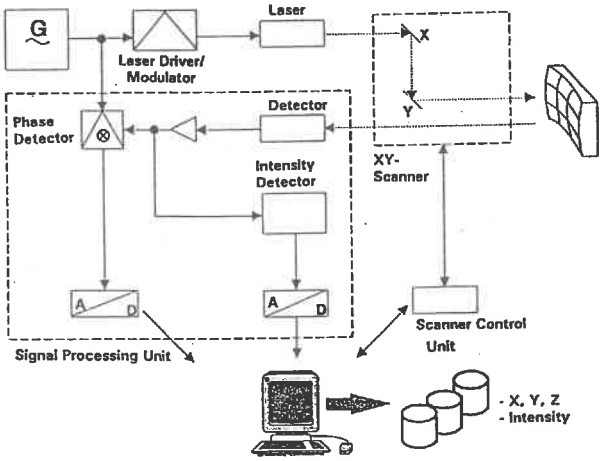

Figure 7.8: The 4D Mapper (after Hartl et al., 1992)

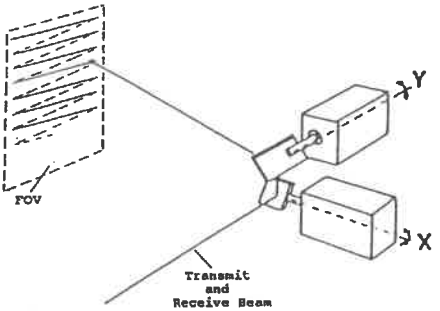

Figure 7.9: Motion of laser beam across rock discontinuity (adapted from Hartl et al., 1992)

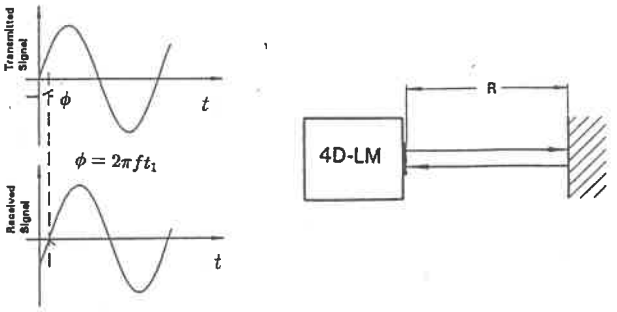

Figure 7.10: Phase difference and range measurement (after Hartl et al., 1992)

7.5.2 Fundamental

If the speed of light, an electromagnetic wave is c and R is the distance between the scanning unit and the surface of the discontinuity, a wave front which leaves the source at time $t = 0$ will travel a distance $2R$ (see figure 7.10) and arrives at the detector of the reflected ray at time $t = t_1$. The time t_1 can be calculated from

$$t_1 = \frac{2R}{c}$$

The phase difference between the transmitted and received beam is

$$\phi = 2\pi f t_1$$

where f is the frequency with which the laser beam is modulated. R is calculated from

$$R = \frac{1}{4\pi f} c\phi$$

The above calculations are automated. Two rock samples— granite sample 4 and sandstone sample 8 were scanned with the laser maper. Each scanned surface consisted of data 20 700 points.

7.6 Suitability Test

The experimental setup for the physical simulation and suitability test is shown schematically in figure 7.11 and photographically in figure 7.12. Tank T3 which

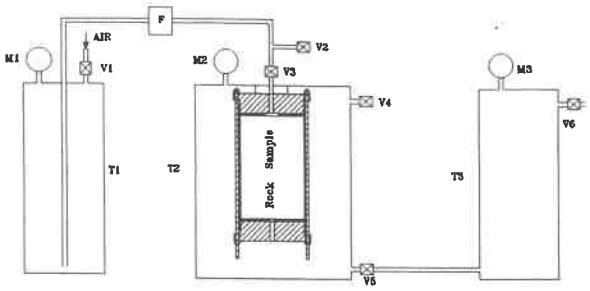

Figure 7.11: Experimental setup for the suitability test

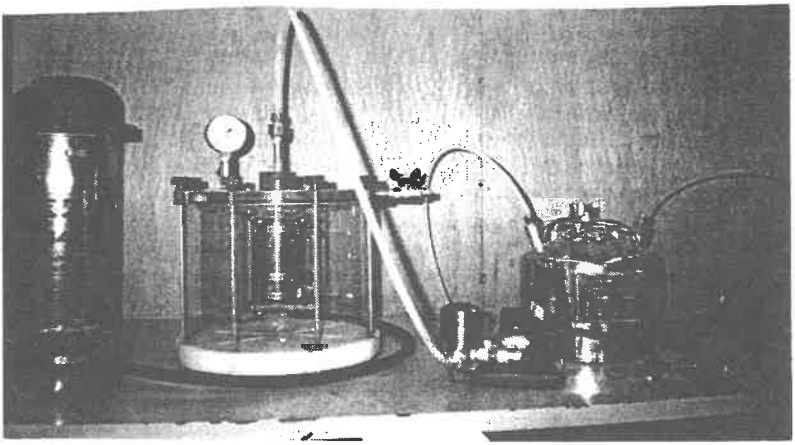

Figure 7.12: Photograph of the experimental setup for the suitability test

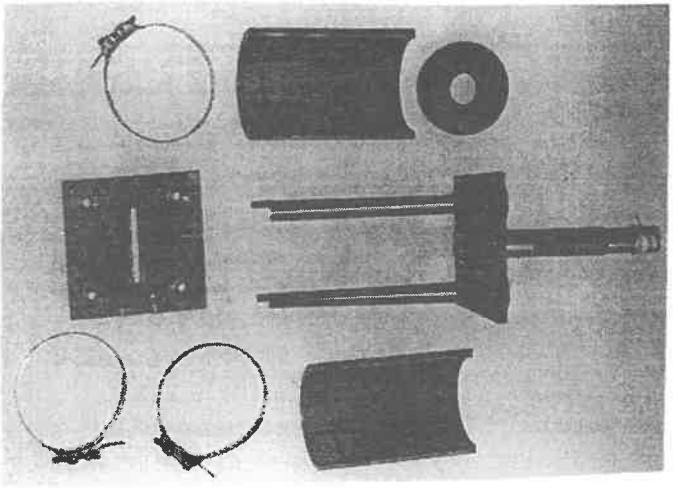

Figure 7.13: The sample holder

is connected to a hand pump through valve V6 is used to pressurize tank T2, thus simulating groundwater pressure. Tank T1 is used for the injection of both water and the cement suspension. It is connected to compressed air network through valve V1 which maintains constant pressure in tank T1. Tank T2 contains the specimen holder (SH) (see figure 7.13) which consists basically of two flat plates and long screws for clapping the sample. The upper and lower plates have a hole which facilitates injection. The flowmeter is only used for the water pressure test. The flow rate of the cement suspension was measured by monitoring the changes in weight of the injection tank, T1. The samples were reassembled and surrounded by tight fitting neoprene rubber and stiffened by a steel tube diametrically cut into two and held together by three metal bands. The ends of the samples were sealed with silicon rubber situated between the upper and lower plates of the specimen holder (figure 7.13). The water in tank T2 was kept at 10kPa for the all the suitability tests. For the granite sample G1, G2, G3 and sandstone samples S1 and S2 the water pressure were implemented at 100 kPa, 200 kPa, 300 kPa and 400 kPa.

Experimental Procedure

The experimental procedure is as follows

1. Execution of water pressure test (WPT) to assess permeability of the discontinuity and calculation of T_0.

2. Injection of cement suspension and measurement of its flow rate .

3. Repeat water pressure test to assess effectiveness of the cement suspension against water 24 hours after injection and calculation of T_1.

4. Calculation of Grout Effectiveness defined in equation 7.13.

$$\frac{T_0 - T_1}{T_1} \tag{7.13}$$

where T_0 is area between the flow rate/pressure curve the pressure axis before grouting T_1 is area between the flow rate/pressure curve and the pressure axis for a given configuration of discontinuities, 24 hours after grouting. The maximum pressure used for the water pressure test must be stated always since Grout Effectiveness is a function of the maximum pressure used.

7.7 Computations

The transmission line modeling method and its implementation are described in Chapter 6. The numerical inversion process is described in Chapter 4. In this section, specific details on the use of TLM for the one dimensional case within the current work are described. The required parameters for the numerical simulation of the water pressure test are — viscosity of water, ν, and the elasticity, E, and the poisson ratio, ν of the rock. For the numerical simulation of grouting, the required parameters are the yield stress, τ_y, and the plastic viscosity, μ_p, of the grout and the elasticity modulus, E, and poisson ratio, ν, of the rock.

The initial conditions was set: $p = p_g$, $v = 0$ at $t = 0$ at the injection end of the sample, $l = 0$. p_g is the grouting pressure. The boundary conditions are: $p = p_g$ for $0 < t < t_e$ in which t_e is the time at the of simulation. The average velocity,v, was calculated at the injection end of the sample by multiplying the flowrate with the cross sectional area.

The flow path was discretized into 200 units to correspond with the scanning points obtained from the mapper. since it was impossible to visually (e.g. by using camera) follow the spread of the grout within the rock discontinuity, calculation of time, within which the discontinuity get blocked was calculated. For the gradient, $\mathcal{J}_{crit}$ on the basis of local distance between the walls of the discontinuity and yield stress, τ_y of the grout. As explained in Chapter 5 blockage of the discontinuity was assumed to occur once the local pressure gradient within a unit becomes equal to or less that less than $\mathcal{J}_{crit}$ for that unit.

For the numerical inversion computation, iteration was stopped once the latest series of $\mathbf{a}_s$ are all within 10% of the corresponding penultimate $\mathbf{a}_s$ values. Numerical simulation results are presented in Chapter 8.

Chapter 8

Analysis of Results

Research procedure are discussed in Chapter 7. In this chapter, the results obtained from the procedures are presented and discussed.

8.1 Characterization of Grout

The range of density for all the mixes is 1.3 -1.37 g/ml. Figures A.1 and A.2 show typical results of rheological tests while table 8.1 shows the summary of the rheological parameters for all the mixes tested.

From the table and figures, the effectiveness of the fluidizer in reducing the flow parameters of the grout is obvious. On the basis of the results in table 8.1, for the particular grout mix, there exit a critical concentration of IH 1 at which its effect very pronounced. This critical concentration for grout mix with water/cement = 1 lies between 2% and 3%. For the rest of the mixes test it lies between 1% and 2 %.

8.2 Characterization of Void Geometry

Typical surface generated from the surface geometry data obtained from the laser mapper is shown in figure A.3. The of average distance between the walls of the discontinuity for the two surfaces whose surfaces were scanned are shown in figures A.4 and figure A.5.

Figure A.6 shows the typical transient flowrate curve. The result of this test was used for the inversion analysis (see Chapter 4) to obtain the variation in the geometry of the flow path. In figures A.4 and A.5, the void geometry obtained from the inversion of the result of transient water pressure test is labeled synthesized while that obtained from the surface geometry data acquired with the laser mapper is labeled *measured*.

w/c ratio	conc. of IH 1 [%]	Yield Stress, τ_y [Pa]	Plastic Viscosity, μ_p [mPa.s]
1.0	0	18.28	157.78
	2	12.40	136.30
	3	4.18	48.04
	5	1.80	21.27
1.1	0	17.01	140.91
	1	12.00	126.54
	2	10.93	52.73
	3	2.61	28.01
1.2	0	16.05	125.89
	1	11.86	111.60
	2	9.59	40.01
	3	2.06	22.05
1.3	0	15.01	119.98
	1	8.23	102.78
	2	5.41	46.29
	3	3.04	20.08
1.4	0	14.89	109.87
	1	6.76	100.82
	2	3.01	40.44
	3	1.67	20.05
1.5	0	14.63	97.50
	1	6.11	97.00
	2	2.28	36.25
	3	-	-

Table 8.1: Rheological parameters of cement grout

Comparison of the two curves shows that the values of the average distance between the walls obtained from the two methods are similar only at locations close to the injection point. The values are however different at locations farther away from the injection point. From this, one can conclude that the transient water pressure test as performed within this research program can only be used to predict the size of the voids at distance close to the injection point. This distance was about 20% of the total length of the discontinuities used.

8.3 Simulation of Rock Grouting

Figures A.7,A.8,A.9,A.10 and A.11 shows flowrate-time curve during grouting of the different samples while table 8.2 is the summary for the grouting simulation test. All the samples used for this test were injected with a grout: water/cement ratio 1% and 3% IH 1. Because the inversion of the result the transient water pressure was not capable of predicting the sizes of voids at distances between the walls of the discontinuity for the total length of the sample, numerical simulation of grouting was done only for the samples G6 and S3 using the void geometry obtained from the surface geometry. Table 8.2 show that the summary of the result of the simulation. The numerical results were lower than the experimental result but were within a deviation of 20%.

Sample	Experimental Blockage Time[min]	Numerical Blockage Time
G4	2.8	-
G5	5.3	-
G6	6.5	5.3
S3	3.1	2.6
S4	2.1	-

Table 8.2: Summary of blockage time

8.4 Suitability

Typical results for the suitability test are shown in figures A.12 and A.13. Rock samples G3 and S2 were injected with grout mix with water/cement ratio 1 without IH 1. Table 8.3 is the summary of the suitability test for all samples tested. Figure A.14 shows grouted sample.

For all the cases, the injected grout was able to withstand the maximum achievable pressure of 400 kPa in the first series of tests and 250 kPa in the second series without being washed out. Granite samples showed consistently higher grout effectiveness than sandstone samples. From these preliminary observations it seems the void volume in the rock matrix affects its grout effectiveness. Furthermore, it was noted, that during injection, for a constant grouting pressure and constant length of specimen the flowrate of the grout decreases with time until the flow stopped completely. The grouted rock samples were examined after the test. Some were easily separated while it was impossible to separate others. The distribution of voids within the discontinuity played a predominant role in determining whether the sample can easily be separated after injection or not. In general, separation of the samples with fairly uniform void distribution was not possible. Separation of the sample was not possible in cases where the void at the injection end was larger than farther away. However separation was easy if the void at injection end was smaller than farther away. The relative size of the discontinuity at the injection end determines the retention of grout within the discontinuity. On the penetration of the grout into fine voids, the grout penetrated very fine voids at the absence of larger connected voids within its vicinity. However, fine discontinuities were not filled with presence of larger connected voids.

Interestingly, 100% grout effectiveness was achievable when sand paper glued

Sample	Grout Effectiveness [%]
G1	93.80
G2	99.76
G3	92.24
G4	97.82
G5	98.47
G6	91.40
S1	82.63
S2	87.5
S3	92.5
S4	85.17

Table 8.3: Summary — suitability test results

to Plexiglas was used to simulate rock discontinuity (Akinrogunde, 1994). However, this was not possible with real rock discontinuities.

Chapter 9

Conclusions

There is a lot of room for improvement in rock grouting as it is currently being practiced. The research reported here was aimed at understanding the physics of rock grouting and the development of a test which can be used as a quality assessment tool in grouting projects.

The superplasticizer (IH 1) supplied with the ultrafine cement was highly effective in reducing both the yield stress and plastic viscosity of the grout. IH 1 is chemically active and its long term effect on the environment is yet to be investigated. Although the manufacturer claimed that IH 1 is environmentally compatible, it is most probable that the use of such additive might be outlawed in the future. Fortunately, the apparatus for the suitability test developed within this research work can be use to assess the long term effects of the cement grout which contains fluidizer.

Until now all the available theories on the flow of grout within rock discontinuities concentrated mainly on the rheological properties of grout. The walls of the discontinuities were simply assumed to be parallel. Consequently, laboratory models were constructed with smooth surfaced material (in most cases Plexiglas). Interestingly, results of flow simulations within these models always correspond with numerical simulations. However, the similarity between the constructed models and real rock discontinuities was never investigated. It was not surprising therefore that these models do not explain the observed flow behaviour of grout within real rock discontinuities. Within this report, the importance of the geometry of the flow path in explaining observed grout flow behaviour was demonstrated. Acquisition of geometric information of the flow path within the rock discontinuities which are not accessible constituted a problem. Furthermore, the process of solving Navier-Stokes equations, which governs the flow of fluids, for a flow domain in rock discontinuities with irregular and dynamic boundary is a formidable task.

These two problems were solved within this research by developing simplified equations for the flow of fluids within rock discontinuities and through the

numerical inversion of the result of water pressure test during transient flow stage. However, this approach make automatic acquisition of flow data mandatory. This should not pose problems as the trend in grouting is towards automation.

The application of the developed solution on the laboratory scale showed that information on the geometry of the flow path within the rock discontinuity at distances close to the injection point can be obtained from the numerical inversion of the result of transient water pressure test. Flow path geometry at locations farther away from the injection point were not obtainable. This pointed to the need for more data acquisition point at locations farther away from the injection point. With the information acquired from additional locations, numerical inversion can be used to obtain complete information on the geometry of the flow path.

Until now, there is no generally available simple test for the assessment of quality of injected grout. Within the framework of this research, a test — suitability test for rock grouting materials has been developed. This test is essentially a quality assurance test. It is used to assess the injectability and sealing effectiveness of injected grout. Other tests such as the resistance of grout to chemically contaminated water can also be investigated with the apparatus developed. The test results showed that ultrafine cement can penetrate very fine discontinuities and has good sealing characteristics. However, complete sealing of the discontinuities was not achieved. The suitability test can be used to write specifications for grouts by stating , for example, the minimum *grout effectiveness* for a project.

The result of simulation of injection of grout using transmission line modeling looks promising. Testing of the method in the field is recommended. An important feature of the transmission line is it is unconditional stability. Preliminary work on direct inversion of the transmission line method is currently being undertaken. Current effort are restricted to lossless transmission lines. Perhaps, future development may be extended to lossy line such as use in this work.

Only fine (mated) discontinuities could be investigated within this work because of the necessity to apply pressure around the sample to present leakage. The use of an apparatus within which distance between the walls of the discontinuity can be varied would provide more information. However, such apparatus will be very complex and expensive. In addition, a repeat of the investigation discussed in this report in the field will eliminated the need for a very complex apparatus, but it will also be expensive. For the field investigation, advantage of tunneling projects in rock can be taken by grouting discontinuities which can later be examined as tunneling progresses.

The suitability test developed within this research is a simple quality assurance test. During the planning stage of grouting projects, it can be used in selecting suitable materials or grout mixes to assess the permeability of different grouting materials. At the construction site, it can be used to assess the permeabilty of injected materials by using cores as test pieces.

Finally, a new theory of rock grouting was developed. The unique feature of the theory is that it extends currently available theory by incorporating the effect of the irregularity in the geometry of the flow path into the physics of rock grouting. The theory emphasizes that blockage of the flow path is a progressive phenomenon which occurs as grouting progress. It is recognized that more work still have to be done on the transmisssion line analysis as used in this research work, it is envisaged that the its practical application in combination with the suitability method should be as shown in Figure 9.1

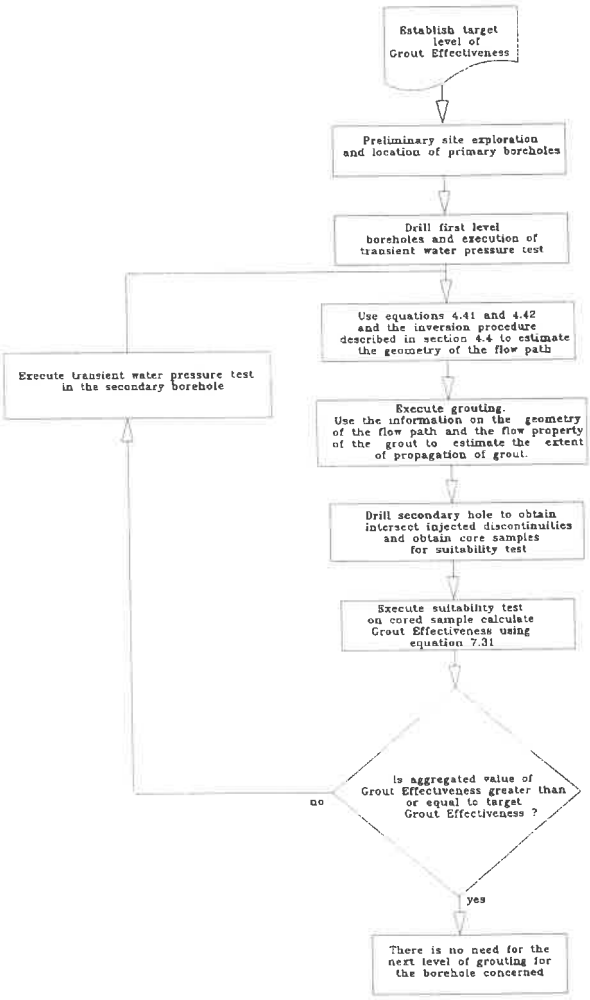

Figure 9.1: Proposed chart for using suitability test and transmission line modelling

Appendix

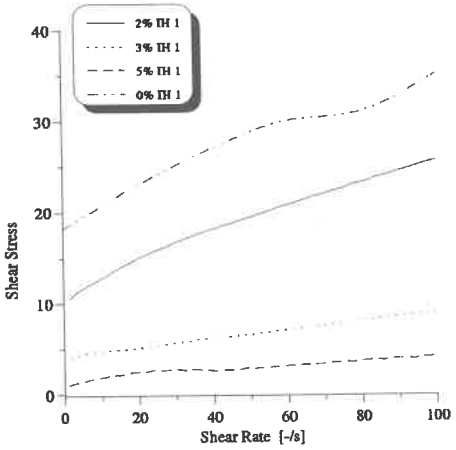

Figure A.1: Flow curve for grout with water/cement ratio 1

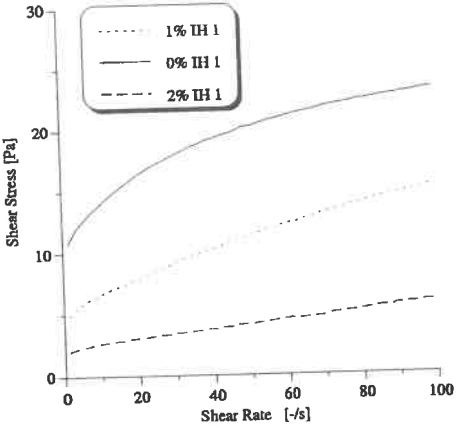

Figure A.2: Flow curve for grout with water/cement ratio 1.5

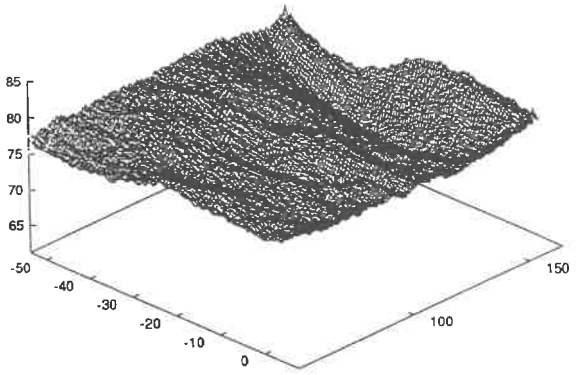

Figure A.3: One of the generated surfaces of sample S3 from the laser mapper data

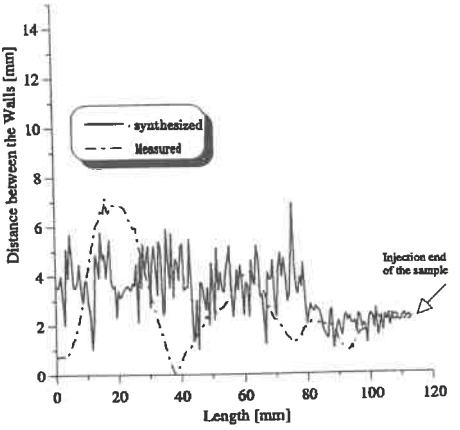

Figure A.4: Flow path geometry for sample S3 — measured and synthesized

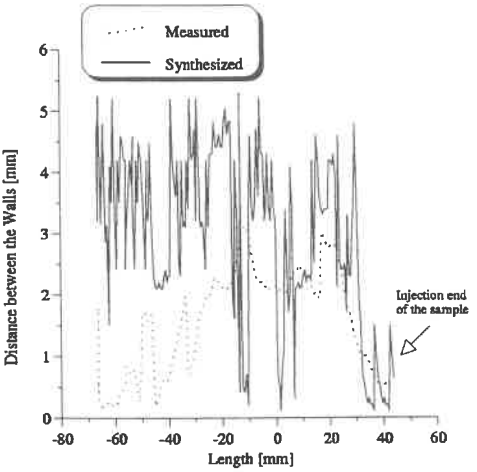

Figure A.5: Flow path geometry for sample G6 — measured and synthesized

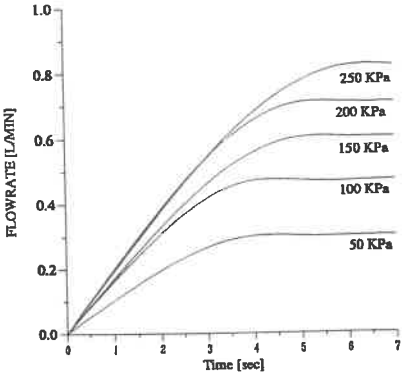

Figure A.6: Transient flowrate-time curve for granite sample G4

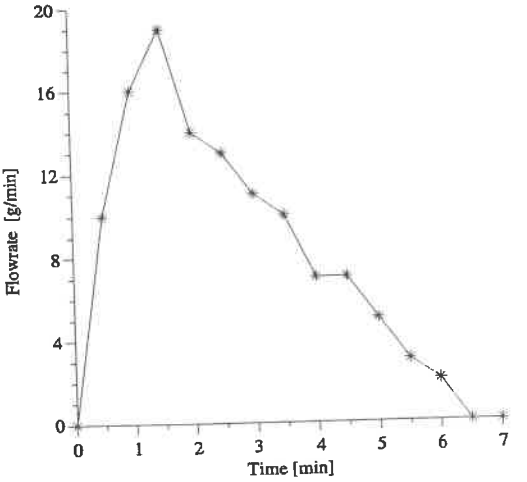

Figure A.7: Flowrate-time curve for granite sample G4

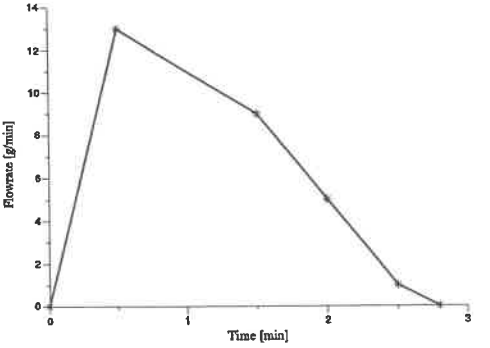

Figure A.8: Flowrate-time curve for granite sample G5

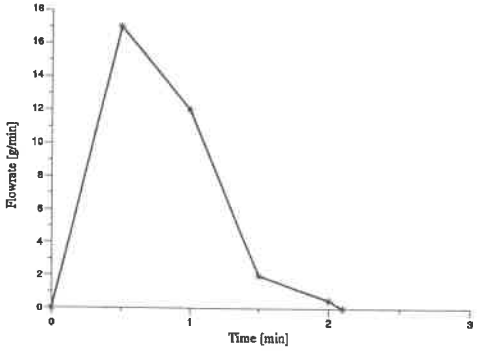

Figure A.9: Flowrate-time curve for granite sample S4

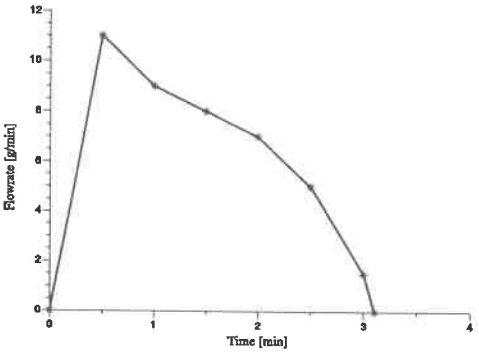

Figure A.10: Flowrate-time curve for sandstone sample S3

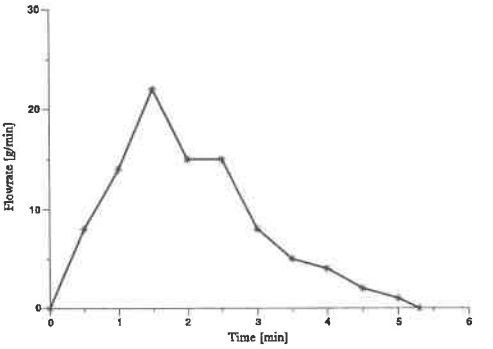

Figure A.11: Flowrate-time curve for sandstone sample G5

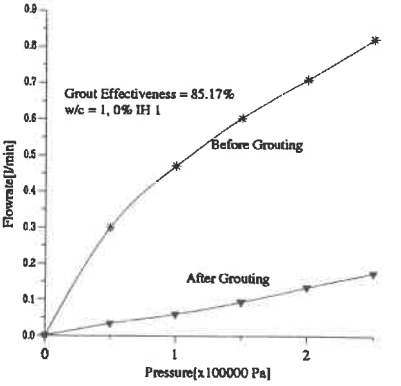

Figure A.12: Result of suitability test for sample G1

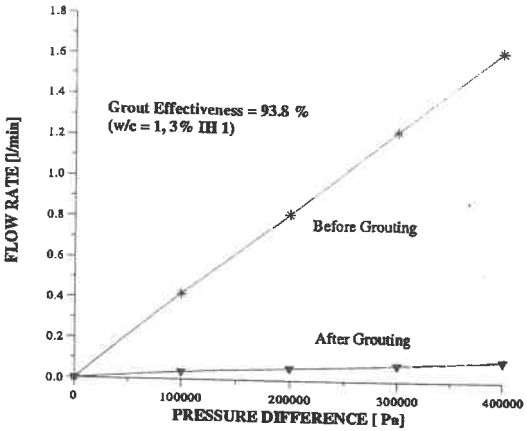

Figure A.13: Result of suitability test for sample S4

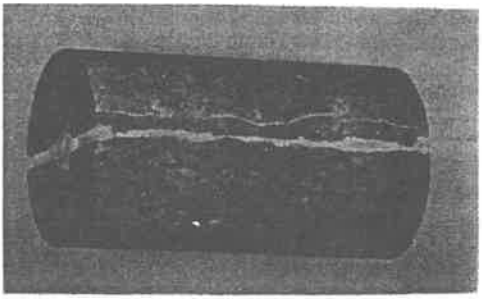

Figure A.14: Grouted sample

Bibliography

Abdali, S.S, E. Mitsoulis and N.C. Markatos (1992): Entry and Exit Flows of Bingham Fluids. . *J. Rheol.*, Vol. 36, No. 2., p389-407.

Abelin, H, L. Birgersson, L.Moreno, H. Widen, T. Agren and I. Neretnieks (1991): A large-Scale flow and Tracer Experiment in Granite 2. Result and Interpretation. *Wat.* Res. Research.. Vol. 27, No. 12, p3119-3135.

Acton, F.S., (1990): *Numerical Methods that Usually Work.* The Mathematical Association of America Washington D.C.

Anderson, J.D., (1995): *Computational Fluid Mechanics.* McGraw-Hill.

Alvarado, D.A. and S.S. Marsden,(1979): Flow of Oil-in-Water Emulsion Through Tubes and Porous Media. *Soc. of Pet. Journal*, Vol. 19. p369-377.

Akinrogunde, E. A. (1994): *Documentation of the Research on Fundamental Studies of Rock Grouting.* Unpublished report.

ANON, (1983): Micros Step into Dam Grouting. *Engg. News Record*, Dec. 15, p 31.

ANON, (1984): BuREC Grout Monitoring Automated on Utah Dam .*Engg. News Record*, July, 5, p 20-21.

Ashikmen, V.A. and L.E. Pronina, (1985): Rheological Properties of Dispersed Cement Grout. *G*idroteknidchesko Stroitel'stvo (translated from Russian), No. 10, p34-38.

Aydan, Ö, Y, Shimizu and T. Kawamoto (1996): The Anisotropy of Surface Morphology Characteristics of Rock Discontinuities. *R*ock Mech. and Engg. Vol. 29 No. 1 p47-59.

Baker, J.W. (1955): Flow in Fissured Formations. *Proc. 4th World Petroleum Congr.,*, p 379-393.

Barnes, H.A. and Walter, K. (1985): The Yield Stress Myth. *Rheo.* Acta. Vol. 24, p323-325.

Barton, N and V. Choubey, (1977): The Shear Strength of Rock Joints in Theory and Practice. *Rock Mech.*, Vol. 10 p1-54

Barton, N., S. Bandis and K. Bakhtar (1985): Strength Deformation and Conductivity Coupling of Rock Joints. *Int. J. Rock Mechs. Min. Sci. and Geom. Abstr.*, Vol. 22 No. 3, p121-140.

Börgesson, L and R. Pusch,( ): Sealing of Fracture Rock Grout Composition and Grout Properties.

Bourke, P.J. (1987): Channeling of Flow Through Fractures in Rock. in *Proc. GEOVAL-87, Swedish Nuclear Power Inspectorate (SKI)*, Stockholm, Sweden.

Bradbury, H.W.(1987): Grout and Grouting . *C*ivil Engineering (ASCE), Jan. p45.

Brown, C.A., P.D. Charles, W.A. Johnsen and S. Chesters, (1993): Fractal Analysis of Topographic Data by Patchwork Method. *W*ear Vol. 161, p61-67).

Brown, E.T. and P.I. Boodt, (1987): Permeability Determination for a Discontinuous, Crystalline Rock Mass. *P*roc. 6th Inter. Congr. on Rock Mech, Montreal p23-30.

Brown, S.R. (1987): Fluid Flow Through Rock Joints: The Effect of Surface Roughness. *J.* of Geophy. Res. Vol. 92, No. B2, p1337-1347.

Brown, S.R. and C. Scholz. (1985): Broad Bandwidth Study of the topography of Natural Rock Surfaces. *J. of Geophysical Research* Vol. 90 No. B14 p12575-12582.

Bureau of Reclamation, (1987): *C*ement Grout Flow Behavior in Fractured Rock. REC-ERC-87-7. U.S. Department of the Interior.

Christopoulos, C. (1995): *The Transmission-Line Modeling Method.* IEEE Press.

Churchill, S.W. (1997): Comprehensiv correlating Equation for Laminar, Assisitng, Forced and Free Convection. *AIChE Journal*, Jan., p10-16

Computational Science Foundation (1995): *Mathematical Optimization.* http://einstein.drexel.edu/csep/MO/MO.html.

Dershowitz, W.S. and H.H. Einstein (1988): Characterizing Rock Joints Geometry with Joint system Model. *R*ock Mechanics and Rock Engineering, Vol. 21, p21-51.

Donier, C and J. Tichy, (1992): Behaviour of a Bingham-like viscous Fluid in Lubrication Flows. *J.* Non-Newtonian Fluid Mech. 45 (1992) p 291-310.

Dwyer, B.P. (1994): Feasibility of Permeation Grouting for Constructing Subsurface Barriers. *Proc. 33rd Hanford Symp. Health Envir. on Instue Remediation: Scientific basis for Current and Future Technologies*, Pasco, Washington, Nov. 7-11.

Ewert, F.-K, (1985): *Rock Grouting with Emphasis on Dam Sites*. Springer Verlag.

Ewert, F.-K, (1996): The GIN-Principle: A Helpful Method for Rock Grouting? Part 1. *W*at. Power and Dam. Feb., p17-19

Ewert, F.-K, (1996): The GIN-Principle Part 2. *W*at. Power and Dam. April., p36-40.

Franklin, J.A. and M.B.Dusseault, (1989): *Rock Engineering*. McGraw-Hill.

Gale, J.E. (1987): Comparision of Coupled fracture Deformation and Fluid Flow with Direct Measurement of Fracture Pore Structure and Stress-Flow Properties. *Proc. 28th Us Symposium on Rock Mechanics*, Tucson 29 June to 1 July, 1987, p1213-1223.

Gustafson, G and H. Stille. (1996): Prediction of Groutability from Grout Properties and Hydrogeological Data. *Tunnelling and Underground Space Technology.*, Vol. 11, No. 3, p325-332.

Hässler, L. (1991): Grouting of Rock - Simulation and Classification. Department of Soil and Rock Mechanics, Royal Institute of Technology, Stockholm.

Håkansson, U., L. Hässler and H. Stille. (1992): Rheological Properties of Microfine Cement Grouts. *Tunnelling and Underground Space Tech.*, Vol. 7 No. 4, p453-458.

Hakami, E. and N. Barton, (1990): Aperture Measurements and flow Experiments Using Transparent Replicas of Rock Joints. in Barton and Stephasson (eds.) *Rock Joints Balkema*, Rotterdam, p383-390.

Haimoni, A and D.J. Hannant, (1988): Development in Shear Vane Test to Measure the Gel Strength of Oilwell Cemement Slurry. *Advances in Cement Research.* Vol. 1, No. 4 p221-229.

Harper, T.R and D.V. Hinds, (1977): The Impression Packer: A Tool for Recovery of Mass Fracture Geometry. *Proc. !st Int. Symp on storage in Excavation Rock Caverns, Stockholm, 5-8 Sept.*, Vol, 2, p 259-266.

Hartl, A. , A. Wehr, G. Pritschow and M. Ioannides. (1992): 4D-Laser Scanning Followd by Internal Computer Model Generation. Proc. 17th Internation Society of Photogrammetry and Remote Sensing., Washington, D.C. p522-527.

Hoefer, W.J.R. (1985): The Transmission-Line Matrix Method—Theory and Applications. *IEEE Trans. on Microwave Theory and Techniques*, Vol. MTT-33, No. 10, p882-893.

Hooton, R.D. and L. Konecny (1990): Permeability of Grouted Fractures in Granite. *Concrete International* July, p48-56.

Houlsby,A.C. (1992): Grouting in Rock Masses, in Bell, F.G. (ed.), *Engineering in Rock Masses.* Butterworth Heineman, p334-350

Houlsby, A.C. (1990):*Construction and Design of Cement Grouting*. John Wiley and Sons. Inc.

Huang, S.L., S.M. Oelfke and R.C. Speck (1992): Applicability of Fractal Characterization and Modeling of Rock Joint Profiles. *Int. J. of Rock Mech. Min. Sci. and Geomech. Abstr.* Vol. 29, No. 2 p89-99.

Huit, J.L. (1956): Fluid Flow in Simulated Factures. *AIChE Journal*, Vol. 2 No. 2 p256-264.

Hwang, N.H.C and R.J. Houghtalen (1996): *Fundamentals of Hydraulic Engineering (3rd Edition).* Prentice Hall.

Iwai, K. (1976): *Fundamental Studies of Fluid Flow Through a Single Fracture*. Ph.D Thesis, University of California.

Jähde, H, (1953): *Injektionen zur Verbesserung von Baugrund und Bauwerk*, VEB Verlag Technik Berlin.

Johns, P.B. and R.L. Beurle (1971): Numerical Solution of 2-Dimensional Scattering Problems Using Transmission -Line Matrix.*Proc. IEE*, Vol. 118, No. 9. p1203-1208.

Johns, P.B. (1974): A New Mathematical Model to Describe the Physics of Propagation. *The radio and Electronic Engineer*. Vol. 44, No. 12. p 657-666.

Johnson,C.D. (1984): *Network Analysis for Technology*. Macmillan Publishing Company.

Keller, A.A., P.V. Roberts and P.K. Kitanidis (1995): Prediction of Single Phase Transport Parameters in A Variable Aperture Fracture" *Geophysical Research Letters*, Vol. 22, No. 11 p1425-1428.

Keller, K and B.P. Bonner, (1985): Automatic Digital System for Profiling Rough surfaces.*Rev. of Sci. Instr.* Vol. 56 No. 2 p330-331.

Kennedy, T.B. (1958): Pressure Grouting Fine Fissures. *J.* Soil Mech. and Found. Div. Proc. ASCE, Paper 1731, p1731-1 - 1731-36

Kleinschnittger, M and K. Holtgrene, (1989): Ergebnisse der Einpreßversuche zur Abdichtung der streckennahen Bereiche. *Vorträge des Seminars Geotechnische Fragestellungen bei Untertagedeponien und Transportvorgängen*, Institut für Grundbau, Bodenmechanik, Felsmechanik und Verkehrswasserbau, RWTH Aachen, p 157-181.

Kollbrunner, C. F. (1948): *Fundation und Konsolidation Band II — Baugrundverbesserungen Baugrube Flachfundation-Tieffundation*. Schweier Druck & Verlaghaus.

Knoblauch, H. (1987): Vergleich versciedener Meßverfahren zur Bestimmung der Fliesßfähigkeit von Einpreßmörteln in bezug auf ihre Genauigkeit und gute Handhabung. *Beton+Fertigteil+Technik*. No. 3, p169-176.

Koerner, R.M. (1984): *Construction and Geotechnical Methods in Foundation Engineering*. McGraw Hill Inc. p 287.

Kosmatka, S.H. (1990): *Cementitious Grouts and Grouting*. Portland Cement Association

Kutzner, C. (1991): *Injektionen im Baugrund*. Ferdinand Enke Verlag, Stuttgart.

Kutzner, C. (1964): Theoretisch Betrachtungen zuir Felsinjektion mit Zement und praktische Folgerungen für die Winterarbeit. *Die Bautechnik*, No. 1, p 2-8.

Kutzner, C and K. Schetelig, (1985): Abdichtung und Vergütung von stark geklüftetem Fels um einer Kraftwerkskaverne (Philippinen). *Geotechnik*, Vol. 8, p 109-114.

Lau, J.S.O., L.F.Auger and J.G. Gibson, (1987): Subsurface Fracture Survey Using a Borehole Television Camera and Acoustic Televiewer. *Can. Geotech. J.*, Vol.24, p499-508.

Lau, D and A. Crawford, (1986): The Cement Grouting of Discontinuities in Rock Masses. *Proc. 27th U.S. Symposium Rock Mechanics*, P854-861.

Lious, C. (1967): *Strömungsvorgänge in klüftigen Medien und ihre Wirkung auf die Standsicherheit von Bauwerken und Böschungen im Fels.* Dissertation, Universität TH Karlsruhe.

Lombardi, G. (1985): The Role of Cohesion in Cement Grouting of Rock. *Proc. Inter. Congr. on Large Dams*, Lausanne., p235-260

Lombardi, G and D.Deere, (1993): Grouting Design and Control using the GIN Principle. *Wat. Power and Dam.*, June, pp 15 -22.

Longwell, P.A., (1966): *Mechanics of Fluid Flow*. McGraw-hIll. 433p.

Lopez, R.s, S.C.H. Cheung, and D.A. Dixon, (1984): The Canadian Program for Sealing Underground Nuclear Fuel Waste Vaults. Can. Geotech. J., Vol. 21, 593-596.

Louis, C. (1967): *Strömungsvorgänge in klüftigen Medien und ihre Wirkung auf die Standsicherheit von Buawerken und Böschungen in Fels.* Dissertation, University of Kalsruhe.

Mannheimer, R.J., (1983): Effect of Slip on Flow Properties of Cement Slurries. *Oil and Gas Journal*, Dec. p144-147.

Magnusson, P.D. (1965): *The Transmission Lines and Wave Propagation.* Allyn and Bacon Inc., Boston.

Marsland, A and A.G. Loudon, (1963): The Flow Properties and Yield Gradient of Bentonite Grout in Sand and Capillaries, *Grouts and Drilling Mud in Engineering Practice*. Butterworth, p15-21.

Moller, D.W., H. L. Minch and J.P Welsch (1983): Ultrafine Cement Pressure Grouting to Control Water in Fractured Granite Rock. *Publication SP 83-8 (81-AB)*. Amer. Conc. Inst. p129-151.

Mooney, M., (1931): Explicit Formulas for slip and Fluidity. *J. Rheology*, Vol. 2, No. 2, p210 -222.

Mouxaus, J. (1978): Boring Devices for Recording Soil Data to Avoid Pollution of Grout and to Predict Unfavourable Tunnelling Under Difficult Conditons in Kutamura (ed.). *Proc. Internation Symposium on Tunneling* , Tokyo.

Müller, R.E. (1994): Monitoring of Pumping Tests and Grouting Operations. *Rock Mech. and Rock Engg.*, Vol. 17, p 51-59.

Müller, R.E. (1993): Geräte für die moderne Injektionstechnik. *Grouting in Rock and Concrete* (ed. Widmann, R), p185-193

Murata, J and H. Kikukawa, (1992): Viscosity Equation for Fresh Concrete. *ACI Material Journal*, May-June, p230-237.

National Research Council, (1996): *Rock Fractures and Fluid Flow*. National Academy Press, Washington, D.C.

Neuzil, C.E. and J.V. Tracy, (1981): Flow Through Fractures. *Wat. Resource. Res.*, Vol. 17, No. 1 p191-199

Nonveiller, E (1985): *Grouting Theory and Practice*. Elsevier Publisher Inc.

ÖDK, (1991): *Remidial Project for Kölbrein Arch Dam: Design and Construction.* ÖDK.

Odling, N.E. (1994): Natural Fractures Profiles, Fractal Dimension and Joint Roughness Coefficient. *Rock Mech. and Rock Engg.* Vol. 27, No. 3 p 135-153.

Papanastasiou, T.C. (1987): Flows of Materials with Yield.*J. of Rheology* , Vol. 31, No. 5, p385-404.

Pearson, J.R.A.(1994): On Suspension Transport in a Fracture: Framework for a Global Model. *J. Non-Newtonian Fluid Mech.*, Vol. 54, p503-512.

Pierau, B., (1996): Einpressugen von Feinstbindemitteln zur Abdichtung der streckennahen Bereiche einer Untertagedeponie. *Geotechnik* , Sonderheft. p118-123

Piggott, A.R. and D. Elsworth, (1993): Characterization of Frature Aperture by Inverse Analysis. *Can. Geotech. Journal*, Vol. 30, p 637-646

Poon, C.Y., R.S. Sayles and T.A. Jones, (1992): Surface measurement and fractal characterization of naturally fractured rocks. *Phy D., Appl. Phys.*, Vol.25, p1269-1275.

Power, W.L and T.E. Tullis, (1991): Euclidean and Fractal Models for the Description of Rock Surface Roughness. *J. of Geophys. Res.* Vol. 96, No. B1, p415-424.

Powell, M.J.D., (1964): An efficient Method for Finding the Minimum of a Function of Several Variables Without Calculating Derivatives, *Comp. J.*, Vol. 7. p155-162.

Pomeroy, S. (1991): What is TLM?
http://wwwLboro.ac.uk/department/el/research/tlm/index.html

Press, W.H., S.A. Teukolsky, W.t. Vetterling and B.P. Flannery, (1992): *Numerical Recipes in C* Cambridge University Press.

Rißler, P.(1977): *Bestimmungen der Wasserdurchlässigkeit von Klüftigem Fels*. Inst. für Grundbau, Bodenmechanik, Felsmechanik und Verkehrswasserbau der RWTH, Aachen, Publication No. 5.

Roach, D.E. and A.D. Fowler, (1993): Dimensionality Analysis of Patterns: Fractal Measurements. *Computers and Geosciences*. Vol. 19 No. 6 p849-869.

Robinson, R., (1996): Boston' Home Run. *Civil Engineering*. ASCE, July, p36-43.

Rushton, K.R. and S.C. Redshaw(1979): *Seepage and Groundwater Flow: Numerical analysis by Analog and Digital Methods*. John Wiley and Sons.

Sharp, J.C and Y.N.T. Maini, (1972): Fundamental Considerations on the Hydraulic characterisitics of Joints in Rock. *Proc. Symp. Percolation Through Fissured Rock*, Stuttgart pT1-F1 - T1-F15

Saari, K (ed.), (1988): *The Rock Engineering Alternative*. Finish Tunnelling Association.

Schulze, B., J Brauns und I Schalm, (1991): Neuartige Baustellenmeßgeräte zur Bestimmung der Fließgrenze von Suspension. *Geotechnik*, No. 3, p125-131.

Smoltczyk, U and E.A. Akinrogunde, (1995): Grouting of Fine Rock Fissures. *Proc. 10th DECSMFE*, Mamaia, Feb 12-15, Sept.

Soudain, M., (1997): Toxic Grout sales Suspended. *New Civil Engineer*, Nov. 1997, p 5.

Trenkić, V., (1995): *The Development and Characterization of Advanced Nodes for TLM Method.* Ph.D Thesis, University of Nottingham.

Tsang, Y.W. and C.F. Tsang, (1987): Channel Model of Flow Through Fractured Media. *Wat. Res. Res.*, Vol 23, No. 3. p 467-479.

Tsang, Y.W. and C.F. Tsang, (1989): Flow channeling in a Single Fractue as a Two Dimensional Strongly Heterogeneous Permeable Medium. *Wat. Res. Res.*, Vol 25, No. 9. p 2076-2080.

Umlauf, R., (1993): Die rheologische Characterisierung von Feinzement-Suspensionen Untersuchungen mit einem Schubspannungsgesteuerten Rheometer. *Berichte der Int. Konf. betreffend Injektionen in Fels und Beton*, Salzburg 11-12, Okt. p117-123.

US Department of Energy, (1995): Evaluation of two Flowable Grout Materials and Application Techniques. *www.em.doe.gov/rainland/land410.html*

US Department of Energy, (1995): Verification of Subsurface Barriers Using Time Domain Reflectometry with Waveguides. *www.em.doe.gov/rainplum/plum28.html*

Walsh, J.B., (1981): Effects of pore pressureand confining pressure on fracture Permeability. Int. Journal Rock Mechanics min. Sci. & Geomech. Abstr., Vol. 18. 429-435.

Wallner, M., (1976) : *Ausbreitung von sedimentationsstabilen Zementpasten in klüftigem Fels*. Institut für Grundbau, Bodenmechanik, Felsmechnaik und Verkehrswasserbau, RWTH, Aachen

Wang, J.S.Y. and T.N. Narasimhan, (1988): Aperture Correlation of a Fractal Fracture. *J. Geophy. Res.* Vol. 93, No. B3 p2216-2224.

Witherspoon, P.A., J.S.Y. Wang, K. Iwai and J.E. Gale, (1980): Validity of cubic law for fluid flow in deformable rock fracture. *Water Resources Research*. Vol 16, p1016.

Wittke, W., (1968): zur Reichweite von Injektionen in klüftigen Fels. *Felmechanik u Ingeniuergeol.* Supp. IV p79-89.

Whorlow, R.W., (1980): *Rheological Techniques.* Ellis Horwood Ltd. , Sussex.

Wylie, D.C., (1992): *Fondations on Rock.* E & FN Spon.

Yoshimura, A and R. K. Prod'homme, (1988): Wall slip correction for coutte and Parallel Disk Viscometers. *J. of Rheology*, Vol. 32, p53-67

Mitteilungen des Instituts für Geotechnik
Herausgegeben von Prof. Dr.-Ing. U. Smoltczyk

Nr. 1	Thamm, B.R.	(1974)	Anfangssetzungen und Anfangsporenwasserüberdrücke eines normalverdichteten wassergesättigten Tones DM 10,--
Nr. 2	Gußmann, P.	(1975)	Einheitliche Berechnung von Grundbruch und Böschungsbruch DM 5,--
Nr. 3	Feeser, V.	(1975)	Die Bedeutung des Kalziumkarbonats für die bodenphysikalischen Eigenschaften vom Löß DM 10,--
Nr. 4	Du Thin, K.	(1976)	Standsicherheit von Böschungen: Programm-Dokumentation **vergriffen**
Nr. 5	Smoltczyk, U./ Pertschi, O./ Hilmer, K.	(1976)	Messungen an Schleusen in der UDSSR. Schleusennorm der UDSSR (SN 30365) **vergriffen**
Nr. 6	Hilmer, K.	(1976)	Erddruck auf Schleusenkammerwände. DM 18,--
Nr. 7	Laumans, Q.	(1977)	Verhalten einer ebenen, in Sand eingespannten Wand bei nichtlinearen Stoffeigenschaften des Bodens DM 18,--
Nr. 8	Lächler, W.	(1977)	Beitrag zum Problem der Teilflächenpressung bei Beton am Beispiel der Pfahlkopfanschlüsse DM 15,--
Nr. 9	Spotka, H.	(1977)	Einfluß der Bodenverdichtung mittels Oberflächenrüttelgeräten auf den Erddruck einer Stützwand bei Sand DM 15,--

Nr. 10	Schad, H.	(1979)	Nichtlineare Stoffgleichungen für Böden und ihre Verwendung bei der numerischen Analyse von Grundbauaufgaben DM 20,--
Nr. 11	Ulrich, G.	(1980)	Verschiebungs- und kraftgesteuerte Plattendruckversuche auf konsolidierenden Böden
	Gußmann, P.		Zum Modellgesetz der Konsolidation DM 20,--
Nr. 12	Salden, D.	(1980)	Der Einfluß der Sohlenform auf die Traglast von Fundamenten DM 25,--
Nr. 13	Seeger, H.	(1980)	Beitrag zur Ermittlung des horizontalen Bettungsmoduls von Böden durch Seitendruckversuche im Bohrloch DM 25,--
Nr. 14	Schmidt, H.H.	(1981)	Beitrag zur Ermittlung des Erddrucks auf Stützwände bei nachgiebigem Baugrund DM 25,--
Nr. 15	Smoltczyk, U./ Schweikert, O.	(1981)	Vorstudie über bauliche Alternativen für Durchgangsstraßen in Siedlungen DM 12,--
Nr. 16	Malcharek, K./ Smoltczyk, U.	(1981)	Vergleich nationaler Richtlinien für die Berechnung von Fundamenten DM 15,--
Nr. 17	Gruhle, H.D.	(1981)	Das Verhalten des Baugrundes unter Einwirkung vertikal gezogener Ankerplatten als räumliches Problem des Erdwiderstandes DM 30,--
Nr. 18	Kobler, W.	(1982)	Untersuchungen über Böschungs- und Grundbruch bei begrenzten Lastflächen DM 25,--

Nr. 19	Lutz, W.	(1983)	Tragfähigkeit des geschlitzten Baugrunds neben Linienlasten DM 25,--
Nr. 20	Smoltczyk, U.	(1983)	Studienunterlagen "Bodenmechanik und Grundbau"; überarbeitete Ausgabe 1993 DM 40,--
Nr. 21	Schweikert, O.	(1984)	Der Einfluß des Böschungswinkels auf die Berechnung des aktiven Erddrucks DM 20,--
Nr. 22	Vogt, N.	(1984)	Erdwiderstandsermittlung bei monotonen und wiederholten Wandbewegungen in Sand **vergriffen**
Nr. 23	Buchmaier, R.	(1985)	Zur Berechnung von Konsolidationsproblemen bei nichtlinearem Stoffverhalten DM 25,--
Nr. 24	Schad, H.	(1985)	Möglichkeiten der Böschungssicherung bei kleinen Baugruben
	Smoltczyk, U./ Schad, H./Zoller, P.		Sonderkonstruktionen der Böschungssicherung DM 35,--
Nr. 25	Gußmann, P.	(1985)	Die Methode der Kinematischen Elemente DM 20,--
Nr. 26	Steinmann, B.	(1985)	Zum Verhalten bindiger Böden bei monotoner einaxialer Beanspruchung DM 25,--
Nr. 27	Lee, S.D.	(1987)	Untersuchungen zur Standsicherheit von Schlitzen im Sand neben Einzelfundamenten DM 25,--
Nr. 28	Kolb, H.	(1988)	Ermittlung der Sohlreibung von Gründungskörpern unter horizontalem kinematischen Zwang DM 25,--

Nr. 29	Ochmann, H.	(1988)	Ebene Grenzzustände von Erdböschungen im stochastischen Sicherheitskonzept DM 25,--
Nr. 30	Breinlinger, F.	(1989)	Bodenmechanische Stoffgleichungen bei großen Deformationen sowie Be- und Entlastungsvorgängen DM 30,--
Nr. 31	Smoltczyk, U./ Breinlinger, F./ Schad, H./Wittlinger, M.	(1989)	Beitrag zur Bemessung von Tunneln in offener Bauweise DM 25,--
Nr. 32	Gußmann, P./ Schanz, T./ Smoltczyk, U./ Willand, E.	(1990)	Beiträge zur Anwendung der KEM (Erddruck, Grundbruch, Standsicherheit von Böschungen) DM 30,--
Nr. 33	Gruhle, H.D.	(1990)	Der räumliche Erdwiderstand vor überwiegend horizontal belasteten Ankerplatten DM 30,--
Nr. 34	Henne, J.	(1995)	Zur Bewehrung von verformten Bodenschichten durch Einsatz zugfester Geokunststoffe DM 30,--
Nr. 35	Wittlinger, M.	(1994)	Ebene Verformungsuntersuchungen zur Weckung des Erdwiderstandes bindiger Böden DM 30,--
Nr. 36	Schad, H.	(1992)	Zeit- und geschwindigkeitsabhängiges Materialverhalten in der Geotechnik - Experimentelle Erfassung und numerische Analyse DM 30,--
Nr. 37	Belz, I.	(1992)	Zur Ermittlung dynamischer Bodenkennwerte in situ aus der Systemantwort des Erregers DM 30,--
Nr. 38	Ma, J.	(1994)	Untersuchungen zur Standsicherheit der durch Stützscheiben stabilisierten Böschungen DM 30,--

Nr. 39	Smoltczyk, U.	(1994)	Sonderheft: 25 Jahre Lehre und Forschung in der Geotechnik DM 30,--
Nr. 40	Rilling, B.	(1994)	Untersuchungen zur Grenztragfähigkeit bindiger Schüttstoffe am Beispiel von Lößlehm DM 35,--

Mitteilungen des Instituts für Geotechnik
Herausgegeben von Prof. Dr.-Ing. P.A. Vermeer

Nr. 41 (1)	Vermeer, P.A.	(1996)	Deponiebau und Geotechnik DM 35,--
Nr. 42	Vermeer, P.A.	(1997)	Baugruben in Locker- und Festgestein DM 35,--
Nr. 43	Brinkmann, C.	(1998)	Untersuchungen zum Verhalten von Dichtungsübergängen im Staudammbau DM 35,--
Nr. 44	Fiechter-Scharr, I.	(1998)	Beeinflussung von Erdbaustoffen durch Beimischen eines organophilen Bentonits DM 35,--
Nr. 45	Schanz, T.	(1998)	Zur Modellierung des mechanischen Verhaltens von Reibungsmaterialien DM 35,--
Nr. 46	Akinrogunde, A. E.	(1999)	Propagation of Cement Grout in Rock Discontinuities Under Injection Conditions DM 35,--

Weitere Veröffentlichungen des Institutes für Geotechnik Stuttgart und seiner Mitarbeiter ab 1997:

---

[1] Vermeer, P.A.: Materialmodelle in der Geotechnik und ihre Anwendung. Beiträge der Tagung FEM `95 - Finite Elemente in der Baupraxis, S. 609-618, Stuttgart, 1995.

[2] Vogt, C., Salden, D.: Schraubanker zum Rückverhängen von Spundwänden. Bautechnik 72, Heft 12, S. 800-802, 1995.

[3] Schanz, T.: Zur geotechnischen Bewertung von Beton-Recycling-Material. Bautechnik 72, Heft 12, S. 810-816, 1995.

[4] Schanz, T., Gussmann, P.: Bearing capacity of strip footing on layered subsoil. Proceedings 5th International Conference on Numerical Models in Geomechanics (NUMOG V), Davos, pp. 583-587, Balkema, Rotterdam, 1995.

[5] Smoltczyk, U., Gussmann, P., Schanz, T., Salden, D.: Zuverlässigkeitsuntersuchungen des Grundbruchs auf geschichteten Böden. Institutsbericht 3 des Institutes für Geotechnik der Universität Stuttgart, Universität Stuttgart, 1995.

[6] Vermeer, P.A., Schanz, T.: Zum Steifemodul von Sanden. Mitteilungen des Institutes für Geotechnik der Technischen Universität Dresden, Heft 3, S. 123-142, TU Dresden, 1995.

[7] Vermeer, P.A., Schanz, T.: Angles of friction and dilatancy of sand. Géotechnique 46, No. 1, pp. 145-151, 1996.

[8] Schanz, T., Vermeer, P.A.: Angles of friction and dilatancy of sand. Géotechnique 47, No. 4, pp. 887-892, 1996.

[9] Vermeer, P.A., Salden, D.: Die Geotechnik des Dammbaus – Wechselwirkungen. Jahrbuch 1996 aus Lehre und Forschung der Universität Stuttgart, S. 86-97, Stuttgart, 1997.

[10] Schanz, T., Vermeer, P.A.: Das Torsionsödometer. Institutsbericht 7 des Institutes für Geotechnik der Universität Stuttgart, Universität Stuttgart, 1997.

[11] Stolle, D.F.A., Bonnier, P.G., Vermeer, P.A.: A soft soil model and experiences with two integration schemes. Proceedings 6th International Conference on Numerical Models in Geomechanics (NUMOG VI), Montreal, pp. 123-128, Balkema, Rotterdam, 1997.

[12] Schanz, T., Bonnier, P.G.: Verification of a soil model with predicted behaviour of a sheet pile wall. Proceedings 9th International Conference on Computer Methods and Advances in Geomechanics, Wuhan/China, Vol. 2, pp. 953-959, Balkema, Rotterdam, 1997.

[13] Vermeer, P.A., Stolle, D.F.A., Bonnier, P.G.: From the classical theory of secondary compression to modern creep analysis. Proceedings 9th International Conference on Computer Methods and Advances in Geomechanics, Wuhan/China, Vol. 4, pp. 2469-2478, Balkema, Rotterdam, 1997.

[14] Vermeer, P.A., Bayreuther, C.: Tiefe Baugruben in weichen Böden. Tagungsband 1. Kolloquium Bauen in Boden und Fels, Technische Akademie Esslingen, Ostfildern, 1997.

[15] Raisch, D., Vogt, C.: Gründungssanierung der Außenwände des Museums in Tübingen. Deutsches Architektenblatt 6/97, 29. Jg., S. 927 f., Forum-Verlag, Stuttgart, 1997.

[16] Schanz, T., Desrues, J., Vermeer, P.A.: Comparison of sand data on different plane strain devices. Proceedings IS-Nagoya`97 International Symposium on Deformation and Progressive Failure in Geomechanics, pp. 289-294, Pergamon, 1997.

[17] Schanz, T.: Die Berücksichtigung von unterschiedlichen Materialsteifigkeiten bei geotechnischen Berechnungen. Tagungsband Numerik in der Geotechnik, Workshop des AK 1.6 der DGGT, S. 107-120, Stuttgart, 1997.

[18] Schanz, T.: The leaning tower of St. Moritz. Plaxis bulletin 4, pp. 4-7, 1997.

[19] Schanz, T., Gussmann, P., Smoltczyk, U.: Study of bearing capacity of strip footing on layered subsoil with the kinematical element method, Proceedings XIVth International Conference on Soil Mechanics and Foundation Engineering, Vol. 1, pp. 727-730, Hamburg, 1997.

[20] Vermeer, P.A., Schanz, T.: Die Steifigkeit des Bodens und ihr Einfluß auf die Fußeinspannung einer Stützwand. OHDE-Kolloquium`97, Mitteilungen des Institutes für Geotechnik der Technischen Universität Dresden, Heft 4, S. 247-264, TU Dresden, 1997.

[21] Vermeer, P.A., Neher H.: Bemessung von Baugruben in weichen Böden. Tagungsband 3. Stuttgarter Geotechnik-Symposium, Baugruben in Locker- und Festgestein, Mitteilungen des Institutes für Geotechnik der Universität Stuttgart, Heft 42, S. 73-82, Universität Stuttgart, 1997.

[22] Vermeer, P.A., Vogt, C.: Tragverhalten horizontaler Schraubanker in nichtbindigen Böden. Tagungsband 2. Kolloquium Bauen in Boden und Fels, Technische Akademie Esslingen, Ostfildern, 1997.

[23] Haarer, R., Vogt, C.: Geotechnische Aspekte der Planung und Ausführung von Grundwasserwannen mit Sohlverankerung im Oberrheintal. Tagungsband 3. Stuttgarter Geotechnik-Symposium, Baugruben in Locker- und Festgestein, Mitteilungen des Institutes für Geotechnik der Universität Stuttgart, Heft 42, S. 119-126, Universität Stuttgart, 1997.

[24] Vermeer, P.A.: Non-associated plasticity for soils, concrete and rock. Proceedings NATO Advanced Study Institute on Physics of Dry Granular Media, pp. 163-196, Kluwer Academic Publisher, Dordrecht, 1997.

[25] Meier, C.P., Schanz, T.: Verformungsabschätzungen für Gründungen mittels Rüttelstopfverdichtung. Tagungsband 5. Darmstädter Geotechnik-Kolloquium, Mitteilungen des Institutes für Geotechnik der Technischen Universität Darmstadt, Heft 39, S. 59-79, TU Darmstadt, 1998.

[26] Neher, H., Schanz, T., Köhler, L.: Das Torsionsödometer – ein neuartiges geotechnisches Versuchsgerät. Messen in der Geotechnik `98, Mitteilungen des Institutes für Grundbau und Bodenmechanik der Technischen Universität Braunschweig, Heft 55, S. 259-272, TU Braunschweig, 1998.

[27] Schanz, T.: A constitutive model for cemented sands. Proceedings 4th International Workshop on Localization and Bifurcation Theory for Soils and Rocks, Gifu, pp. 165-172, Balkema, Rotterdam, 1998.

[28] Vogt, C.: Experimentelle und numerische Untersuchung tiefliegender dreidimensionaler Bruchvorgänge am Beispiel horizontaler Schraubanker. Tagungsband 25. Baugrundtagung, Forum für junge Geotechnik-Ingenieure, S. 25-26, Stuttgart, 1998.

[29] Vogt, C., Bonnier, P.G., Vermeer, P.A.: Analyses of NATM-tunnels with 2D and 3D finite element method. Proceedings of the 4th European Conference on Numerical Methods in Geotechnical Engineering, pp. 211-219, Udine/Italy, 1998.

[30] Schanz, T., Vermeer, P.A.: On the stiffness of sands. Géotechnique 48, pp. 383-387, 1998.

[31] Vermeer, P.A., Neher H.: A soft soil model that accounts for creep. Proceedings of a Workshop on Stability of Embankments on soft Soils, Delft, 1998.

[32] Vermeer, P.A., Meier, C.P.: Standsicherheit und Verformungen bei tiefen Baugruben in bindigen Böden. Tagungsband 25. Vorträge der Baugrundtagung 1998 in Stuttgart, S. 133-150, Stuttgart, 1998.

[33] Bauduin, C.M., De Vos, M., Vermeer, P.A.: Back analysis of staged embankment failure. Zur Veröffentlichung in: Tagungsband Plaxis-Symposium, Amsterdam, 1999.

[34] Stolle, D.F.E., Vermeer, P.A., Bonnier, P.G.: A consolidation model for a creeping clay. Zur Veröffentlichung in: Canadian Geotechnical Yournal, 1999.

[35] Schanz, T., Vermeer, P.A., Bonnier, P.G.: The Hardening Soil Modell – Formulation and Verification. Zur Veröffentlichung in: Tagungsband Plaxis-Symposium, Amsterdam, 1999.